CHARACTERISTICS, SOURCES AND FORMATION MECHANISMS OF ORGANIC AEROSOLS IN THE ATMOSPHERE OF HONG KONG

YAO DAWEN

PhD

The Hong Kong Polytechnic University

2023

The Hong Kong Polytechnic University
Department of Civil and Environmental Engineering

Characteristics, Sources and Formation Mechanisms of Organic Aerosols in the Atmosphere of Hong Kong

Yao Dawen

A thesis submitted in partial fulfillment of the requirements for
the degree of Doctor of Philosophy
August 2022

CERTIFICATE OF ORIGINALITY

I hereby declare that this thesis is my own work and that, to the best of my knowledge and belief, it reproduces no material previously published or written, nor material that has been accepted for the award of any other degree or diploma, except where due acknowledgment has been made in the text.

Signature: _____

Name of Student: Yao Dawen

ABSTRACT

Due to rapid industrialization and urbanization in recent years, particulate matter (PM) pollution has become an annoying environmental problem in megacities like Hong Kong. Organic aerosols (OA), comprising a broad spectrum of compounds with different volatilities and properties, are the major components of ambient PM. OAs in the atmosphere contain primary OA (POA) directly emitted from anthropogenic and natural sources, and secondary OA (SOA) formed through chemical evolutions of organic compounds. Due to dynamic changes in emission profiles, POAs vary significantly across time and locations. In addition to various precursors in the atmosphere, SOA formation is influenced by many factors, such as atmospheric oxidative capacity or underlying aqueous processes. Hence, it is of great significance to quantify the contributions of primary emissions and secondary formation to OAs, and to further understand the formation mechanisms and evolution processes of OAs at different locations in the atmosphere. This thesis aims (1) to investigate the variations and composition of non-refractory sub-micron particulate matter (NR-PM_1) and OAs in the roadside and urban background environments in Hong Kong, (2) to understand the OA sources and their contributions to OAs in various micro-environments, (3) to probe the potential formation and evolution of OAs through various precursors in different environments, and (4) to compare changes in aerosol chemistry over different years.

To understand the characteristics, sources and evolution processes of atmospheric organic aerosols in the roadside environment, a sampling campaign was conducted at an urban roadside site in Hong Kong from November to December in 2017 using a high-resolution time-of-flight aerosol mass spectrometer (HR-ToF-AMS) to monitor

compositions of NR-PM_1. The results showed that organic matter in the roadside environment contributed the most to NR-PM_1 with an average proportion of 57.7 ± 0.2%. The aerosol size distributions of bulk composition of NR-PM_1 and ions indicated that the proportion of primary organic particles caused by the intensive emissions of primary organics at this site was larger. Positive matrix factorization (PMF) analysis was applied to the measurement data and four OA sources were identified, which included a hydrocarbon-like OA (HOA) factor, a cooking organic aerosol (COA) factor, and two oxygenated OA (OOA) factors with different oxidation levels, i.e., less oxidized OOA (LO-OOA) and more oxidized OOA (MO-OOA). Surprisingly, the proportion of primary source of COA was higher than that of another primary source of HOA (p<0.01) even at this roadside site with heavy traffic fleet. Moreover, the contribution of MO-OOA was the highest among all the four factors, suggesting a high degree of oxidation and/or a high regional background in the roadside environment. The COA concentration reached the highest value at 20:00 with an average of 8.2 ± 0.8 μg/m^3. Especially on Sundays, the average maximum COA concentration was 16.1 ± 3.0 μg/m^3. Comparing the results with previous studies at the roadside sites in Hong Kong, the COA levels were consistently higher than HOA, regardless of season and sampling location. All these indicated that cooking emissions were more dominant than vehicle emissions in urban Hong Kong, even in high-traffic areas. To explore the evolution of cooking OA sources, the ratio of $C_3H_3O^+$ / $C_3H_5O^+$ was used to represent the degree of COA oxidation in the atmosphere. The average ratio of $C_3H_3O^+$ / $C_3H_5O^+$ and the inverse pattern with O_x (O_3 + NO_2) during daytime hours suggested that COA underwent some degree of oxidation when transported to the site. The findings implied that cooking activities are a significant source of organic aerosols in Hong Kong, even on busy roads. Control measures should focus on both cooking and traffic emissions in Hong Kong.

SOA formation in the atmosphere is influenced by many factors. To study the formation mechanisms and evolution of OAs in Hong Kong, a sampling campaign was conducted in November 2018 at an urban background site for characterization of secondary air pollution. A HR-ToF-AMS together with other on-line instruments was used to monitor the composition of NR-PM_1 and OA molecular makers. Organics constituted the largest fraction (43.8%) of NR-PM_1, and 86.5% of the organics was contributed by OOAs. The formation mechanisms of a dominant and more variable component of a less-oxidized OOA (LO-OOA1) and the more-oxidized OOA (MO-OOA) were explored. Based on multilinear regressions with molecular markers of OA (e.g., hydroxybenzoic acids and 2,3-dihydroxy-4-oxopentanoic acid) measured by Thermal-desorption Aerosol Gas-chromatography (TAG), we speculated that anthropogenic organic compounds, especially aromatics, were the most likely precursors of LO-OOA1. The correlations between OOAs and the odd oxygen O_x ($O_x = O_3 + NO_2$) were examined to understand the role of photochemical oxidation, and MO-OOA correlated well with O_x. Moreover, the concentration of MO-OOA responded positively to the increase of liquid water content (LWC) in NR-PM_1, indicating that the formation of MO-OOA involved photochemical oxidation and aqueous processes at this site. Besides, MO-OOA exhibited the best correlation with malic acid, which can be formed by oxidation of various precursors. Furthermore, it was plausible that LO-OOA1 was further oxidized to MO-OOA through aqueous processes, as indicated by the consistent diurnal variations of MO-OOA to LO-OOA1 ratio and LWC. This study highlights the important roles of anthropogenic emissions and aqueous processes in SOA formation in coastal areas downwind of cities like Hong Kong.

In addition, OA pollution in the atmosphere can be affected by changes in emissions and meteorological conditions. As such, a detailed comparison of aerosol chemistry from different years is indispensable. A comprehensive sampling campaign was carried

out at the above urban background site in October – November 2020 to investigate changes in aerosol sources and formation mechanisms. Organics was the most dominant component of all the measured substances with an average percentage (51.0 ± 0.5 %) higher than in 2018 (43.8 ± 0.7 %). The diurnal variations of all bulk compositions in NR-PM_1 and secondary air pollutants showed the highest peaks in the same hour around 15:00, indicating intensive photochemical formation of secondary aerosols at this site. In addition, higher levels of O_x observed during the day than in 2018 suggested that there may be stronger photochemical processes in 2020. This was further confirmed by higher O:C ratios during the day in 2020 than in 2018. Furthermore, the diurnal variations of MO-OOA and LO-OOA1 also showed the same peak as O_x at 15:00, and the levels generally increased with the increase of O_x values, implying that the formation of both OOAs was associated with photochemical oxidation. By combining the measured molecular OA markers, we sought to explore the formation mechanisms and precursors of these OOAs. The diel cycles of secondarily-formed malic acid, citramalic acid, 2,3-dihydroxy-4-oxopentanoic acid (DHOPA), hydroxybenzoic acids (OHBAs) and monoterpene SOA tracers (MT-SOA-T) all showed their highest peaks in the afternoon, consistent with OOAs and O_x, indicating that photochemical oxidation played an important role in the formation of SOAs, regardless of the anthropogenic or biogenic origins at this site. By combining LO-OOA1 and MO-OOA with OA markers, we found that biogenic SOA contributed to the formation of MO-OOA. These findings could further enhance our understanding of OAs in urban background areas.

To sum up, this thesis explored the characteristics, sources and formation processes of organic aerosols in the atmosphere of Hong Kong. Differences in variations and formation of OAs in the roadside environment and urban background environment were investigated. The formation mechanisms and evolution processes of OOAs and COA

were understood. The possible precursors of OOAs were also identified. The findings deepen the understanding of the origins and chemical evolution of OAs in Hong Kong and provide a scientific basis for controlling OA pollution. The outcomes may be applicable to other similar cities around the world and provide guidance for policymakers.

THE NOVELTY OF THIS STUDY

With the rapid economic development in recent years, particulate matter (PM) pollution has become an environmental concern in megacities such as Hong Kong. Organic aerosols (OA), as the main component of ambient PM, consist of primary OA (POA) directly emitted from sources and secondary OA (SOA) formed in the atmosphere. POAs vary by time and location due to dynamic changes in emission profiles, while SOA formation is influenced by many factors, such as various precursors, atmospheric oxidative capacity and/or underlying aqueous processes. This thesis aimed to fill the gaps in OA studies in Hong Kong and deepen the understanding of OA characteristics in urban roadside and background environments. The characteristics, sources and evolution and formation processes of OAs were deeply studied. This study is expected to provide new insights into the cross-year and inter-location of OA pollution in Hong Kong. The novelty of this study is summarized as follows:

1) A detailed study of POAs at a high-traffic site found that the significant contribution of cooking emissions was even greater than that of vehicular emissions. The oxidation degree of cooking emissions was first investigated in an urban roadside environment in Hong Kong. **This study is the first** to use the ratio of $C_3H_3O^+$ / $C_3H_5O^+$ to describe the oxidation degree of cooking emissions, which changed in contrast to the daytime pattern of O_x, suggesting that COA emitted elsewhere was progressively oxidized, resulting in enhanced OOA in the roadside environment.
2) The formation and evolution of SOA were studied at an urban background site on the southern coastline of China. SOA-dominated organics in NR-PM_1 were high. **This is the first time** that OAs measured by HR-ToF-AMS were

combined with online measurements of OA makers by TAG in Hong Kong. It was demonstrated **for the first time** that one of the LO-OOA components was mainly formed through the photochemical oxidation of aromatics in the atmosphere of Hong Kong.

3) **For the first time**, the formation of OOAs was found to be related to photochemical oxidation and aqueous processes, while the potential transformation from LO-OOA to MO-OOA involved aqueous processes in the atmosphere in Hong Kong.
4) **For the first time**, detailed comparisons of online measurements of organic aerosols in different years were carried out at an urban background site in Hong Kong. Temporal variations in chemical species and oxidation degree of OAs suggested more photochemically reactive at this site in 2020 than in 2018. It was found that photochemical oxidation of anthropogenic and biogenic VOCs was one important pathway for SOA formation, and POAs could still be detected at this background coastal site. The diurnal patterns of SOA markers supported the inference that MO-OOA and LO-OOA1 were more correlated with photochemical processes in 2020, due to stronger photochemical capacity in the atmosphere.

RESEARCH OUTPUTS

1. **Yao DW**, Lyu XP, Lu HX, Zeng LW, Liu TY, Chan K Chak, Guo H*, Characteristics, sources and evolution processes of atmospheric organic aerosols at a roadside site in Hong Kong. Atmospheric Environment 252, 118298, doi: 10.1016/j.atmosenv.2021.118298, 2021 (Impact factor: 4.798; Grade A).
2. **Yao DW**, Lyu XP, Murray F, Morawska L, Wang Y, Wang JY, Guo H*. Continuous effectiveness of replacing catalytic converters on liquefied petroleum gas-fueled vehicles in Hong Kong. Science of the Total Environment 648, 830-838, 2019 (Impact factor: 4.9; Grade A).
3. **Yao DW**, Guo H*, Lyu XP, Lu HX, Huo, YX. Secondary organic aerosol formation at an urban background site on the coastline of South China: Precursors and aging processes. Environmental Pollution, 119778, 2022.
4. Lu HX, **Yao DW**, J Yip, CW Kan, Guo H*, Addressing COVID-19 spread: Development of reliable testing system for mask reuse. Aerosol & Air Quality Research 20: 2309–2317, 2020 (Impact factor: 2.735; Grade B)
5. Lyu XP, Guo H*, **Yao DW**, Lu HX, Huo YX, Xu W, Kreisberg N, Goldstein AH, Jayne J, Worsnop D, Tan Y, Lee SC, Wang T, In situ measurements of molecular markers facilitate understanding of dynamic sources of atmospheric organic aerosols. Environmental Science & Technology 54, 11058-11069, 2020 (Impact factor: 7.27; Grade A)
6. Zhou LY, Liu TY, **Yao DW**, Guo H, Cheng CL, Chan CK*, Primary emissions and secondary production of organic aerosols from heated animal fats. Science of the Total Environment 794, 148638, 2021 (Impact factor: 7.693; Grade A).
7. Lyu XP, Guo H*, Zhang WH, Cheng HR, **Yao DW**, Lu HX, Zhang LY, Zeren

YZ, Liu XF, Qian Z, Wang SM, Ozone and its precursors in a high-elevation and highly forested region in central China: origins, in-situ photochemistry and implications of regional transport. Atmospheric Environment 259, 118540, 2021 (Impact factor: 4.798; Grade A).

8. Lyu XP, Huo YX, Yang J, **Yao DW**, Li KM, Lu HX, Zeren YZ, Guo H*, Real-time molecular characterization of air pollutants in a Hong Kong residence: implication of indoor source emissions and heterogeneous chemistry. Indoor Air 00, 1-13, DOI: 10.1111/ina.12826, 2021 (Impact factor: 4.739; Grade A).

9. Zeng LW, Fan G-J, Lyu XP, Guo H*, Wang J-L, **Yao DW**. Atmospheric fate of peroxyacetyl nitrate in suburban Hong Kong and its impact on local ozone pollution, Environmental Pollution, https://doi.org/10.1016/ j.envpol.2019.06.004, 2019 (Impact factor: 5.099; Grade A).

10. Liu TY, Zhou LY, Liu QY, Lee BP, **Yao DW**, Lu HX, Lyu XP, Guo H, Chan CK. Secondary organic aerosol formation from urban roadside air in Hong Kong. Environmental Science and Technology 53 (6), 3001–3009, doi: 10.1021/acs.est.8b06587, 2019 (Impact factor: 6.198; Grade A).

11. Lyu XP, Guo H*, Cheng HR, Wang XM, Ding X, Lu HX, **Yao DW**, Xu C, Observation of SOA tracers at a mountainous site in Hong Kong: Chemical characteristics, origins and implication on particle growth. Science of the Total Environment 605-606, 180-189, 2017 (Impact factor: 4.9; Grade A).

12. Huo Y, Guo H*, Lyu XP, **Yao, DW**, Emission characteristics, sources, and airborne fate of speciated organics in particulate matters in a Hong Kong residence. Indoor air, 32(3), e13017, 2022.

13. Xing, L., Fu, T. M., Liu, T., Qin, Y., Zhou, L., Chan, C. K., Guo, H., **Yao, D.**, Duan, K., Estimating organic aerosol emissions from cooking in winter over the Pearl River Delta region, China. Environmental Pollution, 292, 118266, 2022.

14. Nie, W., Yan, C., Huang, D. D., Wang, Z., Liu, Y., Qiao, X., Guo, Y., Tian, L., Zheng, P., Xu, Z., Li, Y., Xu, Z., Qi, X., Sun, P., Wang, J., Zheng, F., Li, X., Yin, R., Dallenbach, K. R., Bianchi, F., Petäjä, T., Zhang, Y., Wang, M., Schervish, M., Wang, S., Qiao, L., Wang, Q., Zhou, M., Wang, H., Yu, C., **Yao, D.**, Guo, H., Ye, P., Lee, S., Li, Y., Liu, Y., Chi, X., Kerminen, V., Ehn, M., Donahue, N., Wang, T., Huang, C., Kulmala, M., Worsnop, D., Jiang, J., Ding, A., Secondary organic aerosol formed by condensing anthropogenic vapours over China's megacities. Nature Geoscience, 15(4), 255-261, 2022.

ACKNOWLEDGEMENTS

Five years have passed since I studied for my PhD degree at The Hong Kong Polytechnic University (PolyU), and it has left an indelible mark on my heart. Over the years, I have met many people who have given me kindness, support and encouragement. My time at PolyU was one of the most unforgettable experiences in my life. Here, I would like to express my sincere thanks to them.

First of all, I would like to express my heartfelt thanks to my supervisor, Prof. Hai GUO. He supported and guided my PhD research. His doors are always open to students, and he gave me a lot of advice and guidance during discussions. Those face-to-face discussions or emails inspired me a lot to complete my PhD study. He also offered me all the sources, such as instruments or laboratory equipment needed for my research work. Besides, every time when I sent him my manuscripts or thesis, he always did a lot of detailed revisions and modifications. Without his supervision, this Ph.D. would not be completed.

Secondly, I sincerely thank all my group mates. Special appreciation goes to Dr. Xiaopu LYU, who helped me a lot in my studies such as experiments, data analysis and paper writing. His kind help significantly improved my work. Thanks also go to Dr. Yu WANG, Dr. Lewei ZENG, Dr. Pei ZENG, Dr. Xufei LIU, Dr. Yangzong ZEREN and Dr. Haoxian LU, for always supporting me in my work and daily life. I also thank Dr. Jingcui XU, Dr. Kaiming LI, Miss Beining ZHOU, Miss Yunxi HUO, Miss Jin Yang, Miss Luyao ZHANG, Miss Jiaying WANG and Mr. Enyu XIONG, who offered a lot of good advice during my daily work.

Thirdly, I like to express my thanks to Mr. Jazz CHAN, Mr. W. F. TAM and Mr. Steven POON for their technical support on my experiments and sampling campaigns.

Fourthly, my thanks go to all the people I met at PolyU, including but not limited, Mr. Ziyang HAN, Miss. Xue LUO, Mr. Zhuoxuan ZHUANG, Miss. Ruixing LIANG, and Miss. Yue LUO, and special thanks go to Miss Xiaolin ZHOU for everything.

Fifthly, this work was supported by the Research Grants Council of the Hong Kong Special Administrative Region via the Collaborative Research Fund (C5004-15E), the Theme-Based Research Scheme (T24-504/l7-N), the NSFC/RGC Joint Research Scheme (N_PolyU530/20), the General Research Fund (PolyU 152052/16E and PolyU 15212421), and the Strategic Focus Area scheme of The Research Institute for Sustainable Urban Development at The Hong Kong Polytechnic University (1-BBW9), and the Hong Kong Polytechnic University internal fund (4-BCF6).

Finally, I deeply thank my families for their generous love and endless support, especially my parents and Lingling HUANG. They were very supportive of me in every situation.

Contents

Chapter 1 Overview

1.1 Research background

Airborne particulate matters (PM) influence climate change (Seinfeld and Pandis, 2008; Jacob and Winner, 2009) and pose a threat to public health (Dockery et al., 1993, Pope and Dockery, 2006). PM also has adverse effects on air quality and our visibility (Cheung et al., 2005; Han et al., 2016). With the development of modern industry, urban PM pollution has become an annoying problem in many countries and led to frequent haze days in recent years. Extensive research has been carried out to understand and address PM pollution around the world. In the atmosphere, a large proportion (20-90%) of the mass of submicron particles is organic aerosols (OAs) (Kanakidou et al., 2005; Jimenez et al., 2009), which consist of a broad spectrum of compounds with different volatility and properties (De Gouw and Jimenez, 2009; Zhang et al., 2011).

OAs include primary organic aerosols (POAs) from direct emissions of various anthropogenic and natural sources, and secondary organic aerosols (SOAs) formed in the atmosphere by the chemical evolution of organic compounds (Donahue et al., 2006; Kroll and Seinfeld, 2008; Li et al., 2016). Many sources, such as vehicular emissions, coal combustion, cooking emissions, can lead to different POAs of different species and compositions. These POAs could further form SOAs through a series of atmospheric reactions in the real atmosphere. Apart from local sources, the evolution and formation of OAs are also influenced by multiple factors such as atmospheric oxidation capacity, reaction media, and meteorology (Hu et al., 2017; Xu et al., 2017; Brege et al., 2018; Paglione et al., 2020). Thus, it is crucial to investigate the OAs in the atmosphere so that appropriate control strategies can be proposed.

Traditional method for ambient PM analysis is to collect PM on filters and perform offline chemical analysis of the collected particles. However, offline filter analysis is prone to various artifacts during sample collection, shipping or storage (Turpin et al., 1994; Dillner et al., 2009). In addition, offline sampling methods typically require 24 – 48 hours of collection time to obtain sufficient particles for chemical analysis, resulting in coarse temporal resolution to capture rapidly evolving processes in the atmosphere. The state-of-the-art instruments are usually capable of providing measurement data at a sampling location with a temporal resolution of seconds to a few minutes (Hallquist et al., 2009). With the rapid development of online measurement mass spectrometry techniques, the Aerodyne High Resolution - Time of Flight - Aerosol Mass Spectrometer (HR-ToF-AMS) is currently one of the widely used technologies to identify the size-resolved abundance and composition of organic and inorganic components of non-refractory submicron particulate matter (NR-PM_1) (Jayne et al., 2000; Canagaratna et al., 2007). Furthermore, we can extract the sources of OAs in the atmosphere by combining the OA mass spectra gained from AMS high-resolution data with source receptor models, e.g. positive matrix factorization (PMF) model (Zhang et al., 2005; Lanz et al., 2007).

With the information of aerosols with a high temporal resolution from HR-ToF-AMS, we can identify the sources of OAs as POAs (e.g. hydrocarbon-like OA (HOA), cooking OA (COA), coal combustion OA (CCOA)) and oxygenated OAs (OOAs) at each specific sampling site (Jimenez et al., 2009; Zhang et al., 2019). Depending on the degree of volatility or oxidation, the OOAs can be further categorized into SV-OOA (semi-volatile OOA) and LV-OOA (low-volatility OOA) or LO-OOA (less oxidized OOA) and MO-OOA (more oxidized OOA). While these POAs and OOAs make substantial contributions to OAs, the proportion varies at the same site as the POAs

emissions are different and the OOAs can be formed locally or transported regionally. Moreover, extensive studies have demonstrated that airborne pollutants emitted from primary sources can form SOA during photochemical aging (Nordin et al., 2013; Gordon et al., 2014; Klein et al., 2016; Liu et al., 2018). However, discrepancies are found with respect to the role of each process at different sites/sampling campaigns (Xu et al., 2017; Huang et al., 2020; Xiao et al., 2021), implying that the formation processes and mechanisms of OAs may vary by time and location. Furthermore, HR-ToF-AMS has been extensively used to study the evolution of OAs in the atmosphere (DeCarlo et al., 2010; He et al., 2011; Kim et al., 2017). However, based on AMS data alone, it is difficult to determine the precursors and specific formation pathways of SOA, as AMS fails to provide any molecular information. Nevertheless, with the aid of other unambiguous measurements, the interpretability of AMS data can be enhanced (Xu et al., 2015; Lyu et al., 2020).

Hong Kong, an Asian metropolis in southern China adjacent to the rapidly developing Pearl River Delta (PRD) region of mainland China, has been affected by PM pollution over the past decades (So et al., 2007; Cheung et al., 2015). Due to large number of on-road motor vehicles and extremely high population density, local sources such as vehicle and cooking emissions contribute significantly to OAs. Although a series of control measures implemented by the local government have reduced vehicle exhaust emissions to a certain extent (HKEPD, 2017), the importance of cooking emissions to OAs should be paid more attention in urban areas of Hong Kong (Lee et al., 2015; Liu et al., 2019). In addition, regional and even superregional transport exacerbate particulate pollution in Hong Kong, especially in cool seasons when prevailing winds bring in polluted air masses from mainland China (Wang et al., 2017; Lyu et al., 2020). Furthermore, the high relative humidity and strong photochemical capacity of Hong

Kong favor aqueous processes and photochemical oxidation in SOA formation (Li et al., 2013; Qin et al., 2016). Thus, mitigating particulate pollution in Hong Kong remains a huge challenge that requires further research.

In this work, a HR-ToF-AMS, together with other real-time instruments, was utilized to continuously measure NR-PM_1 components and other air pollutants at an urban roadside site and an urban background site during three sampling campaigns in Hong Kong. Temporal variations of NR-PM_1 components and sources of OAs at the two sites were discussed. The characteristics and sources of OAs at different locations and in different years were compared. The evolution processes and formation mechanisms of OA components at each site were also investigated. These findings deepen our understanding of the characteristics and chemical evolution of OAs in urban atmosphere and provide scientific basis for controlling PM pollution.

1.2 Scope of this study

This thesis aims to probe the characteristics, sources and formation processes of organic aerosols in the atmosphere of Hong Kong. The objectives of the thesis are as follows:

- To investigate the variations and composition of NR-PM_1 in roadside and urban background environments in Hong Kong.
- To explore the sources and contributions of OAs in different locations and compare the characteristics of OA sources across time and locations.
- To examine the formation and evolution of OAs in Hong Kong and discuss the impact of each process on the formation of different OAs in different locations.
- To reveal potential precursors of different OAs and find out the formation mechanisms of OAs through different precursors in the atmosphere.

This work aims to fill gaps in OA studies in Hong Kong and to improve understanding of the compositional characteristics of OAs in urban roadside and urban background locations. It also attempts to further advance our knowledge of the formation of different OAs by in-depth study of the evolution and formation processes of each OA. In addition, this study is expected to provide new insights into the inter-annual and inter-location of OA pollution in cities around the world by exploring OAs in different locations and years in Hong Kong. These findings provide scientific support for the remediation of OA pollution and guide policymakers in formulating and implementing control measures.

1.3 Outline of this thesis

This thesis is divided into seven chapters including 'Overview', 'Literature Review', 'Methodology', three chapters of results and discussion (Chapters 4-6, which are 'Characteristics, sources and evolution processes of atmospheric organic aerosols at a roadside site in Hong Kong', 'Secondary organic aerosol formation at an urban background site on the coastline of South China: precursors and aging processes' and 'Changes in aerosol chemistry at an urban background site in Hong Kong before and during the COVID-19 pandemic'), and the final chapter of 'Conclusions and suggestion for future study'.

Chapter 1 'Overview'. In this chapter, the basic knowledge of photochemical pollution is introduced and the research background and knowledge gaps are presented. The contents and objectives of this study are also listed and highlighted.

Chapter 2 'Literature review'. This chapter looks back previous studies on atmospheric aerosols from the aspects of sources and evolution processes. Earlier research on on-line measurements using HR-ToF-AMS is reviewed and summarized. Relevant studies in Hong Kong are also discussed.

Chapter 3 'Methodology' describes data sources, sampling locations, and instrumentation. Details of HR-ToF-AMS are presented. In addition, the description and configuration of models are illustrated.

Chapter 4 'Characteristics, sources and evolution processes of atmospheric organic aerosols at a roadside site in Hong Kong'. In this chapter, the sources and evolution processes of organic aerosols at a roadside site is studied.

Chapter 5 'Secondary organic aerosol formation at an urban background site on the coastline of South China: precursors and aging processes'. In this chapter, variations of

OA sources at an urban background site are investigated. The formation mechanisms and evolution processes of OOAs are evaluated.

Chapter 6 ‘Changes in aerosol chemistry at an urban background site in Hong Kong before and during the COVID-19 pandemic’. This chapter studies the characteristics and sources of OAs at the urban background site in 2020 and compares the results with those found in 2018. Differences in relationship to precursors between the two years are discussed.

Chapter 7 ‘Conclusions and suggestion for future study’. This chapter summarizes the key findings and highlights the novelty of this study. The limitation of this study is discussed and the suggestion for future research is given.

Chapter 2 Literature Review

2.1 Organic aerosols in the atmosphere

In the atmosphere, a large fraction (20-90%) of the submicron particulate mass is organic aerosol (OA). which contains primary organic aerosol (POA) from direct emissions of various anthropogenic and natural sources, and secondary organic aerosol (SOA) formed in the atmosphere from gas-phase precursors. While emissions from various sources make substantial contributions to OAs, the proportion varies at the same site as the POAs emissions are often different and the SOAs can be formed locally or transported regionally. Jimenez et al. (2009) described the atmospheric evolution of OA, in which OA and OA precursor gases evolved by becoming increasingly oxidized, less volatile, and more hygroscopic, leading to the formation of oxygenated organic aerosols (OOAs) in the atmosphere. Ng et al. (2010) compiled and presented results from factor analysis of 43 datasets. SOAs with volatility were diagnosed and ambient OA would converge towards highly aged LV-OOA with atmospheric oxidation.

Extensive studies have demonstrated that primary emissions such as vehicular exhaust (Chirico et al., 2010; Nordin et al., 2013; Gordon et al., 2014) and cooking activities (Klein et al., 2016; Liu et al., 2017a; Liu et al., 2018) can form SOA during photochemical aging. Gordon et al. (2014) investigated the photochemical aging on emissions from 15 light-duty gasoline vehicles. Emissions from some vehicles generated 6 times the amount of SOA than the primary PM after 3 hours of oxidation, resulting in the formation of substantial SOA. Nordin et al. (2013) studied SOA formation in gasoline exhaust gas at idle and cold start of three passenger vehicles through photo-oxidation experiments. It was found that SOA was readily formed in gasoline exhaust, and its characteristic aerosol mass spectrum was similar to that of

oxidized organic aerosols, which usually dominated the mass spectra of organic aerosols downwind of urban areas. For cooking emissions, Liu et al. (2018) examined the characteristics of SOA from cooking emissions of seven different oils heated and photo-oxidized in a smog chamber. The results suggested that cooking style and atmospheric oxidative conditions affect ambient COA components and proportion. But most of these studies are based on chamber experiments and cannot fully represent the real atmosphere. Therefore, it is still of great significance to quantify the contributions of primary emissions and secondary formation to OAs, and to further understand the formation mechanisms and evolution processes of OAs in the atmosphere.

Except for the precursors, SOA formation is also affected by various factors such as atmospheric oxidative capacity, reaction media, and meteorology (Hu et al., 2017; Xu et al., 2017; Brege et al., 2018; Paglione et al., 2020). Xu et al. (2017) studied the roles of photochemical oxidation and aqueous processes in altering the composition and oxidation degree of oxygenated OA (OOA) in Beijing. It was shown that aqueous processes dominated the formation of the more oxidized OOA (MO-OOA). Xiao et al. (2021) found that the contribution of MO-OOA to OA increased with increasing relative humidity and O_x, suggesting the promotion of SOA formation by aqueous-phase processes and photochemical oxidation. The joint effects of RH and O_x indicated that aqueous-phase process was more prominent than photochemical formation in MO-OOA formation and SOA aging. Huang et al. (2020) inspected the dependence of OOA components on O_x and liquid water content (LWC) at a background site of the Yangtze River Delta region in summer. They found that the formation of OOA at higher oxidation state was mainly driven by photochemical oxidation. Furthermore, Xu et al. (2018) investigated the changes in aerosol chemistry in winters from 2014 to 2016 in Beijing. While cooking OA decreased substantially, the contribution of biomass

burning OA increased slightly. In addition, the changes in aerosol and OA composition varied differently at different pollution and relative humidity levels. Such discrepancies indicated that SOA formation mechanisms might not always be consistent. It is critical to conduct more research on the sources and formation processes of SOAs in the atmosphere.

2.2 Online measurements of organic aerosols

Traditionally, filter-based method is used to collect samples and analyze the composition and origin of OAs in the atmosphere. Due to limited time-resolution and time consuming of offline sample analysis, it is difficult to capture the dynamic variations and evolution of OAs in real environment (Turpin et al., 1994; Dillner et al., 2009). With the development of mass spectrometry techniques, on-line instruments are usually capable of providing measurement data with a temporal resolution of seconds to a few minutes (Hallquist et al., 2009). The Aerosol Mass Spectrometer (AMS) is currently one of the most popular technologies used to identify the size-resolved abundance and composition of both organic and inorganic components of NR-PM_1 in the atmosphere (Jayne et al., 2000; Canagaratna et al., 2007).

The high-resolution version of the AMS (i.e. HR-ToF-AMS) instrument allows the separation of ions with the same mass/charge ratio but different elemental compositions. For example, at m/z 43 the following fragments could be resolved: $C_2H_3O^+$ and $C_3H_7^+$. This facilitates the identification and differentiation of the spectra of POA sources and SOA components (Ulbrich et al., 2009; Hallquist et al., 2009). Statistical techniques are also used to enhance the interpretability of the data. Aiken et al. (2007) developed a method to determine the O/C, N/C and H/C atomic ratios of organic matter with high time resolution. In addition, OA sources can be resolved by combining OA mass spectra gained from AMS high-resolution data with source receptor models. Zhang et al. (2005) achieved the first quantification of OA composition using AMS data collected in Pittsburgh. Two prominent components, i.e. oxygenated organic aerosol (OOA) and hydrocarbon-like organic aerosol (HOA), accounted for the majority of the OA mass. The OOA had a mass spectrum typical of highly oxygenated species and was identified as a surrogate for SOA. The spectrum of HOA contained reduced species of

hydrocarbons and was considered a surrogate for POA. Lanz et al. (2007) applied a positive matrix factorization (PMF) model to AMS spectra and provided details on POA and SOA components. OOAs were further differentiated into two OA components with different volatility in this study. This means that high time resolution analysis of the whole organic mass becomes possible using AMS data (Hallquist et al., 2009).

To date, AMS measurement data has been widely used to study the OAs in the atmosphere (Jimenez et al., 2009; DeCarlo et al., 2010). Jimenez et al. (2009) reviewed and summarized OA observations in the Northern Hemisphere. It was proposed that OA and OA precursor gases evolve by becoming more oxidative and less volatile, leading to the formation of oxygenated organic aerosols (OOAs). In these previous studies, sources and evolution of OAs have been extensively investigated. However, based on AMS data alone, it is difficult to determine the precursors and specific formation pathways of SOA, as AMS cannot provide any molecular information. With the aid of other explicit measurements of OA tracers, the interpretability of AMS data on OAs can be largely enhanced. For example, Xu et al. (2015) identified an isoprene-derived SOA based on a correlation of AMS data with particle-phase 2-methyltetrols measured by semi-volatile thermal desorption aerosol gas chromatograph. The effect of sulfate on isoprene-OA was discussed and the mediating effect of sulfate on this component was found in the southeastern United States. Lyu et al. (2020) found time series and diurnal patterns of anthropogenic SOA consistent with AMS-resolved more-oxidized oxygenated organic aerosols (MO-OOA). Combining AMS data with SOA tracers measured by Thermal-desorption Aerosol Gas-chromatograph (TAG), formation processes of some anthropogenic SOAs were determined at a regionally urban background site in Hong Kong. Interaction of air pollutants, and atmospheric oxidative capacity might enhance PM pollution in continental and marine air. These findings suggest that our ability to capture the dynamic variations and evolution processes of

OAs can be enhanced by comprehensive measurements in the atmosphere.

2.3 Studies of OAs in Hong Kong

Hong Kong has suffered from PM pollution for decades (So et al., 2007; Cheung et al., 2015). The composition, origin and evolution of OA in Hong Kong have been extensively studied (Lee et al., 2013; Li et al., 2015; Lee et al., 2015). A high-resolution time-of-flight aerosol mass spectrometer (HR-ToF-AMS) made the first measurements in 2011 during a field sampling campaign at a coastal site in suburban Hong Kong (Lee et al., 2013). The size-resolved chemical composition of NR-PM_1 was measured and three aerosol components (i.e., hydrocarbon-like organic aerosol, semi-volatile organic aerosol and low-volatile organic aerosol) were generated by source apportionment. The results showed that under the influence of coastal and continental air masses, the larger the particle diameter, the greater the proportion of oxygenated organic aerosols and the higher the organic-to-carbon ratios. Long-term observations of OAs were also carried out in Hong Kong in the past. HR-ToF-AMS was used to conduct a one-month sampling campaign at the same suburban site during each season of the year (Li et al., 2015). The results suggested that air mass origin greatly affected both the NR-PM_1 concentration and the proportion of species in NR-PM_1, with locally produced SOAs higher than those caused by long-range transport in spring and summer. There have been also some studies on the characteristics of OAs in the roadside environment of Hong Kong (Lee et al., 2015; Lee et al., 2017; Liu et al., 2019). Lee et al. (2015) performed the first real-time HR-ToF-AMS measurements of NR-PM_1 at an urban roadside site in Hong Kong in 2013. While fresh POA accounted for two thirds of the total measured organics, the contribution of cooking in organic aerosols exceeded that of vehicle emissions. Moreover, both traffic and cooking emissions at this site contributed substantially to

particle mass in Aitken and Accumulation modes (Lee et al., 2017). Liu et al. (2019) investigated in situ SOA formation in urban roadside air in winter in Hong Kong using an oxidative flow reactor (OFR) combined with HR-ToF-AMS and found that cooking emissions might also have a significant impact on SOA in urban areas. This draws attention to the need for more research elsewhere in Hong Kong to evaluate the importance of different POAs (especially related to cooking emissions) for developing appropriate air pollution mitigation and reduction policies.

In addition to local sources, secondary formation and regional transport can aggravate OA pollution in Hong Kong (Hu and Yu, 2013; Li et al., 2013; Qin et al., 2016). Based on filter-based measurement data, Hu and Yu (2013) inferred the aqueous formation of malic acid through the oxidation of multiple precursors. With on-line measurement data of HR-ToF-AMS, Li et al. (2013) presented the results of the degree of oxygenation of OA at a coastal site from late April to the end of May. Two foggy periods and one hazy period were chosen to compare the changes in the degree of oxygenation of OA. It was found that during the haze, gas-phase oxidation was the main factor affecting the oxidation of organic matters, while aqueous-phase processes may be related to the high oxidation of OA during the foggy periods. Qin et al. (2016) analyzed the evolution of OA during PM episodes at the same site and identified the roles of photochemical oxidation and aqueous processes in SOA formation. Most previous studies (e.g., Li et al., 2013; Qin et al., 2016) aimed to understanding aqueous chemistry were conducted in spring, as Hong Kong has the highest relative humidity and cloud cover from March to June. However, the city is most exposed to photochemical pollution in autumn when ozone levels are significantly higher than many inland cities (Liu et al., 2021). In addition, transboundary transport brings aging air masses from mainland China to Hong Kong in cool seasons. Therefore, SOA formation in autumn is worth investigating when strong photochemical oxidation and aqueous processes interact.

Chapter 3 Methodology

3.1 Description of sampling sites

The sampling campaign was conducted at a location on the campus of The Hong Kong Polytechnic University (PolyU) from 2 November to 13 December 2017. The location of the sampling site and the surrounding environment are shown in Figure 3-1. The site (22.30°N, 114.18°E) was immediately adjacent to the eight-lane entrance and exit of the Cross-Harbor Tunnel, the busiest traffic hub with an average daily traffic flow of approximately 114,000 vehicles in 2017 (HKATC, 2017). Hence, this site is an ideal location to study the impacts of vehicular emissions on OAs. Within 1 km radius, the Tsim Sha Tsui commercial centre is located west of the sampling site, where many shops and restaurants are situated, while to the south is the Victoria Harbor. In the northeast and east of the site are residential areas with densely distributed buildings and numerous restaurants. As a metropolis, Hong Kong possesses many densely populated commercial and residential areas. There are many vehicles driving on the narrow and busy canyon streets, and a lot of restaurants on both sides of the streets. Hence, the air in urban Hong Kong is full of vehicular exhaust and cooking smells. In view of the location of the sampling site and the surrounding environment, it represents a typical roadside environment in Hong Kong. Namely, vehicles and cooking activities are the main emissions in the area around the site, and there are almost no biogenic emissions nearby. The sampling inlet (~2 m long, 3.2 cm i.d.) equipped with a $PM_{2.5}$ cyclone, approximately 3.5 m above the ground, was installed on the rooftop of a container, and the air was drawn into the HR-ToF-AMS and another online instrument at a total flow rate of 16.7 L/min. Before entering the AMS, the sampled air passed through a 0.6m long diffusion dryer filled with silica gel to remove bulk gas- and particle-phase water.

The residence time of less than 6s in the sampling line would reduce the loss of organic vapors (Pagonis et al., 2017). Our previous study calculated and proved the minor losses of organic vapors in the same sampling line (Liu et al., 2019).

Figure 3-1. Location of the roadside sampling site and the surrounding environment

Another sampling campaign was carried out in November 2018 at an air quality monitoring station (Hok Tsui, HT) managed by the Hong Kong Environmental Protection Department (HKEPD). The theme of this field campaign was to observe photochemical pollution in subtropical Hong Kong. The site (22.209°N, 114.253°E) was located at the southeastern tip of Hong Kong, facing the South China Sea to the east and south (Figure 3-2). Local emissions were sparse despite a small village nearby. East-northeast winds prevailed in autumn at the site. Therefore, air pollutants from the

urban areas of Hong Kong and the adjoining Pearl River Delta (PRD) can be transported to the site. For this reason, HT has been regarded as an urban background site in South China (Zhang et al., 2012; Wang et al., 2019; Lyu et al., 2020). The sampling inlet was ~1 m above the roof of a one-story building (~3 m), and a PM_1 cyclone (URG-2000-30EHB) was used to remove large particles from the air drawn into the instruments (Lyu et al., 2020). In addition to HR-ToF-AMS, many other instruments were deployed at the site, which provide auxiliary data for this study.

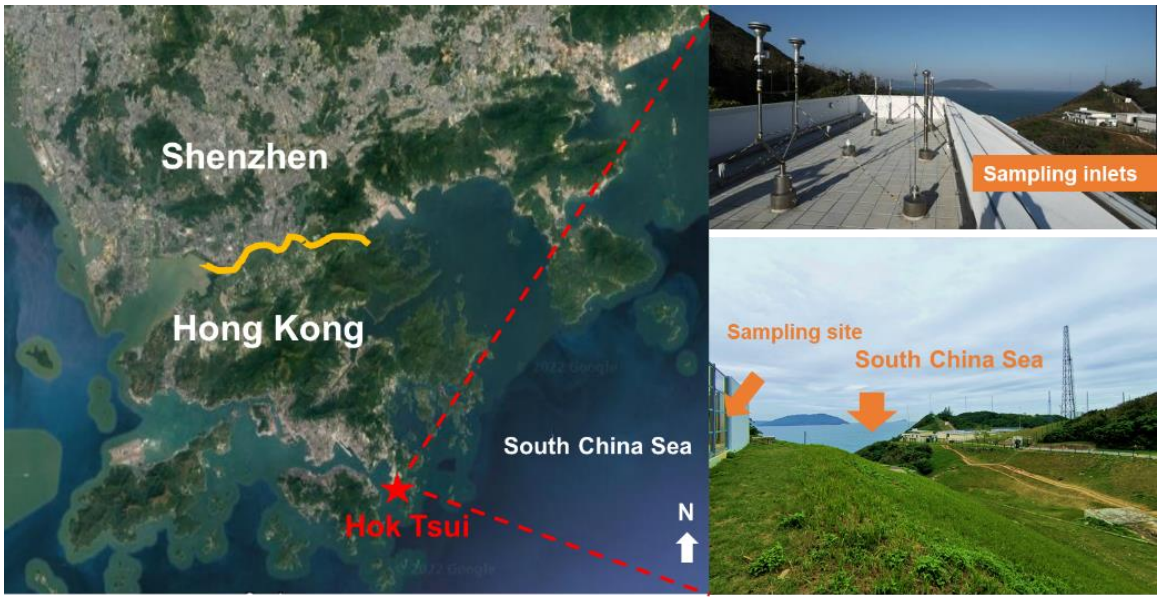

Figure 3-2. Location of the urban background sampling site (star in left panel) and the real scene of sampling inlets and environment (right panels). Boarder line between Shenzhen and Hong Kong is highlighted in yellow.

The third sampling campaign was carried out at the Hok Tsui (HT) site from 29 September to 18 November 2020. To keep consistency with the sampling campaign in 2018, the layout of the instruments, the inlets and the instrument settings remained unchanged. Details were not given again.

3.2 Measurement techniques

3.2.1. Description of the design of HR-ToF-AMS

The NR-PM_1 compositions including total organics, sulfate, nitrate, ammonium and chloride were measured using an Aerodyne HR-ToF-AMS (Jayne et al., 2000; DeCarlo et al., 2006). The instrument is maintained by a bank of pumps, including a diaphragm pump and five turbo pumps, to keep near-vacuum conditions. Ambient air is drawn through a 100 μm critical orifice at a flow rate of around 80 cm^3 /min into a set of aerodynamic lenses to focus ambient particles into a narrow beam. The aerosol beam is then accelerated into the particle flight chamber, where a rotating circular chopper is positioned at the entrance of the flight chamber. The chopper sets the starting point of the aerosol beam, and particle size measurements are obtained by calculating the travel time of the aerosol beams in the chamber. The rotating chopper has three continuous status loops, which are open, close, and chopping. In the open position, the chopper moves completely out of the plane of the particle beam. In the close position, the particle beam is completely blocked by the blade, and the mass spectrometer will only acquire signals from the background air and gas-phase species within the instrument. The difference between open and closed chopper mass spectrometry generates mass spectral signals related to particle composition. In the chopping position, the particle beam is focused on radial slits of the rotating disk, which allows small packets of particles to pass through the chopper. Then different vacuum-aerodynamic particle sizes can be determined from the flight time of the particles over a fixed length of the flight chamber as particles of different sizes attain different velocities. A heated tungsten structure at the end of the flight chamber vaporizes the particle components at a temperature of 600°C. As such, only compounds that instantly vaporize at this temperature are measurable by AMS and are referred to as NR-PM_1 components. The

vapors are exposed to electrons (70eV) from a filament for electron impact ionization. The resulting positive ions are then orthogonally accelerated into a high-resolution ion time-of-flight mass analyzer. A multichannel plate detector (MCP) is used for ion detection, with the signal sent to a data acquisition board for computational processing. The instrument alternated every 5 minutes between two ion optical modes, *i.e.*, V-mode with higher sensitivity and W-mode with higher mass resolution. A complete V mode cycle consisted of 6 sub-cycles, and each sub-cycle of 20s was divided into 10s mass spectrum (MS) mode (5s chopper-open and 5s chopper-close) and 10s particle time-of-flight (PToF) mode. As such, the size distributions of the NR-PM_1 components were measured, where the sizes were in mass-weighted aerodynamic diameter. In each W mode, data were acquired in 12 sub-cycles of 10s MS mode (5s chopper-open and 5s chopper-close). The ions detected in W-mode with high mass resolution (~5000–6000) allowed us to determine the elemental composition of organics (DeCarlo et al., 2006; Aiken et al., 2008; Sun et al., 2011), which therefore were used in source apportionment.

3.2.2. Data processing of HR-ToF-AMS

The collected NR-PM_1 mass concentration and size distribution data were processed in accordance with general principles laid out in previous studies (Jimenez et al., 2003; DeCarlo et al., 2006), employing the standard Tof-AMS Analysis Toolkit 1.59D and Tof-AMS HR Analysis 1.19D based on WaveMetrics Igor Pro 6.37 version available from the Tof-AMS Resource Web page (http://cires.colorado.edu/jimenez-group/ToFAMSResources/ToFSoftware/index.html) and using default Relative Ionization Efficiency (RIE) values of 1.2 for sulfate, 1.1 for nitrate, 1.3 for chloride, and 1.4 for organics (Canagaratna et al., 2007). A RIE of 4.3 was chosen for ammonium based on the average of the RIE values obtained from weekly periodic ionization efficiency (IE) calibrations during the sampling period. By comparing with particle mass concentrations estimated from continuous measurement data of a Scanning

Mobility Particle Sizer (SMPS, model 5.400, GRIMM, Germany) and a Black Carbon Analyzer (BC, model AE16, Magee, USA), a collection efficiency (CE) factor of 0.7 was determined and applied to AMS-derived NR-PM_1 mass concentration (Figure 3-3). Particle-free filtered ambient air was sampled using an inline HEPA-filter for about 60 minutes every two days to obtain background mass spectra and the instrument method detection limit (MDL). The MDLs were also calculated using the background data, which were determined to be 0.201, 0.020, 0.016, 0.012, and 0.010 μg/m^3 for organic, sulfate, nitrate, ammonium and chloride, respectively. CO_2^+ signals were corrected with the time-dependent gas-phase CO_2 contributions. The contributions of organic nitrate and organic sulfate were checked and modified based on the correlation plots between the related fragments. Transmission curves of the standard lens for most AMS instruments were determined in a previous study (Knote et al., 2011), which showed nearly 100% efficient transmission in the range of 100 – 550 nm and fell off at both sides. In this study, we considered the transmission efficiency as part of the combined correction factor CE to avoid additional uncertainties from the application of off-site calibrated lens transmission values. The elemental ratios between oxygen, carbon and hydrogen, as well as the organic mass-to-carbon ratio (OM/OC) of OA, were determined from analysis of the W-mode high-resolution mass spectra (HRMS) data, following the method recently reported by Canagaratna et al. (2015). It should be noted that the neglected H^+ signal from fragmentation of H_2O^+ ions may affect the oxidation state calculations. However, Hildebrandt Ruiz et al. (2014) estimated the impact was minor based on the small variation of H:C ratio (< 3 %).

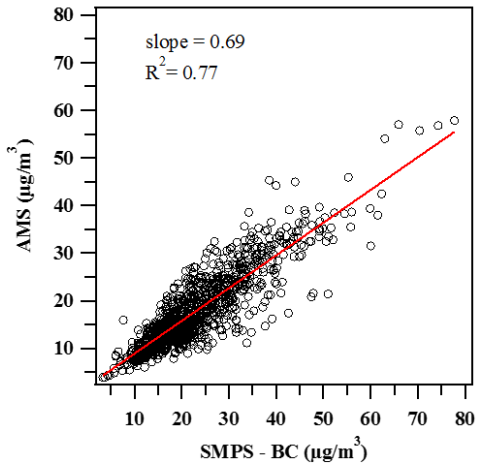

Figure 3-3. Scatter plot of NR-PM_1 concentration measured by AMS vs. particle mass concentration estimated from SMPS and BC measurements during the sampling period. Linear regression fit line, slope and R^2 are also shown.

During the sampling campaigns at the Hok Tsui site, most of the instrument settings remained the same and followed the same standard procedures described above. A RIE of 4.0 was assigned to ammonium based on the weekly periodic ionization efficiency calibration. The ionization efficiency (IE) at m/z 30 and m/z 46 was calibrated using pure ammonium nitrate particles with a size of 350 nm. An air flow calibrator (Drycal DC-Lite) was used to calibrate the sampling flow rate. Particle velocity was calibrated using Nanosphere PSL particles (Duke Scientific, Palo 120 Alto, CA, USA) with sizes of 50, 100, 200, 300, 400, 500 and 600 nm. By comparing the AMS NR-PM_1 with PM_1 minus black carbon measured by the HKEPD, we determined the collection efficiency (CE) as 0.73 (Figure 3-4). The CE factor was applied to all the measured PM_1 components. Particle-free ambient air was sampled through an inline HEPA-filter for ~60 minutes every 2-3 days to obtain the background concentrations, which were subtracted from the ambient data and used to calculate the method detection limits (MDLs). The MDLs were 0.211, 0.022, 0.020, 0.013, and 0.013 µg/m^3 for organics,

sulfate, nitrate, ammonium and chloride, respectively.

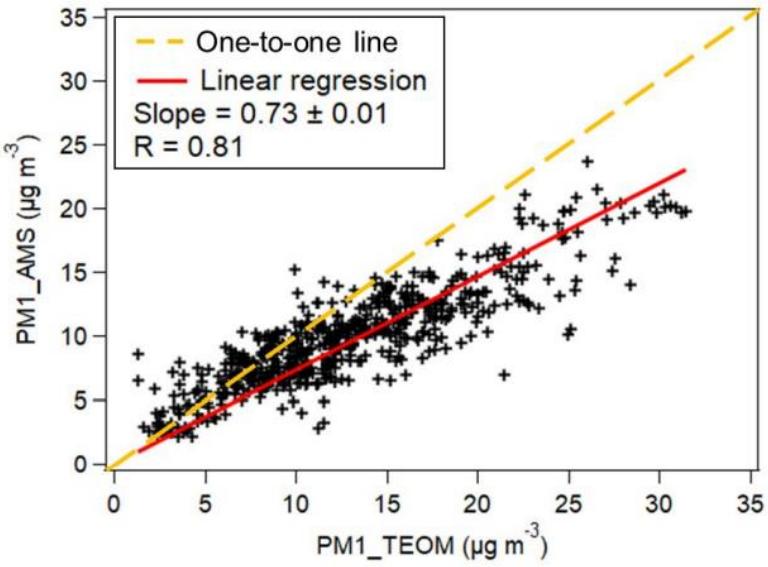

Figure 3-4. Linear regression between PM_1 measured by AMS (PM_1_AMS) and TEOM (PM_1_TEOM). Concentration of black carbon is deducted from PM_1_TEOM.

3.2.3 Other measurements

During the sampling period at a roadside site at PolyU, trace gases including CO, O_3, NO and NO_2 were continuously monitored. CO was measured with a gas filter correlation CO analyser (API model 300 EU). NO–NO_2–NO_x was measured by chemiluminescence technique (API model 200E), and an UV photometric analyzer (API model T400) was used to monitor O_3 mixing ratio. The detection limits for CO, NO, NO_2 and O_3 were 40, 0.5, 0.5 and 2.0 ppbv, respectively. All the instruments were regularly calibrated and tested with quality control and assurance (QC/QA) procedures identical to those in the US air quality monitoring program (Wang et al., 2017). Meteorological parameters including temperature, relative humidity (RH), wind speed, wind direction, atmospheric pressure and solar radiation were measured using a weather

station (Vantage Pro2TM, Davis Instruments Corp., Hayward, CA) installed on the rooftop of a container that hosted all the gas analysers. The time-resolution of the measurements was one minute, which were integrated into hourly data.

During the sampling campaigns at Hok Tsui, criteria air pollutants, nitric oxide (NO) and meteorological parameters were monitored by the HKEPD. Details about the measurements can be found in previous studies (Lyu et al., 2020; Tan et al., 2021). All the instruments were regularly calibrated following the QC/QA protocol identical to that adopted by the US air quality monitoring program (Lyu et al., 2020). The molecular makers of OA used in this study were measured by an online Thermal-desorption Aerosol Gas-chromatograph coupled with time-of-flight mass spectrometry (TAG). Details about the measurement and data processing have been provided in Lyu et al. (2020). Volatile organic compounds (VOCs) were measured using a proton transfer reaction mass spectrometry (Tan et al., 2021). During the sampling period, the average ambient temperature, relative humidity and wind speed were 22.5 ± 0.1 °C (mean ± 95 confidence interval, the same elsewhere), 79.9 ± 0.8 % and 4.6 ± 0.1 m/s, respectively. The prevailing winds were easterly and northeasterly. All data were consolidated into hourly averages for further analysis, except for TAG data. In these campaigns, TAG was run at a resolution of 1.5 hours per sample in 2018 and 2 hours per sample in 2020 sampling campaign. Wherever TAG data were used, other data with higher time resolution were averaged over the TAG sample intervals to match.

3.3 Model configuration

3.3.1 Positive Matrix Factorization (PMF) model

High-resolution MS data for organics were analyzed using the PMF2 algorithm in robust mode (Paatero and Tapper, 1994) with the PMF Evaluation Toolkit (PET ver 2.05) (Ulbrich et al., 2009). A minimum error value was applied to the error matrix, and each ion was assessed and processed according to its signal-to-noise ratio (SNR). Ions with an average SNR of less than 0.2 were removed, and those with a SNR between 0.2 and 2 were down-weighted by increasing their errors by a factor of 2. Furthermore, the errors for ions related to m/z 44 (i.e., CO_2^+, CO^+, H_2O^+, HO^+, and O^+) were also increased by 2-3 folds to reflect the influences of CO_2^+. Isotopes were removed from the matrices, because their signals were scaled to their parent ions rather than being measured directly. The application of PMF in this work and the discussion of the results are presented in later chapters.

3.3.2 Estimation of liquid water content

The liquid water content (LWC) in PM_1 was calculated using the Extended AIM Aerosol Thermodynamics (E-AIM) Model, which was developed for characterization of the gas/liquid/solid partitioning in aerosol systems (http://www.aim.env.uea.ac.uk /aim/aim.php). In this study, the E-AIM IV (Wexler and Clegg, 2002; Friese and Ebel, 2010) was used, where the inorganic composition of PM_1 measured by HR-ToF-AMS, temperature and relative humidity were input into the model. The average LWC during the sampling campaign at Hok Tsui in November 2018 was 10.4 ± 0.6 μg/m^3, comparable to the previously reported level of 12.8 μg/m^3 in autumn in Hong Kong (Li et al., 2013; Qin et al., 2016). It should be noted that organic compounds were not considered in the calculation of LWC values in this study. One reason is that we did not have observational data for these organics during these sampling campaigns, and

another reason is that the range of organics in the E-AIM model generally does not significantly affect LWC values calculated based on ambient datasets. Details were discussed in Chapter 5.2.

Chapter 4 Characteristics, sources and evolution processes of atmospheric organic aerosols at a roadside site in Hong Kong

4.1 Introduction

Atmospheric particulate matters (PM) affect climate change (Racherla et al., 2006; Tai et al., 2010) and pose a threat to public health (Dockery et al., 1993, Pope and Dockery, 2006). In the atmosphere, organic aerosol (OA) accounts for a large fraction (20-90%) of the submicron particulate mass. OA contains primary organic aerosol (POA) from direct emissions of various anthropogenic and natural sources, and secondary organic aerosol (SOA) formed in the atmosphere from gas-phase precursors. The characteristics and evolution of aerosol pollution are affected by multiple factors such as photochemistry, meteorological parameters and regional transport, in addition to local sources that vary from location to location (Hu et al., 2017). To formulate appropriate control strategies, it is crucial to investigate the OAs in the atmosphere.

HR-ToF-AMS can provide information of aerosols with a temporal resolution of minutes, allowing us to understand the rapid changes and formation of aerosols in the real atmosphere (Ng et al., 2010; Hu et al., 2016). In addition, by combining the OA mass spectra gained from AMS high-resolution data with source receptor models, e.g., positive matrix factorization (PMF) model, the sources of OAs can be identified as POAs (e.g., hydrocarbon-like OA (HOA), cooking OA (COA)) and oxygenated OAs (OOAs) at each specific sampling site (Jimenez et al., 2009; Zhang et al., 2019). However, the proportion of each OA source to total organics varied at the same site as the POAs emissions were different and the OOAs could be formed locally or

transported regionally. Besides, POAs from vehicle exhaust (Chirico et al., 2010; Nordin et al., 2013; Gordon et al., 2014a, 2014b) and cooking activities (Klein et al., 2016; Liu et al., 2017a; Liu et al., 2018) can form SOA during photochemical aging. But these studies are mostly based on chamber experiments which cannot fully represent the real environment in the atmosphere. Hence, it is of great significance to quantify the contributions of primary emissions and secondary formation to OAs, and to further understand the formation mechanisms and the aging process of OAs in the atmosphere (Ulbrich et al., 2009; Hu et al., 2017).

Hong Kong, as a highly urbanized city in East Asia, has been influenced by PM pollution in the past decades (So et al., 2007; Cheung et al., 2015). Due to large number of on-road motor vehicles and poor quality of fuel, roadside PM pollution was ever severe (Guo et al., 2009; Huang et al., 2014). The PM levels at roadside have been significantly reduced in recent years after the implementation of a series of control measures by the local government (HKEPD, 2017). However, massive cooking emissions in urban Hong Kong has raised concerns (Lee et al., 2015; Lyu et al., 2017a). Moreover, air pollution in the adjacent Pearl River Delta (PRD) region aggravates the PM pollution in Hong Kong (Louie et al., 2005; Lyu et al., 2017b). In addition, these locally-emitted and regionally-transported air pollutants can be further oxidized into SOA during dispersion and transport, resulting in elevated PM values (Hu et al., 2010). Thus, understanding the sources and evolution processes of organic aerosols in Hong Kong remains a great challenge.

There were several OA studies using HR-ToF-AMS technique in Hong Kong (Li et al., 2013; Lee et al., 2015; Liu et al., 2017b), which helped us understand the sources in different seasons and locations. For instance, SOA dominated (~80 %) the organic portion of NR-PM_1 in suburban area, while POA accounted for two thirds in urban

roadside area (Li et al., 2013; Lee et al., 2015). To investigate the aging processes of OAs in the atmosphere in Hong Kong, Qin et al., (2016) summarized the episode events at a suburban site and examined the photochemical evolution of aerosols during the events. They found that the less oxidized OA was clearly transformed to higher oxidized OA at the later stage of photochemical aging. Liu et al. (2019) investigated in-situ SOA formation from urban roadside air in Hong Kong in winter using an oxidation flow reactor (OFR) and highlighted the importance of potential SOA formation from vehicle and cooking emissions. Although a study reported that the contribution of cooking to OA and POA exceeded that of vehicle emissions at a roadside site in Hong Kong (Lee et al., 2015), the evolution processes from massive cooking emissions is still elusive and needs in-depth investigation. Therefore, it is essential to understand the dynamic and chemical processes of aerosol evolution in the atmosphere, especially for the aerosols from cooking emissions in urban Hong Kong.

In this chapter, a HR-ToF-AMS together with other online instruments for real-time measurements of particulate pollutants was deployed from 2 November to 13 December 2017 at an urban roadside site in Hong Kong. The abundance, variations and size distributions of chemical components in NR-PM_1 were firstly investigated. The characteristics and sources of OAs were then explored. Finally, the evolution processes of OA at the roadside site were elaborated. Specifically, the characteristics and evolution processes of OA, particularly COA, during high PM episode events were investigated. The findings are helpful for us to better understand the PM pollution in the roadside environment.

4.2 General characteristics of aerosols in the roadside environment

4.2.1 Temporal variations of air pollutants

The day-to-day variations and average mass concentrations of the composition of NR-PM_1 are shown in Figure 4-1 ((a)-(b)). The hourly NR-PM_1 concentration ranged from 5.6 to 82.6 μg/m^3 with an average of 26.1 ± 0.7 μg/m^3 (average ± 95 confidence interval). For each bulk composition in NR-PM_1, their concentrations varied greatly while their temporal variations presented similar trends. Organics was the most dominant component ranging from 3.4 to 55.8 μg/m^3 with an average of 15.1 ± 0.4 μg/m^3, accounting for 57.7 ± 0.2% of all the measured components. Sulfate ranked the second with an average mass concentration of 5.8 ± 0.2 μg/m^3 and an average percentage of 23.1 ± 0.2%. The concentrations of nitrate and ammonium were similar, with an average of 2.8 ± 0.2 μg/m^3 and 2.3 ± 0.1 μg/m^3, respectively. The average mass concentration of chloride was the lowest among all components, which was 0.2 ± 0.01 μg/m^3 over the entire sampling period.

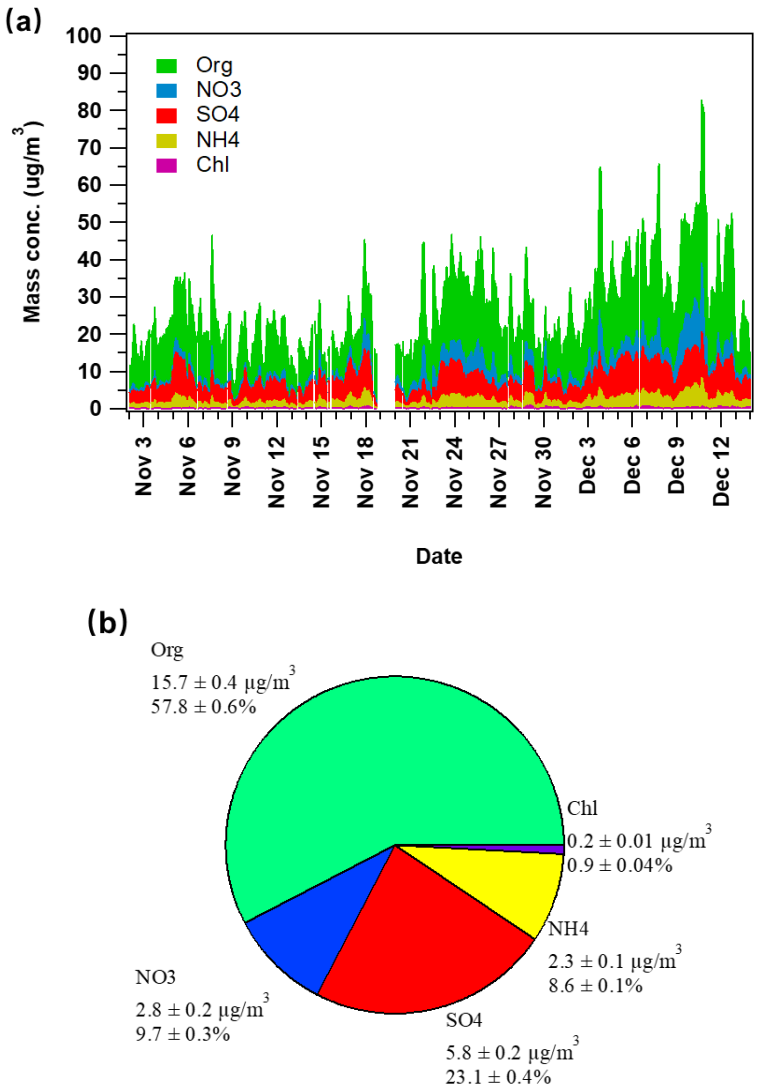

Figure 4-1. Day-to-day variations (a) and average composition (b) of NR-PM_1 components

The variations of hourly meteorological parameters are shown in Figure 4-2. The average ambient temperature, RH, wind speed, atmospheric pressure and daily maximum solar radiation were 22.6 ± 0.2 ℃, 70.2 ± 0.8 %, 0.5 ± 0.02 m/s, 1017 ± 0.2

bar and 442.6 ± 65.3 W/m^2, respectively. The overall weather conditions during the sampling period were relatively stable, with only two short showers recorded. The dominant wind was a low-speed northeasterly wind, which brought in air pollutants from nearby areas.

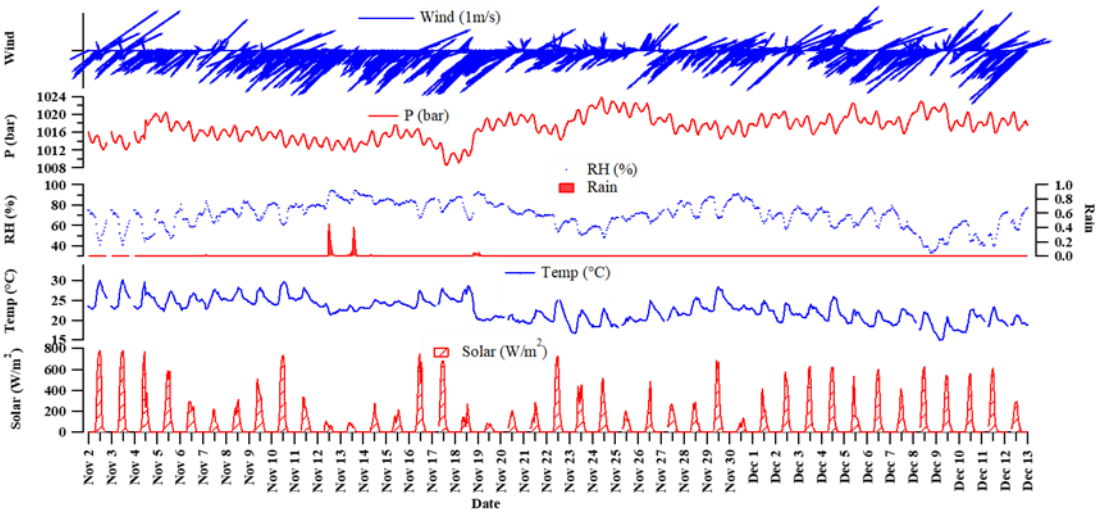

Figure 4-2. Time series of weather conditions during the sampling period

The NR-PM_1 concentrations measured by AMS during this sampling campaign were compared with previous studies conducted in Hong Kong. It was found that the levels of NR-PM_1 in this study were higher than the values at other suburban and roadside sites in Hong Kong in winter, spring and/or summer (Lee et al., 2015; Li et al., 2015; Liu et al., 2019), but analogous to the levels found in autumn and early winter in Hong Kong (Sun et al., 2016), implying that this study site was more strongly affected by anthropogenic emission sources and/or weather conditions. Compared to the values of Liu et al. (2019) at this same sampling site, which was performed one month later than our study, the concentrations of NR-PM_1 were indeed higher in this study. Vehicular emissions did not have significant seasonal differences at this roadside site as the traffic

volumes counted each month were similar (HKATC, 2017). A main reason for this difference was the weather conditions. In this study, our sampling period was in late autumn and early winter, while the study period in Liu et al. (2019) was mainly in winter. The weather in Hong Kong was gloomy and rainy in winter as a cold front over southern China moved across the coastal areas of Guangdong at the beginning of January. The formation of secondary pollutants, such as the oxidation from POA to SOA, might be limited by the colder weather. Furthermore, the stronger northerly winds more readily diluted the air pollutants in the atmosphere of Hong Kong during the sampling campaign in Liu et al. (2019).

The diurnal variations of NR-PM_1 and the compositions are shown in Figure 4-3. The diurnal patterns of NR-PM_1 and total organics were similar (Figure 4-3 (a) – (b)), with the highest peak at 19:00 and two small peaks at 9:00 and 14:00, implying possible contributions of local traffic and/or cooking activities. Relatively flat diurnal cycle was observed for sulfate (Figure 4-3 (d)), due to the regional characteristics of sulfate aerosol (Sun et al., 2015). The diurnal patterns of nitrate, ammonium and chloride (Figure 4-3 (c), (e) – (f)) were similar, with a trough at noon and in early afternoon, and a peak in the evening (19:00 – 20:00), consistent with the previously-observed daytime evaporation of semi-volatile species (Li et al., 2015). In addition, higher boundary layer heights in the midday and afternoon favored the dispersion of air pollutants, resulting in lower concentrations during the day. Furthermore, the lower ambient temperature at night promoted gas–particle partitioning of semi-volatile species (Hu et al., 2017).

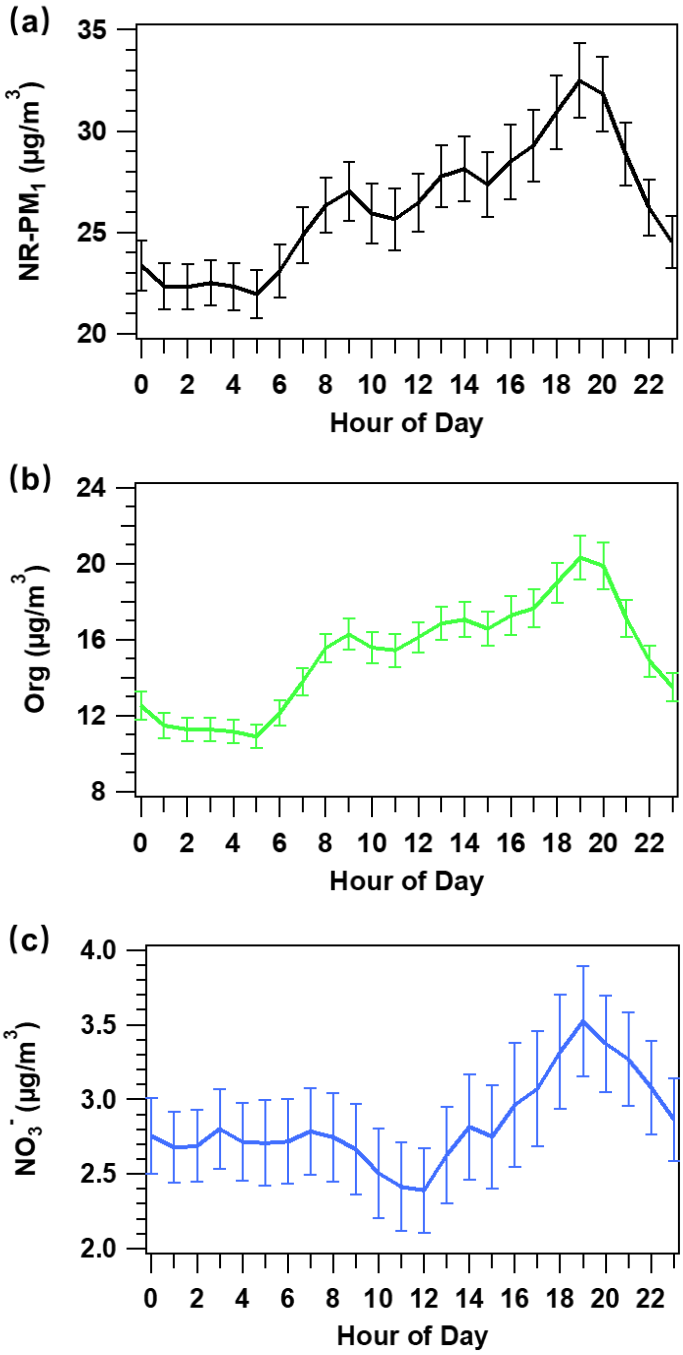
(a)
NR-PM1 (µg/m3)
35
30
25
20
0 2 4 6 8 10 12 14 16 18 20 22
Hour of Day
(b)
Org (µg/m3)
24
20
16
12
8
0 2 4 6 8 10 12 14 16 18 20 22
Hour of Day
(c)
NO3- (µg/m3)
4.0
3.5
3.0
2.5
2.0
0 2 4 6 8 10 12 14 16 18 20 22
Hour of Day

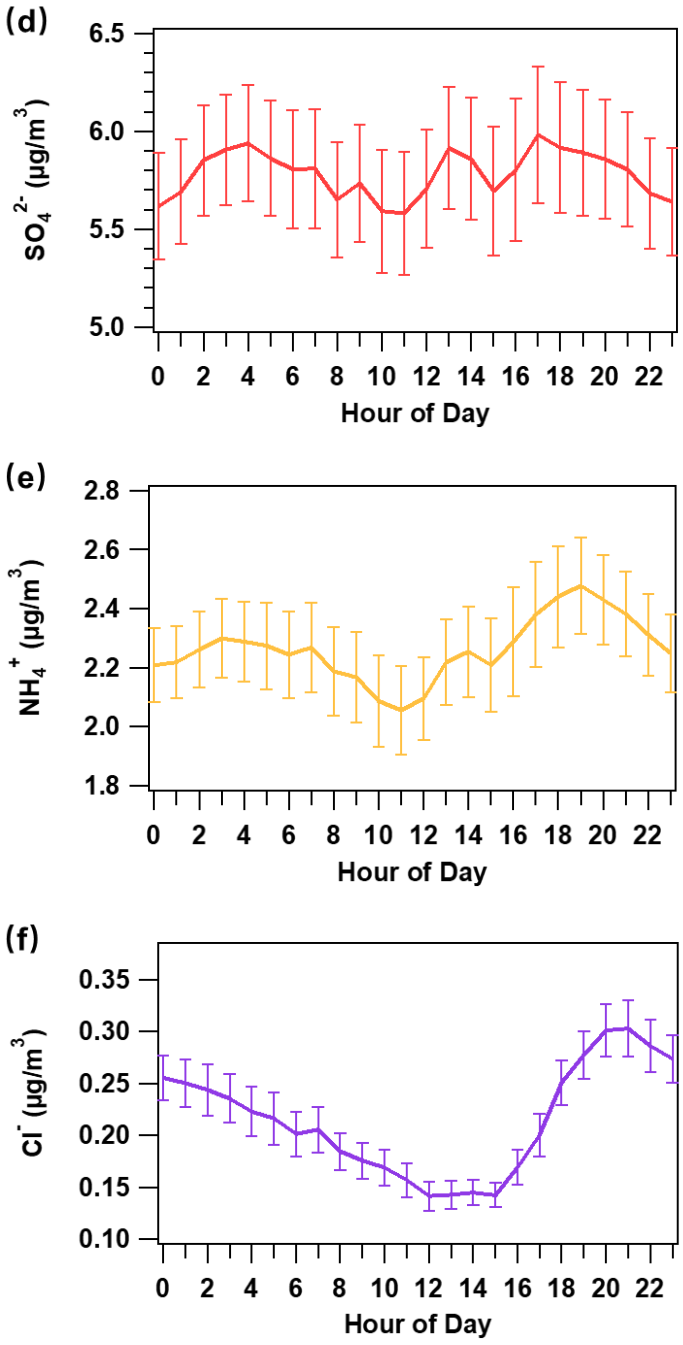

Figure 4-3. Diurnal variations of NR-PM_1 and the components

The diurnal variations of trace gases are presented in Figure 4-4 to further investigate the pollution characteristics in the roadside environment. Both NO and NO_2 showed a peak at 9:00, in accordance with the patterns of NR-PM_1 and total organics, revealing intensive vehicle emissions at this site. It was noted that the NO level in the evening rush hours was much lower than that in the morning. This was associated with the distinct traffic flow characteristics of vehicles in the cross-harbor tunnel, which was highest in the morning rush hour and relatively stable during the rest of the day (HKATC, 2017). In contrast, the diurnal patterns of NR-PM_1 and total organics showed peaks in the evening, especially during dinner time. Thus, the enhancements of NR-PM_1 and total organics in the evening were unlikely related to vehicular emissions but other sources such as cooking activities, which will be further discussed in Sections 4.3 and 4.4. Due to the titration effect of NO on O_3, the O_3 levels were low with an obvious trough in the morning traffic hours at this typical roadside site. In addition, the increase in NO_2 levels in the afternoon also partially implied the conversion from NO titration. The CO levels at this site were relatively stable, mainly due to less regional transport of air masses to the site. The diel cycle of CO experienced a trough around noon as the boundary layer height increased and vehicular emissions decreased during this period.

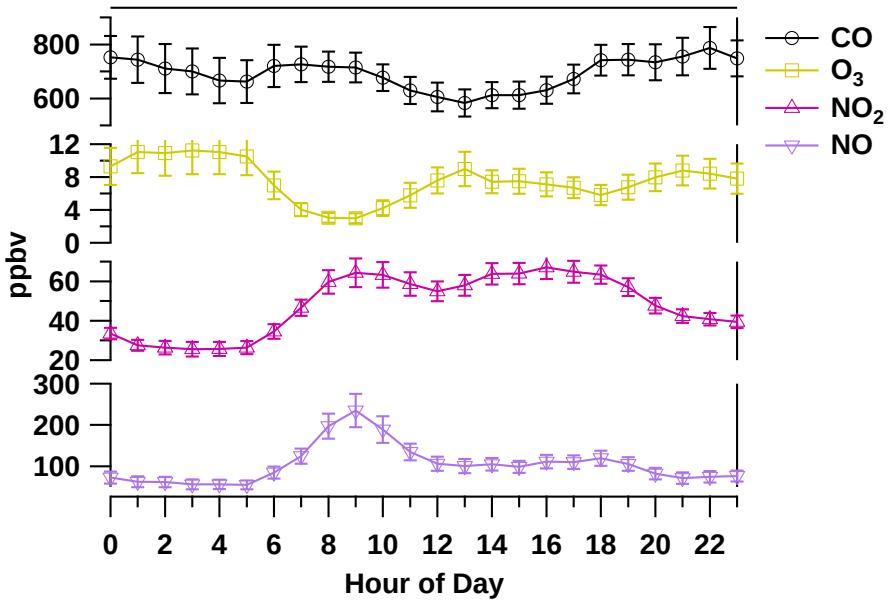

Figure 4-4. Diurnal variations of trace gases during the sampling period

4.2.2. Size distributions of NR-PM$_1$ components

The size distributions of bulk compositions of NR-PM$_1$ are shown in Figure 4-5 (a). All the measured non-refractory components peaked at ~600 nm in vacuum aerodynamic diameter (D_{va}), which suggested that these particles were most likely internal mixtures of the organic and inorganic components (Lee et al., 2015). Furthermore, the total organics exhibited a clear shoulder at 100–200 nm which might be caused by fresh organic aerosols of primary origin. Figure 4-5 (b) presents the size distributions of specific organic ions, i.e. all ions at m/z 43 (mostly $C_3H_7^+$), m/z 44 (mostly CO_2^+), m/z 55 (mostly $C_4H_7^+$ and $C_3H_3O^+$) and m/z 57 (mostly $C_4H_9^+$ and $C_3H_5O^+$). These specific ions were selected as they had remarkable peaks in the spectra. It was found that hydrocarbon-like organics (m/z 43, 55, 57) had higher concentrations at sizes of 100–200 nm than m/z 44 (p<0.01). The small peaks of these typical ions were also found in previous studies, indicating a large contribution of hydrocarbon-like organics from

primary emissions such as traffic to the total organics (Canagaratna et al., 2010; Sun et al., 2011).

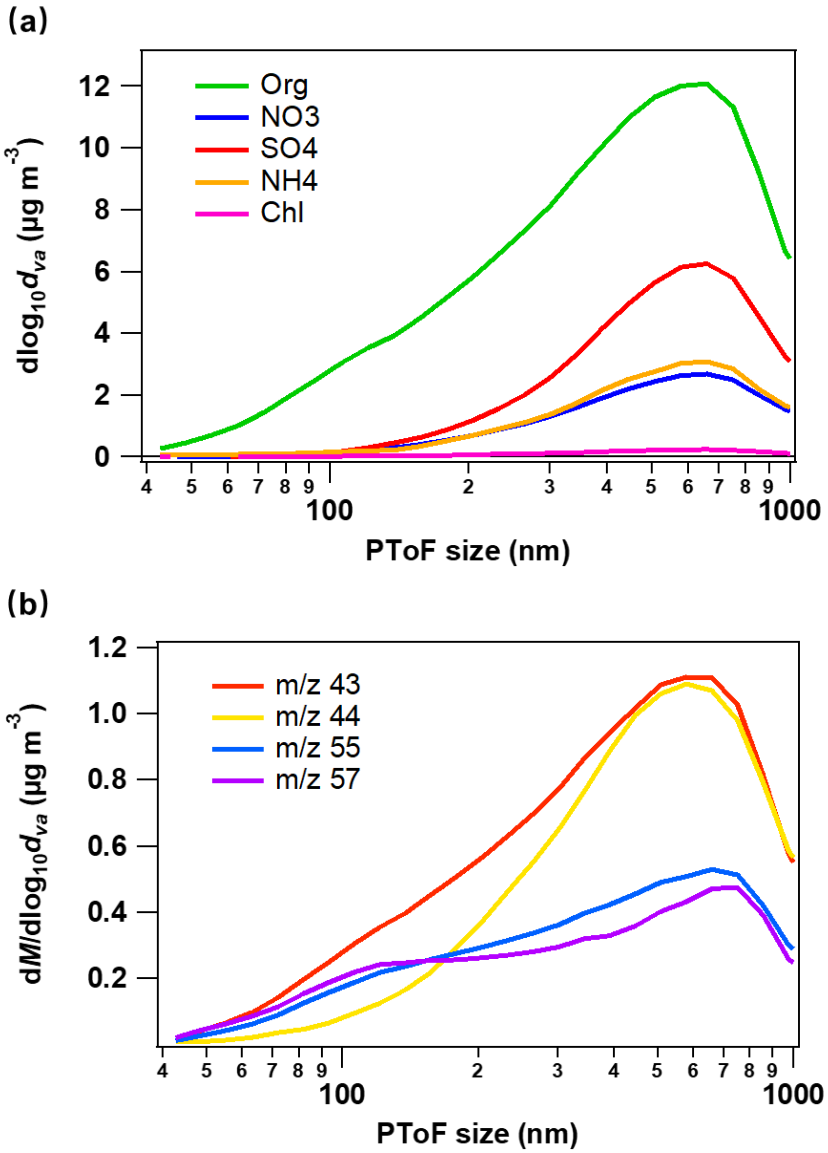

Figure 4-5. Size distributions of bulk compositions (a) and specific m/z ions (b)

The hydrogen-to-carbon molar ratios (H:C) and oxygen-to-carbon molar ratios (O:C) are often used to estimate the average carbon oxidation state (OS_C) and to evaluate the

degree of oxygenation of organics. Based on the measurements of H:C and O:C ratios, the OS_C value can be simply calculated as 2 × O:C – H:C, which more accurately captures the degree of oxidation of organics than the O:C ratio (Kroll et al., 2011). Figure 4-6 shows the diurnal patterns of elemental ratios in this study. The average organic mass to organic carbon ratios (OM:OC), O:C and H:C ratios were 1.77 ± 0.01, 0.47 ± 0.01 and 1.69 ± 0.01, respectively. These values were comparable with the H:C (1.4 – 1.9) and O:C ratios (0.2 – 0.8) previously measured at urban roadside sites in Hong Kong, perhaps due to the similar types of emission sources at these sites (Lee et al., 2015; Liu et al., 2019). The H:C ratio was low in the evening, had a morning peak at 9:00-10:00 with a value of 1.79 ± 0.02, and then decreased with time until 21:00 when a small evening peak appeared, suggesting more intensive primary emissions (e.g. traffic and cooking) in these peak hours and photochemical oxidation of organics in the afternoon and/at dusk, which were proved by the opposite diurnal trend of the O:C ratio; namely troughs at 9:00-10:00 and 21:00 and increase in the afternoon and at dusk. The dramatic decrease of POA emissions at night led to a higher proportion of secondary OA, resulting in the highest O:C ratio from 1:00 to 6:00. Meanwhile, OS_C showed an evening peak and an afternoon peak, with an average of -0.76 ± 0.02 during the whole sampling period.

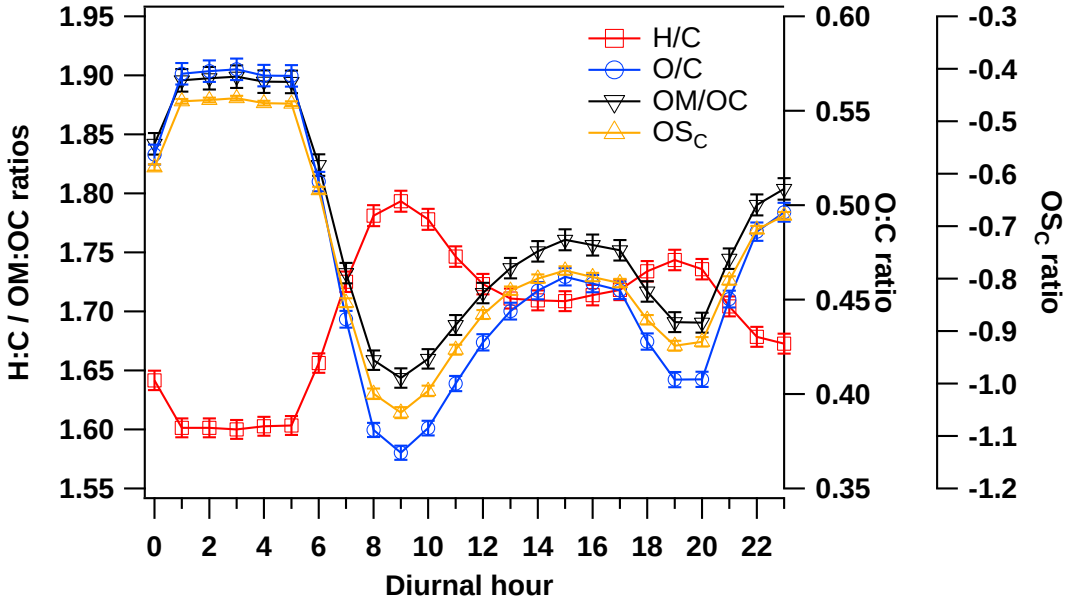

Figure 4-6. Diurnal patterns of OM:OC, H:C, O:C and OS_C ratios.

4.3 Source apportionment of OAs in the roadside environment

4.3.1 Source identification

In order to obtain physically meaningful results, several criteria were used to evaluate and select appropriate number of factors from model simulation in this study (Ulbrich et al., 2009; Zhang et al., 2011; Kim et al., 2017). Figure 4-7 (a) shows the Q/Q_{exp} values for factors 1-6. The Q/Q_{exp} values decreased with the increase of number of factors, and the possible optimal solution should be 6 or more factors. However, when the source profiles of 5 factors are compared (Figure 4-7 (b)), it was found that the two OOA factors had similar spectra and close elemental ratios. In addition, after consideration of the elucidation of the mass spectra of OAs, the ability of 5 factors or more to explain the data was not improved compared to 4 factors. Hence, the result of 4 factors was the most optimal solution. The rotational ambiguity of the optimal solution was examined by the FPEAK value, which ranged from -2 to 2. The uncertainty of each factor was estimated by 50 bootstrapping runs, and the average factor with 1σ variation for each point is shown in Figure 4-7 (c). It is noteworthy that Liu et al. (2019) identified 5 factors at the same site for the campaign, which started 11 days after the campaign in this study. The reason for this difference was that the OA levels and atmospheric oxidative capacity during this sampling period were generally higher. As such, the less oxidized OA factor with the lowest contribution in Liu et al. (2019) was not identified in this study. The similar diel cycles of the four factors in our study to the rest factors in Liu et al. (2019) showed the consistency and reliability of the results, which will be further discussed in section 4.3.2.

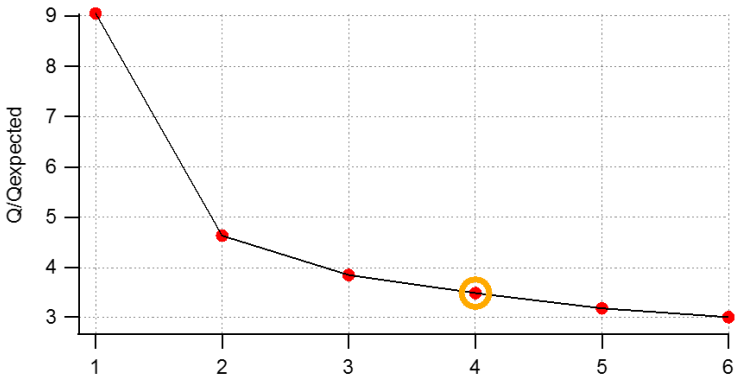
Q/Qexpected
9
8
7
6
5
4
3
1
2
3
4
5
6

(a)

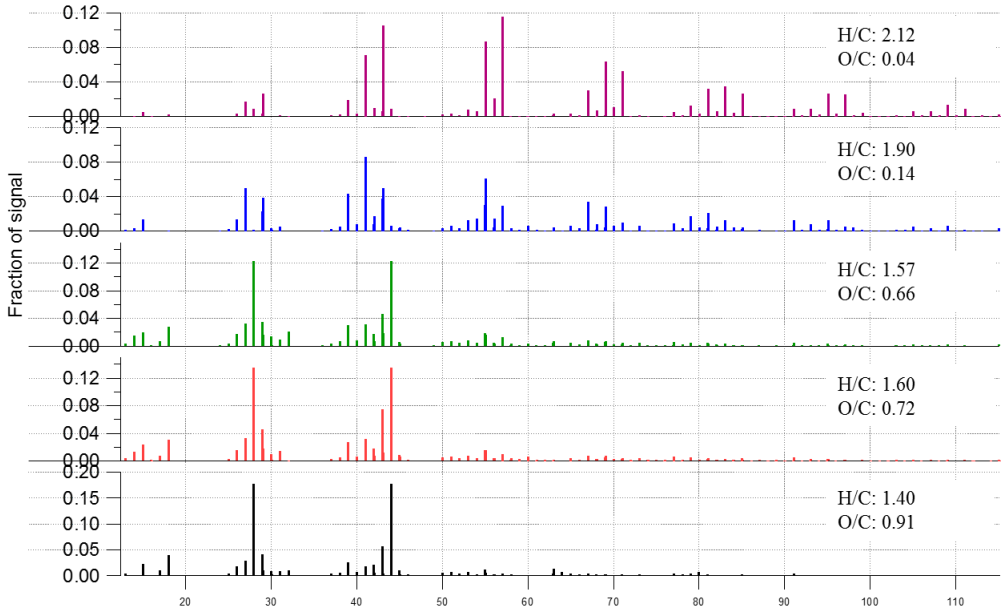
Fraction of signal
H/C: 2.12
O/C: 0.04
H/C: 1.90
O/C: 0.14
H/C: 1.57
O/C: 0.66
H/C: 1.60
O/C: 0.72
H/C: 1.40
O/C: 0.91
0.12
0.08
0.04
0.00
0.20
0.15
0.10
0.05
20
30
40
50
60
70
80
90
100
110

(b)

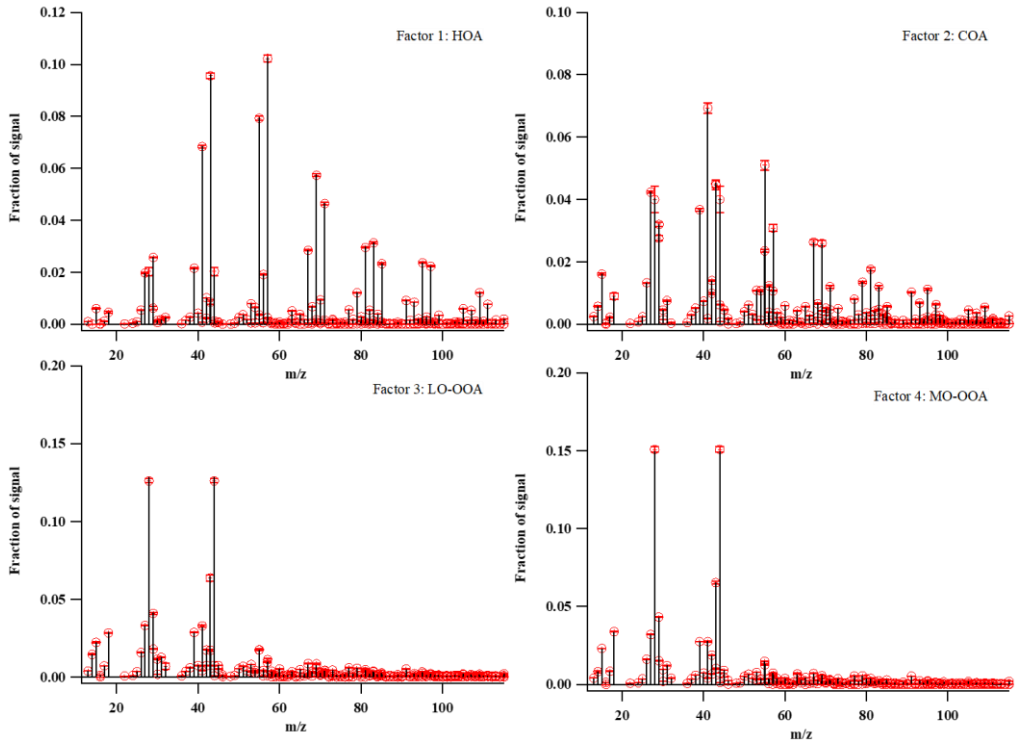

(c)

Figure 4-7. Q/Qexp values for PMF-resolved factors 1-6 (a) Source profiles of 5 factors (b) Results from bootstrapping analysis of the 4-factor solution (c).

In this study, four OA factors were determined, including two POA factors (HOA and COA) and two SOA factors (less oxidized oxygenated OA (LO-OOA) and more oxidized OOA (MO-OOA)). The mass spectra of the four identified factors are shown in Figure 4-8. Table 1 gives the H:C, O:C and OM:OC ratios of the MO-OOA, LO-OOA, COA and HOA factors.

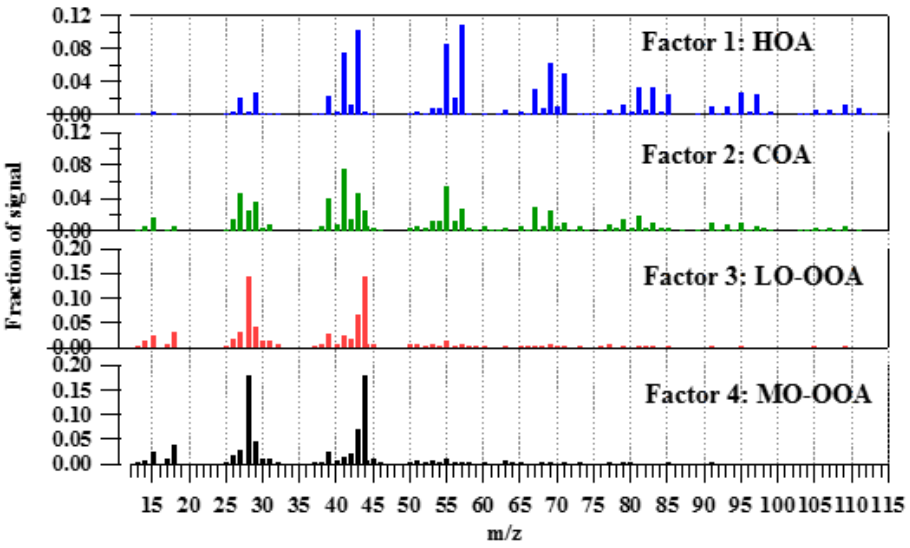

Figure 4-8. Sources profiles of the four factors

Table 1 Elemental ratios of the four factors

	HOA	COA	LO-OOA	MO-OOA
H:C	2.10	1.88	1.53	1.40
O:C	0.03	0.22	0.78	0.97
OM:OC	1.22	1.45	2.18	2.41

Alkyl fragments ($C_nH_{2n+1}^+$ and $C_nH_{2n-1}^+$) made a substantial contribution to the HOA factor. The major peaks of HOA mass spectrum were m/z 41, 43, 55 and 57, which were mostly composed of $C_3H_5^+$, $C_3H_7^+$, $C_4H_7^+$ and $C_4H_9^+$ ions, respectively. These major peaks and the overall abundant alkyl fragments are the typical features of the HOA spectra. This fragmentation pattern was similar to that reported in other studies and was mainly due to the primary aerosols emitted from fossil fuel combustion (Zhang

et al., 2005; Lanz et al., 2008; Ng et al., 2011; Sun et al., 2011). Because of the dominance of chemically-reduced hydrocarbon species, HOA factor had the highest H:C ratio (average: 2.10), and conversely the lowest O:C (0.03) and OM:OC (1.22) ratios. The oxidation degree of the HOA in this study was comparable to the updated values of HOA (O:C ratio: 0.05–0.25) from other studies (Canagaratna et al., 2015). The relatively low O:C ratio was mainly due to the intensive primary emissions from vehicle exhausts at this roadside site.

To a lesser extent, the mass spectrum of COA factor in this study also contained many alkyl fragments. However, this factor had significantly larger amounts of oxygen-containing ions than HOA. While COA shares similar spectra to HOA, it is identified by a high contribution of $C_3H_3O^+$ at m/z 55, and a much lower contribution of ions at m/z 57 than HOA (Mohr et al., 2009; Mohr et al., 2012). Previous studies found that $C_3H_3O^+$ and $C_3H_5O^+$ are in COA as they are the major fragments of aliphatic acids (e.g., linoleic acid and palmitic acid) in cooking oils or animal fat (Sun et al., 2011). It was also reported that $C_5H_8O^+$ (m/z 84) and $C_6H_{10}O^+$ (m/z 98) are the typical tracers in COA (Lee et al., 2015; Kim et al., 2017). Figure 4-9 ((a)-(h)) shows the scatter plots of COA and HOA with the cooking tracers ($C_3H_3O^+$, $C_3H_5O^+$, $C_5H_8O^+$and $C_6H_{10}O^+$). It was obvious that the COA concentration had much better correlations than HOA with these four cooking tracers, confirming that the second source was COA. Despite primary origins for both factors, COA was more oxidized than HOA because it contained some oxidizing components as discussed above. Therefore, the O:C (0.22) and OM:OC (1.45) ratios of COA were higher than those of HOA while the H:C ratio was lower (1.88). Besides, Xu et al. (2018) revealed that COA may include contribution of other OA such as sesquiterpene SOA. In this study, there was almost no biogenic emissions and other sources except vehicular and cooking emissions around the

sampling site, which would exclude the interference from biogenic emissions and other sources. In fact, relatively weaker correlation between COA source and the tracer of biogenic emissions, i.e. $C_5H_6O^+$ at m/z 82 was identified (Figure 4-10), confirming that COA was less interfered by other OAs at this site.

In this study, the two identified OOA factors had less alkyl fragments and more oxygenated species than the HOA and COA. The mass spectra of the two OOAs were characterized by a dominant peak at m/z 44 (CO_2^+), similar to the OOA profiles determined in other studies (Lanz et al., 2007; Ulbrich et al., 2009; Sun et al., 2010, 2011). To distinguish these two OOA factors, it was found that the third factor had a lower fraction of m/z 44 (f44) and less oxidation degree (O:C = 0.78, H:C = 1.53) than the fourth factor (O:C = 0.97, H:C = 1.40). As such, Factor 3 was characterized as LO-OOA while Factor 4 was defined as MO-OOA.

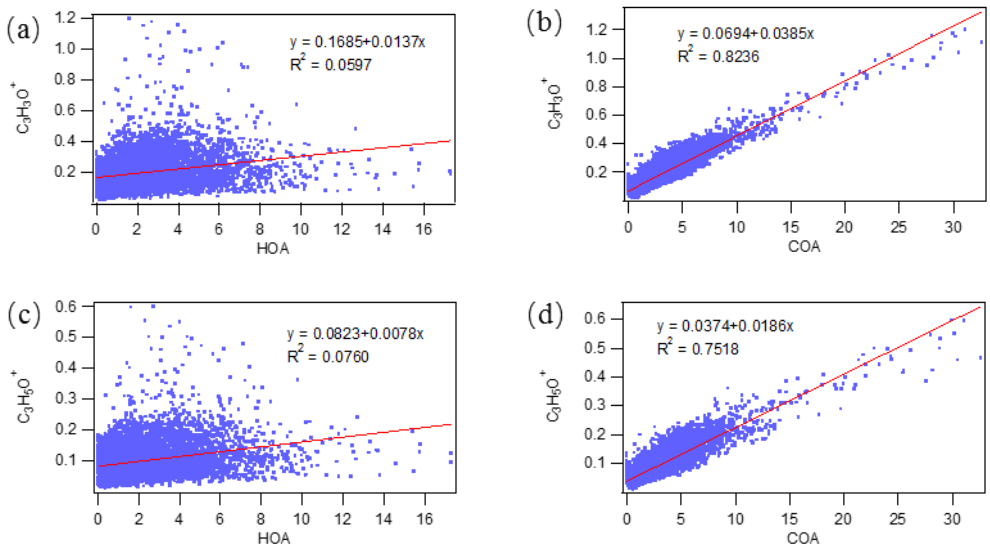

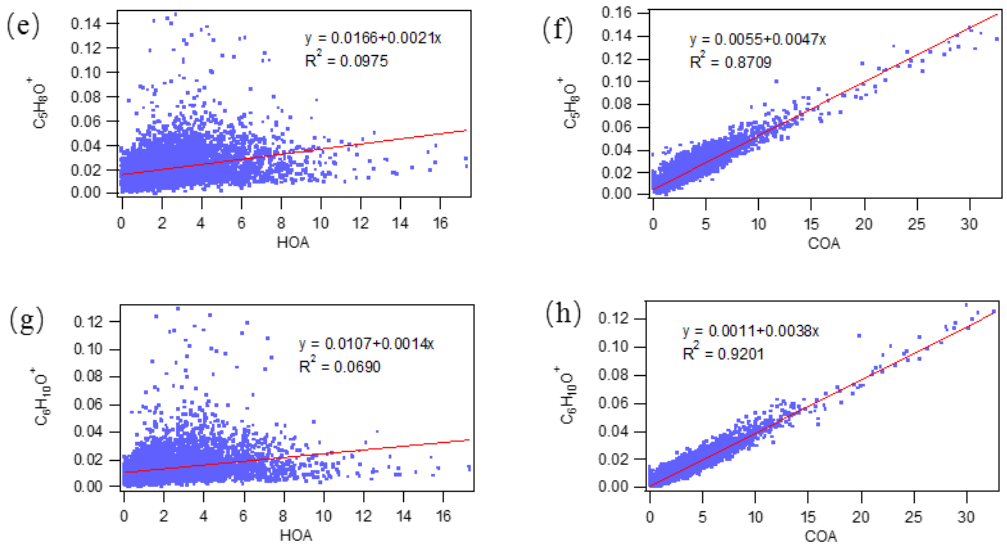

Figure 4-9. Scatter plots between (a) HOA and $C_3H_3O^+$, (b) COA and $C_3H_3O^+$, (c) HOA and $C_3H_5O^+$, (d) COA and $C_3H_5O^+$, (e) HOA and $C_5H_8O^+$, (f) COA and $C_5H_8O^+$, (g) HOA and $C_6H_{10}O^+$, (h) COA and $C_6H_{10}O^+$.

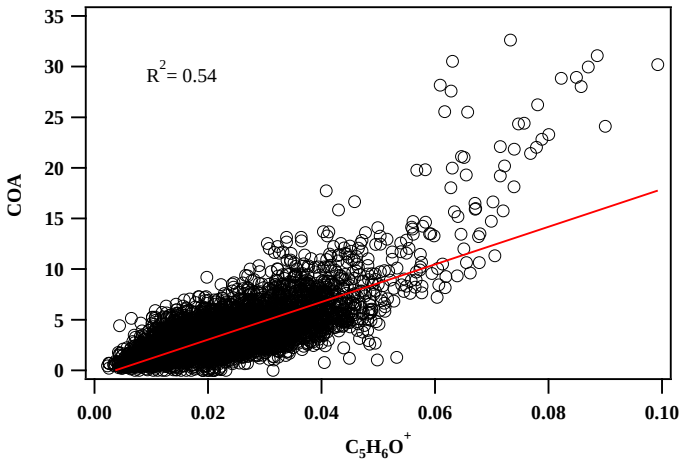

Figure 4-10. Scatter plots between COA and $C_5H_6O^+$

4.3.2. Source contributions

Figure 4-11 presents the contribution of each identified source to OAs in both absolute concentration and percentage. Surprisingly, although this roadside site was proximity to intensive vehicular sources, the contribution of MO-OOA was the highest, followed by COA and LO-OOA, while the contribution of HOA was the lowest. The SOA sources (LO-OOA+MO-OOA) contributed more than the POA sources (COA+HOA), which is consistent with the result of Liu et al. (2019) who collected data at the same site, implying possibly prompt oxidation of OAs and/or high regional background at the roadside site. Moreover, the contribution of LO-OOA was lower than MO-OOA ($p < 0.01$), suggesting high oxidation degree and/or high regional background in the roadside environment. More striking feature was that the contribution of COA was even higher than that of HOA ($p < 0.01$) at this site with very high-density passing vehicles and very few restaurants nearby. This phenomenon implied that the control of vehicular emissions might be efficient while the COA-containing air was full of the urban environment including the roadside environment in Hong Kong.

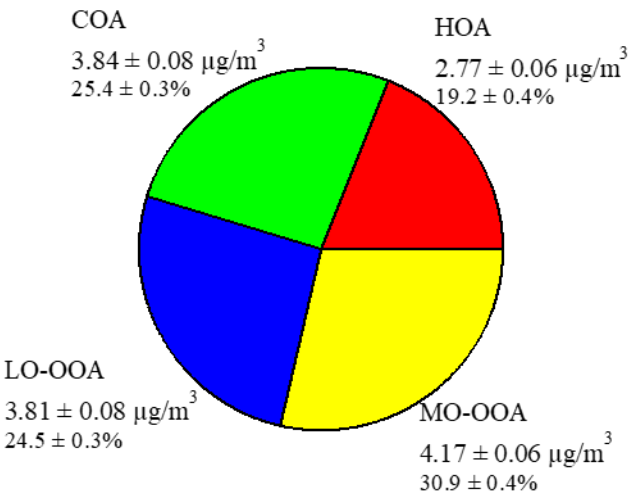

Figure 4-11. Source contributions of four sources to OAs.

Our previous studies found that volatile organic compounds (VOCs) emitted from diesel-fuelled and LPG-fuelled vehicles have dropped during these years due to the control measures in Hong Kong (Lyu et al., 2016, 2017a; Yao et al., 2019), whereas VOCs from gasoline-fuelled vehicles have shown an increasing trend. However, these studies did not measure OAs. Instead, OAs were measured in 2013 at an urban roadside site, i.e. Mong Kok (MK). Similar to the study site, the MK site is also a typical urban roadside site with heavy traffic and minimal biogenic emissions. In comparison, the HOA concentration at MK (2.7 μg/m^3, Table 4-2) was comparable to that in this study (2.8 ± 1.9 μg/m^3) in the same season (autumn and early winter). The comparable HOA values at the roadside sites in different years seemed contradictory to the results of the previous studies, which claimed the efficiency of control measures for vehicular emissions. However, if we looked deeper into the HOA values and considered the traffic volume at MK and at the Cross-Harbor tunnel, we found that the HOA level associated with each vehicle indeed decreased twice from 2013 to 2019, because the average daily traffic of the main road (Nathan Road) immediately next to the MK site was ~50,000, much less than the traffic volume of ~114,000 at the Cross-Harbor tunnel (HKATC, 2017). In addition, it was found that regardless of the season and sampling location, the level of COA was always higher than that of HOA, which further indicated that cooking emissions were more dominant than vehicle emissions even in heavy traffic locations (Table 4-2).

Table 2 HOA and COA levels in urban roadside environments in Hong Kong (mean ± standard deviation)

Time	Sampling time	Site	HOA concentration (μg/m^3)	COA concentration (μg/m^3)	COA proportion
Nov. - Dec. 2017, This study	24h	PolyU	2.8 ± 1.9	3.8 ± 2.9	25.4 ± 1.0
	Mealtime	PolyU	3.0 ± 1.4	5.8 ± 4.0	33.5 ± 10.6

Mar. - May 2013 (Lee et al., 2017)	24h	MK	3.5 ± 2.4	4.4 ± 4.3	34.4
May - Jul. 2013 (Lee et al., 2017)	24h	MK	2.0 ± 1.3	3.6 ± 3.4	46.2
Mar. - Jul. 2013 (Lee et al., 2015)	24h	MK	2.8	4.0	38.6
Sep. - Dec. 2013 (Sun et al., 2016)	24h	MK	2.7	3.6	24.2
	Mealtime	MK	3.2	7.8	36.9

Regarding the diurnal variations of the contributions of the four sources, the HOA source showed a high peak at 9:00 and a small peak at 17:00-18:00 (Figure 4-12), analogous to the pattern of NO due to road traffic. Similarly, two peaks were found for COA source with a small peak at 12:00-13:00 and a big peak at 20:00 (8.2 ± 0.8 μg/m^3). The contrary pattern of NO and similar variations of NR-PM$_1$ and total organics (Figure 4-3) to the COA source in the evening, which is in line with the dinner time in Hong Kong (Lee et al., 2015; Vu et al., 2018), supported the identification of the COA source.

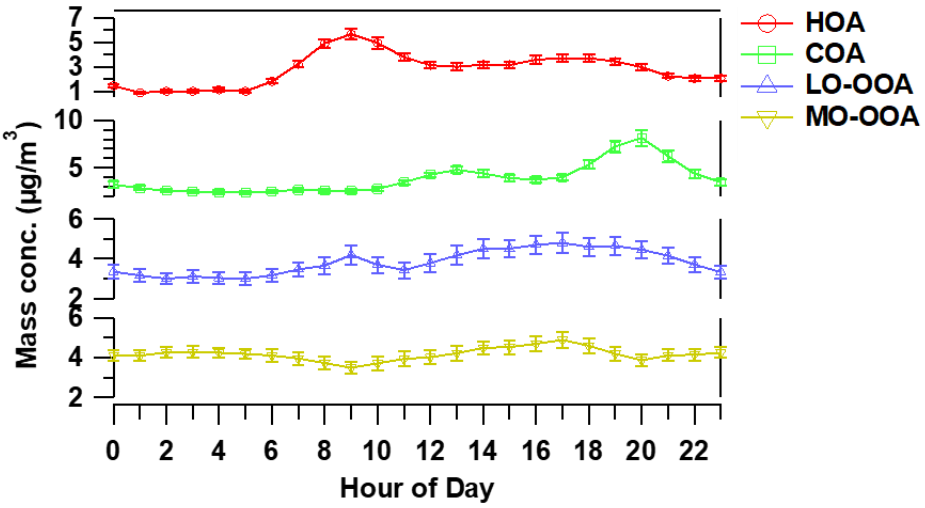

Figure 4-12. Diurnal patterns of the four OA sources.

To further clarify the cooking emissions at this site, the diurnal pattern of oleic acid, a typical tracer of cooking activities (Schauer et al., 2002; Zhao et al., 2007), measured at PolyU (~300 m away from the sampling site) is shown in Figure 4-13. It was clear that the peak value appeared at 20:00, consistent with the diurnal variation of COA source, confirming the intensive cooking emissions during the dinner time in urban Hong Kong. Furthermore, the LO-OOA source presented a bimodal distribution with a peak at 9:00 and another broad peak at 17:00-18:00, which was coincidently opposite to the O_3 pattern, indicating immediate morning formation of LO-OOA from HOA of vehicular exhausts and progressive oxidation in the afternoon (Sun et al., 2016). However, the MO-OOA source was relatively constant throughout the day, inconsistent with the patterns of all the trace gases in Figure 4-4, confirming high regional background value of this source.

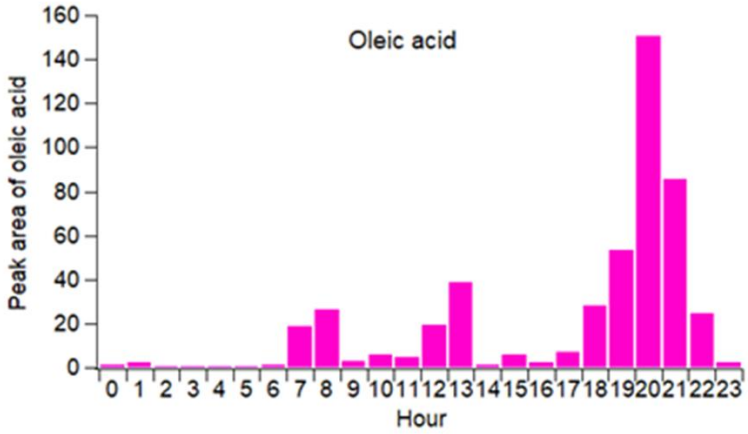

Figure 4-13. Diurnal variations of oleic acid measured at PolyU.

The variations of the percentages of individual sources in the sum of PMF-resolved OAs are shown in Figure 4-14. It was found that the percentage of COA increased with the increase of total PMF-resolved OAs, implying that COA was the major contributor when OA levels were high. HOA showed the same pattern as COA but its increasing

rate was much lower than that of COA. In contrast, the percentage of MO-OOA decreased while LO-OOA remained stable.

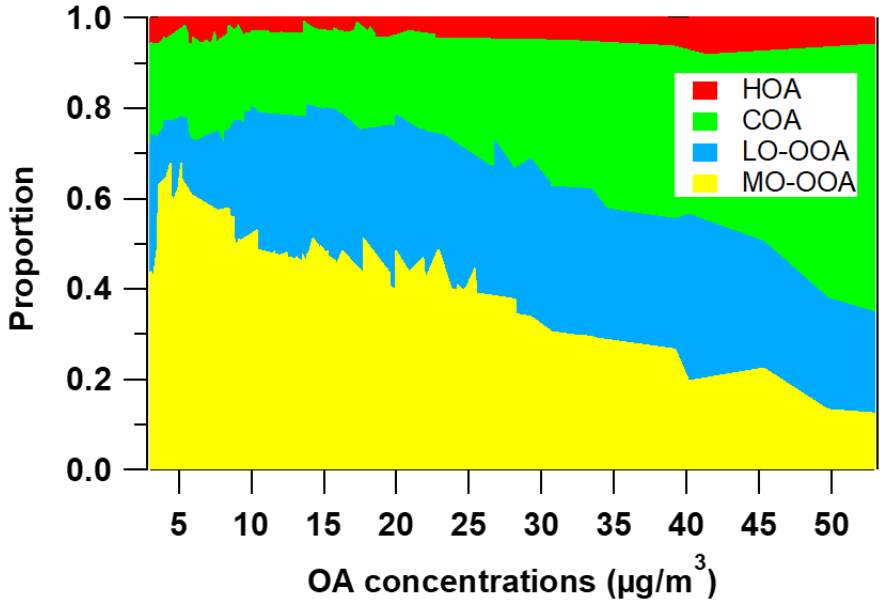

Figure 4-14. Percentage variations of individual sources in the sum of PMF-resolved OAs. The values of the x-axis represent the hourly OA concentrations measured.

To further investigate the HOA and COA sources, the diurnal trends of them on Saturday, Sunday and weekdays are given (Figure 4-15). A much higher HOA morning peak was found on weekdays and Saturday ($p < 0.01$), whereas COA presented a much higher evening peak on Sunday ($p < 0.01$), consistent with the fact that there are much fewer on-road vehicles and much more Hong Kong residents like to have dinner at restaurants on Sunday (Chan, 2010). Indeed, the contribution of COA on Sunday to the overall COA concentration reached 22.3% in this study. Moreover, the COA levels were much higher than the HOA concentrations ($p < 0.01$). Although it is difficult to differentiate the emissions from restaurants from those from domestic cooking due to

lack of survey data, we can infer that emissions from restaurants were much higher on Sunday than on other days, and most likely larger than domestic cooking emissions from the big difference in peak values of COA on Sunday (~15 μg/m^3) and on the other days (~6 μg/m^3) (Figure 4-15). The results suggested that cooking activities particularly in restaurants are a noticeable source of OAs in Hong Kong and much more efforts should be made to control it apart from remediation of vehicular emissions.

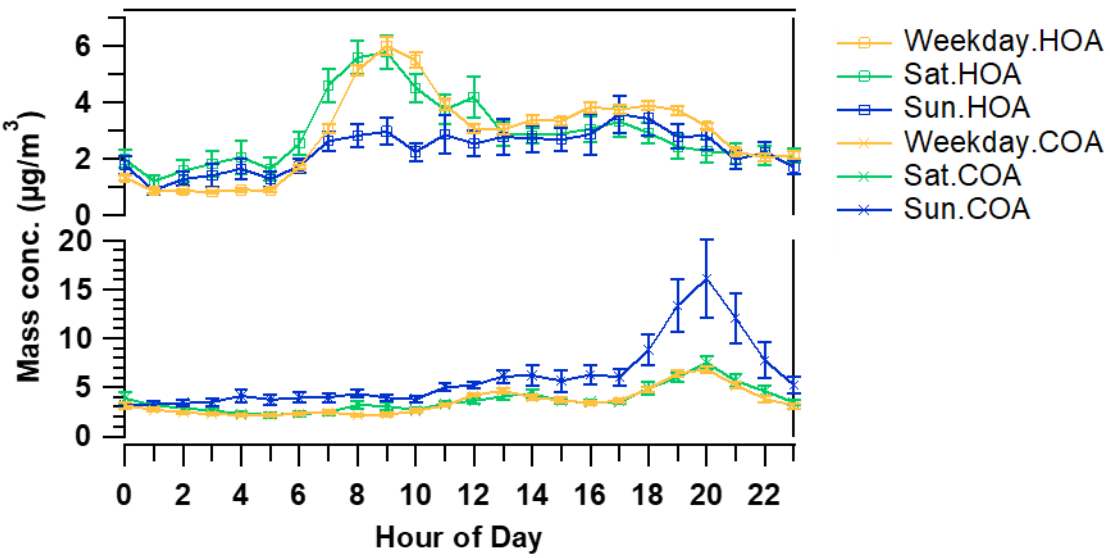

Figure 4-15. Diurnal patterns of HOA and COA on Saturday, Sunday and weekdays.

4.4 Evolution of OA sources

To study the evolution of a specific OA source, typical ions are usually chosen as tracers because they were directly measured by the instrument. Long straight-chain fatty acids, including unsaturated (*e.g.* oleic acid and linoleic acid) and saturated (*e.g.* palmitic acid and stearic acid), are unique markers for cooking emissions as they are from oils during cooking processes (He et al., 2004; Zhao et al., 2007). Based on the source profile of measured COA (Mohr et al., 2012), $C_3H_3O^+$ at m/z 55 and $C_3H_5O^+$ at m/z 57 were

chosen as the proxy of unsaturated fatty acids and saturated fatty acids, respectively. In section 4.3, we also found the strong correlations of these ions with COA factor. Besides, ion CO_2^+ at m/z 44 was regarded as the typical tracer of OOA as it had strong correlations with the OOA sources (R > 0.9). The diurnal patterns of $C_3H_3O^+$, $C_3H_5O^+$ and CO_2^+ are shown in Figure 4-16 (a). The diel cycles of $C_3H_3O^+$ and $C_3H_5O^+$ were the same as that of COA source (Figure 4-16 (a)), confirming their common source of cooking emissions. Different from $C_3H_3O^+$ and $C_3H_5O^+$, CO_2^+ presented a broad peak starting from 10:00 and maximizing at 17:00, suggesting the photochemical oxidation of OAs in the atmosphere.

To further look into the oxidation of OAs at this roadside site, the diurnal patterns of $C_3H_3O^+$/ $C_3H_5O^+$ ratio and total oxidant (O_x = O_3 + NO_2) are illustrated in Figure 4-16 (b). The ratio of $C_3H_3O^+$ / $C_3H_5O^+$ was used to elaborate the oxidation degree of cooking emissions in the atmosphere, because unsaturated fatty acids (*i.e.* $C_3H_3O^+$) have shorter lifetime than saturated fatty acids (*i.e.* $C_3H_5O^+$), which means that unsaturated fatty acids are photochemically destroyed more rapidly than saturated fatty acids, leading to decline of $C_3H_3O^+$ / $C_3H_5O^+$ ratio. Although these two fragmentation ions are not completely derived from fatty acids, the ratio of $C_3H_3O^+$ / $C_3H_5O^+$ can be used as an indicator to investigate the potential evolution processes of COA due to the differences in saturation level. Besides, the level of O_x was used to characterize the atmospheric oxidative capacity (Clapp and Jenkin, 2001). The diurnal variation of $C_3H_3O^+$ / $C_3H_5O^+$ ratio showed one peak at 13:00 (2.04 ± 0.01) and another at 20:00 (2.17 ± 0.01), in consistence with that of cooking emissions. Clearly, during the daytime hours, the ratio of $C_3H_3O^+$ / $C_3H_5O^+$ showed opposite trend to that of O_x, proving the evolution of cooking emissions in the atmosphere. However, the reversed pattern was not observed in the evening even though the cooking emissions reached the highest,

reflecting that the nighttime chemical evolution of cooking emissions on average was insignificant. In addition, the average ratio of $C_3H_3O^+$ / $C_3H_5O^+$ during the whole sampling period was 2.01 ± 0.01, much lower than the ratio of oleic acid/stearic acid (4.8) of the cooking source (Zhao et al., 2007), implying that COA was oxidized to some extent during the transport to the site. Furthermore, the average O_x level during the sampling period was 56.0 ± 1.4 ppbv, analogous to the values (55.9 ± 3.4 ppbv) at another roadside site in Hong Kong (Yao et al., 2019). Previous studies reported that COA could be oxidized in an hour under a moderate O_3 level (Kaltsonoudis et al., 2017). The reversed daytime patterns of $C_3H_3O^+$ / $C_3H_5O^+$ and O_x in this study confirmed this hypothesis, especially in the afternoon when the photochemical reactions were generally strong. The results demonstrated that the COA emitted elsewhere was progressively oxidized, leading to enhanced OOA at this roadside site.

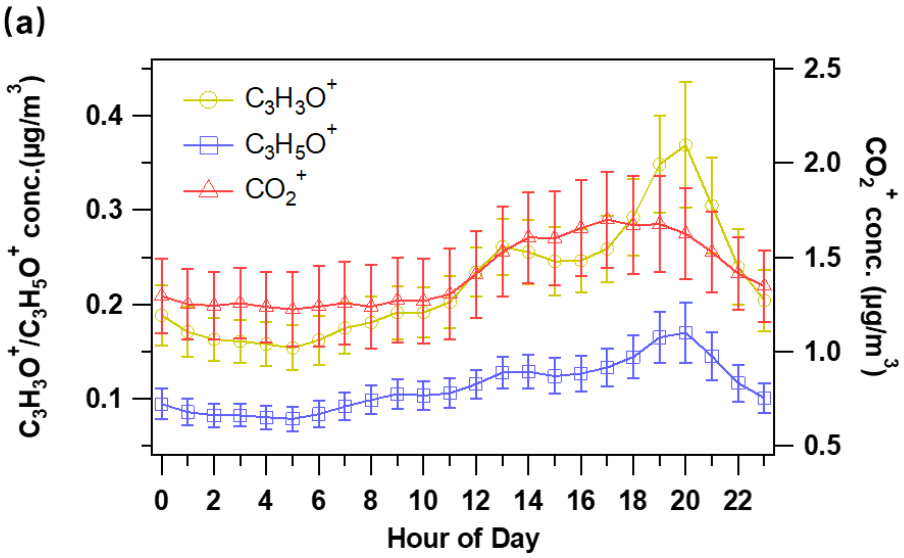

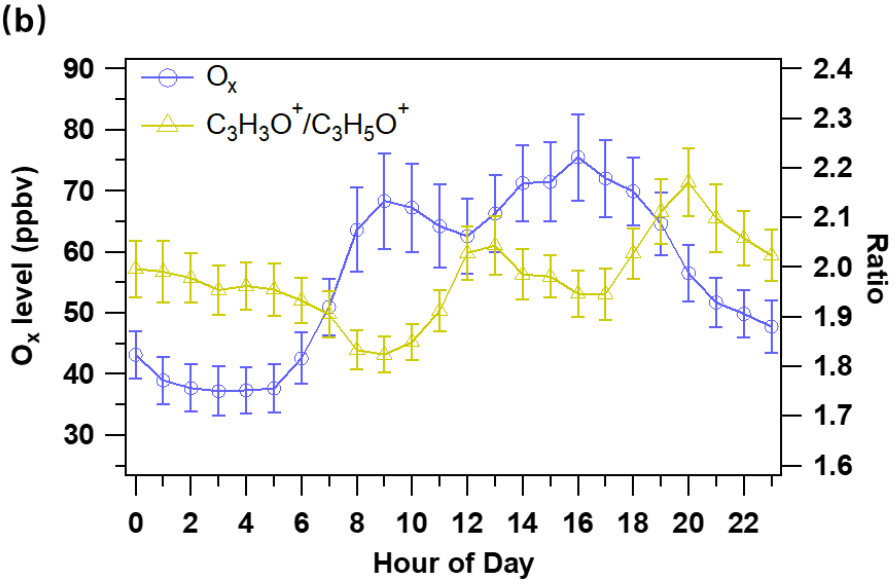

Figure 4-16. Diurnal variations of $C_3H_3O^+$, $C_3H_5O^+$ and CO_2^+ (a) and ratio of $C_3H_3O^+$ / $C_3H_5O^+$ and O_x (b) during the whole sampling period

4.5 Summary

In this chapter, an intensive sampling campaign was conducted for six weeks at a roadside site in Hong Kong. HR-ToF-AMS and trace gas analyzers (*i.e.*, CO, O_3 and NO-NO_2-NO_x) were used to collect data simultaneously to investigate and understand the characteristics, sources and evolution processes of OAs in the roadside environment. Results showed that the average NR-PM_1 concentration was 26.1 ± 0.7 μg/m^3 and OA contributed the most to NR-PM_1 with the proportion of 57.7 ± 0.2%. The aerosol size distributions of all measured NR-species showed an accumulation mode peaked at around 600 nm while there were more primary organics at < 200 nm. PMF analysis identified four OA components (HOA, COA, LO-OOA and MO-OOA), and the proportion of COA was 25.4 ± 0.3%, even higher than that of HOA (19.2 ± 0.4%) at this traffic-busy site. The COA concentration reached the highest value at 20:00 with an average of 8.2 ± 0.8 μg/m^3. Especially on Sundays, the average maximum COA concentration was 16.1 ± 3.0 μg/m^3. Furthermore, with the increase of PMF-resolved total OA concentrations, the proportion of COA increased. The ratio of $C_3H_3O^+$ / $C_3H_5O^+$ was used to elaborate the oxidation degree of cooking emissions in the atmosphere, and the daytime opposite trend of the ratio of $C_3H_3O^+$ / $C_3H_5O^+$ to that of O_x confirmed the evolution of cooking emissions in the atmosphere. This study concludes that cooking activities are an important source of organic aerosols in the urban areas of Hong Kong, and efforts should be made to control emissions from cooking and traffic.

Chapter 5 Secondary organic aerosol formation at an urban background site on the coastline of South China: precursors and aging processes

5.1 Introduction

Secondary organic aerosol (SOA) formation in the atmosphere is influenced by a number of factors, such as atmospheric oxidative capacity, precursors, reaction media, and meteorology (Hu et al., 2017; Xu et al., 2017; Brege et al., 2018; Paglione et al., 2020). Numerous studies have discussed the formation processes of OAs in the atmosphere (Young et al., 2015; Xu et al., 2017; Kim et al., 2018; Huang et al., 2020; Kanawade et al., 2020; Xiao et al., 2021). In China, Xu et al. (2017) studied the roles of photochemical oxidation and aqueous processes in altering the composition and oxidation degree of oxygenated OA (OOA) in Beijing. It was shown that the aqueous processes dominated the formation of the more oxidized OOA (MO-OOA). The consistent findings were reported by Xiao et al. (2021), who examined the joint effects of relative humidity (RH) and odd oxygen (O_x) on SOA formation. Huang et al. (2020) inspected the dependence of OOA components on O_x and LWC at a background site of the Yangtze River Delta region in summer. They found that the formation of OOA at a higher oxidation state was mainly driven by photochemical oxidation. Such discrepancies indicated that SOA formation mechanisms might not always be consistent. AMS has been extensively used to study the evolution of OA in the atmosphere (DeCarlo et al., 2010; He et al., 2011; Kim et al., 2017). However, based on AMS data alone, it is difficult to determine the precursors and specific formation pathways of SOA, as AMS cannot provide any molecular information. With the aid of other unambiguous

measurements, the interpretability of AMS data can be enhanced. For example, Xu et al. (2015) determined the isoprene-derived SOA based on the correlation with 2-methyltetrols and showed the mediation effect of sulfate on this component in the southeastern United States. Lyu et al. (2020) combined AMS data with SOA tracers measured by Thermal-desorption Aerosol Gas-chromatograph (TAG), and determined the formation processes of some anthropogenic SOAs at a regionally urban background site in Hong Kong. These findings indicated that our ability to capture the dynamic variations and evolution processes of OAs can be enhanced with comprehensive measurements in the atmosphere.

Hong Kong has suffered from PM pollution for decades (So et al., 2007; Lin et al., 2018). In addition to local sources, such as vehicular and cooking emissions (Lee et al., 2015; Yao et al., 2021), regional and even superregional transport can aggravate PM pollution in Hong Kong, especially in cool seasons (Wang et al., 2017; Lyu et al., 2020). The composition, sources and evolution of OAs in Hong Kong have been extensively studied (Li et al., 2013; Hu and Yu, 2013). Vehicular and cooking emissions made significant contributions (44.6% - 65.0%) to OA at urban roadside sites (Lee et al., 2015; Yao et al, 2021). Li et al. (2013) indicated that aqueous processes were likely responsible for the high degree of oxygenation for OA at an urban background site during the foggy period in spring. Qin et al. (2016) analyzed the evolution of OAs during PM episodes at the same site and identified the roles of photochemical oxidation and aqueous processes in SOA formation. With the filter-based measurement data, Hu and Yu (2013) deduced aqueous formation of malic acid through the oxidation of multiple precursors. Most of the previous studies (e.g., Li et al., 2013; Qin et al., 2016) aimed at understanding aqueous chemistry were conducted in spring, as Hong Kong has the highest relative humidity and cloud cover from March to June. However, photochemical pollution is the worst in this city in autumn, with ozone levels

significantly higher than many inland cities (Liu et al., 2021). Besides, transboundary transport brought aged air masses from mainland China to Hong Kong in cool seasons. Therefore, SOA formation in autumn merits investigation. Moreover, the AMS-based studies failed to identify the precursors of SOA, and low time resolution was an inherent defect of filter-based studies.

In this chapter, HR-ToF-AMS together with other on-line instruments was used for real-time measurements of NR-PM_1 composition at an urban background site, which was also a coastal site, in Hong Kong. The temporal variations of NR-PM_1 components and the sources of OA at this site are discussed. We focus on the formation mechanisms of two dominant OOA components. The study also sheds light on the potential precursors of OOA. The findings enhance understanding on the chemical evolution of OAs in urban background atmosphere and provide scientific basis for controlling OA pollution that is increasingly concerned.

5.2 General features of aerosols at the background site

The time series of the NR-PM_1 components and the average composition of NR-PM_1 are shown in Figure 5-1. The hourly concentration of NR-PM_1 ranged from 3.0 to 32.4 μg/m^3, with a mean of 13.5 ± 0.4 μg/m^3. The total concentration of organics was 6.0 ± 0.2 μg/m^3, varying between 1.1 μg/m^3 and 16.0 μg/m^3. The fraction of total organics (43.8 ± 0.7%) was followed by that of sulfate (35.8 ± 0.7 %), ammonium (14.4 ± 0.2 %), nitrate (5.4 ± 0.2 %) and chloride (0.7 ± 0.02 %), whose concentration was 4.7 ± 0.1, 1.9 ± 0.1, 0.8 ± 0.05 and 0.08 ± 0.01 μg/m^3, respectively. Mainly due to the lower emissions of POA at HT, the organics fraction was lower than that (>50%) at the urban roadside sites in Hong Kong (Lee et al., 2015; Yao et al., 2021). However, it was markedly higher than that (31%) at another background site (HKUST) about 14 km north of HT (Li et al., 2015). This was attributable to the lower concentrations of other PM_1 components at HT, because the concentrations of organics were comparable (6.0 ± 0.2 μg/m^3 at HT *vs.* 6.0 μg/m^3 at HKUST). In particular, the average concentration of sulfate was 7.4 μg/m^3 at HKUST, 57.4% higher than our observation at HT. Note that the HKUST measurement conducted in 2011 witnessed much higher mixing ratio of sulfur dioxide (3.4 ppbv), compared to the 1.2 ppbv observed at HT in 2018. Therefore, in this study, the lower level of sulfate was likely a result of the declining precursor. Despite the potential concentration reduction over time, the mass fraction of sulfate at HT was significantly higher than that (23.1 ± 0.4 %) measured at an urban roadside site in recent years (Yao et al., 2021). On one hand, regional transport might be partially responsible for the high levels of sulfate at this urban background site. On the other hand, the relatively high levels of relatively humidity (72.7 %) and atmospheric oxidative capacity (reflected by O_x of 49.8 ppbv) in the coastal area could facilitate aqueous formation of sulfate (Li et al., 2015). The aqueous chemistry is confirmed in

analysis of SOA formation mechanisms (chapter 5.3).

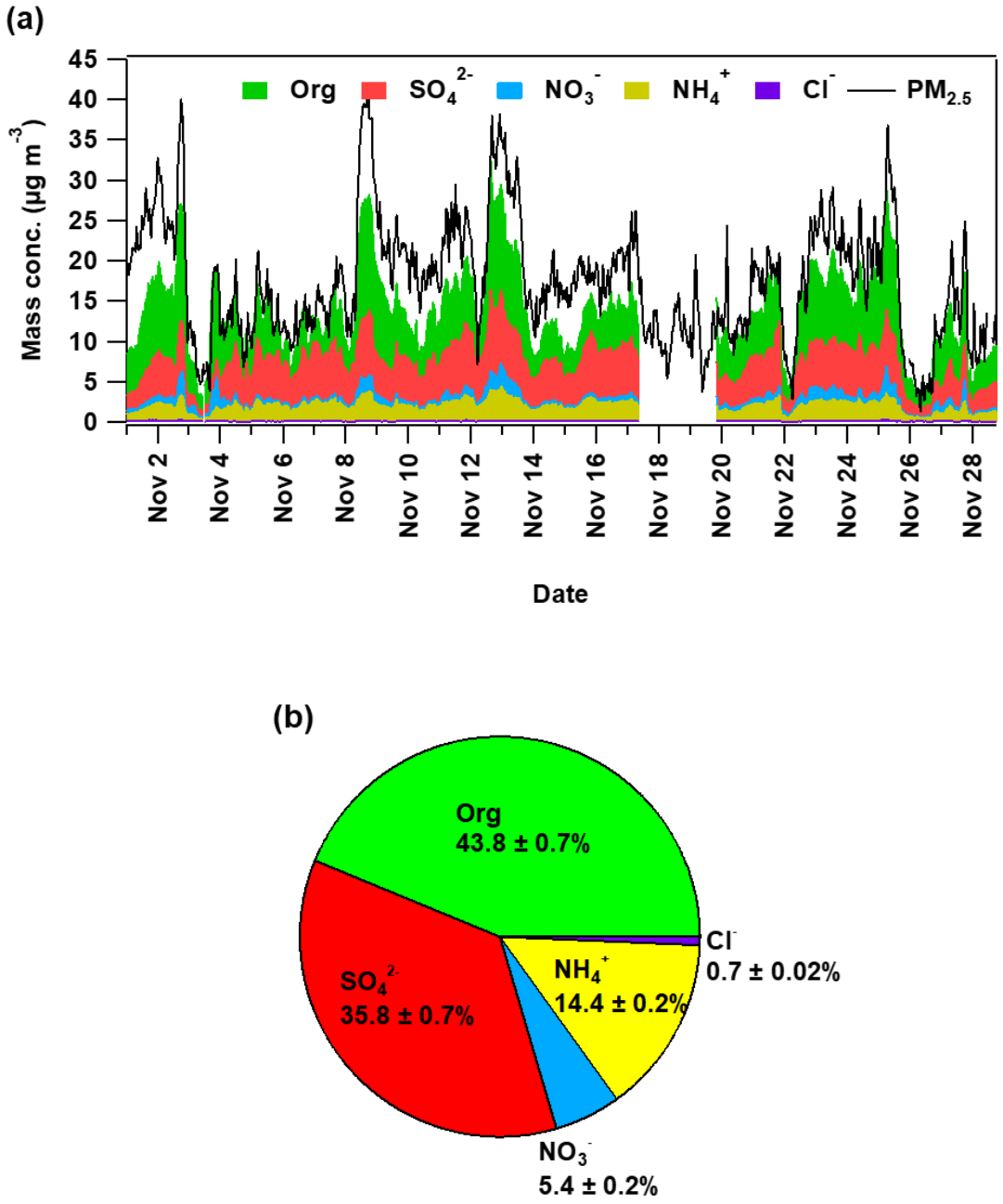

Figure 5-1. Time series of NR-PM_1 components and $PM_{2.5}$ (a); and average composition of NR-PM_1 at HT. Org: total organics, SO_4^{2-}: sulfate, NO_3^-: nitrate, NH_4^+: ammonium, Cl^-: chloride.

Figure 5-2 shows the time series and diurnal patterns of the calculated LWC, temperature and relative humidity during the sampling period. The average LWC during this sampling period was 10.4 ± 0.6 μg/m^3, comparable to the previously reported level of 12.8 μg/m^3 in autumn in Hong Kong (Li et al., 2013; Qin et al., 2016). While the variation of LWC resembled the pattern of relative humidity, the correlation between them was moderate (r^2 = 0.52), mainly due to the influence of water-soluble ions.

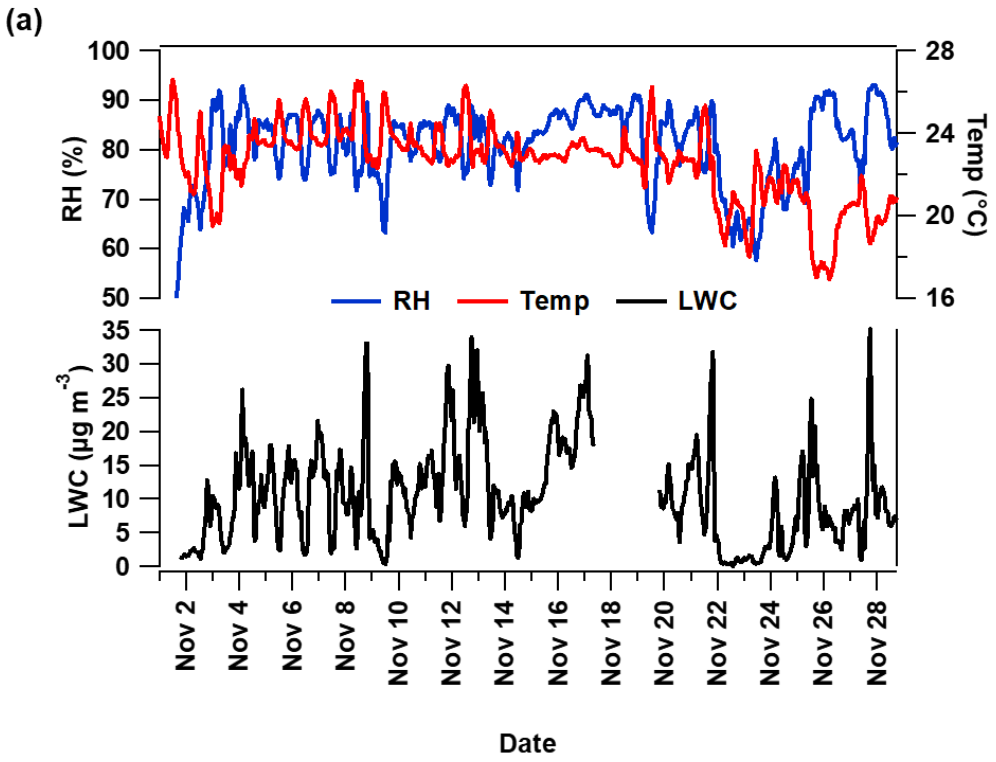

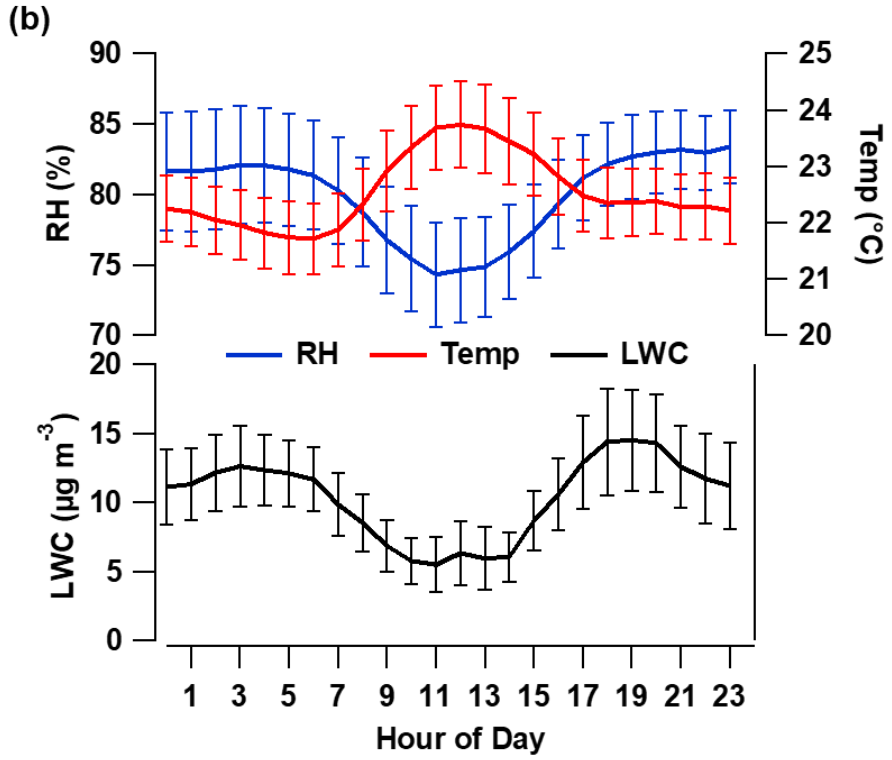

Figure 5-2. Time series (a) and average diurnal variations (b) of the calculated LWC, temperature (temp) and relative humidity (RH) during the sampling period. Error bars in (b) represent 95% confidence intervals (CIs).

The diurnal variations of NR-PM_1 and the components therein are shown in Figure 5-3. Higher levels of NR-PM_1 were observed in daytime, indicating intensive photochemical formation of secondary aerosols, which overwhelmed the effect of higher boundary layer height. The total organics showed a broad peak from 11:00 to 20:00, consistent with the pattern of NR-PM_1. It implied that SOA constituted a significant fraction of the total organics and modulated the diurnal variation of NR-PM_1. Differently, an obvious trough was identified for the diurnal pattern of nitrate during 11:00-14:00, which could be caused by the enhanced evaporation in this period when the temperature was high (Figure 5-2). The diurnal pattern of sulfate differed from that

of the total organics mainly in the afternoon, when the former continued to increase while the latter was relatively stable on the plateau. Due to the increase of LWC from noon to early evening, the rise in sulfate concentration in the afternoon might be attributable to aqueous formation. The relatively stable concentration of total organics between 11:00 and 20:00 did not necessarily indicate no chemical evolution. Instead, we speculate a potential transformation of the organics towards higher oxidation states (chapter 5.4), which might not lead to notable change in the total concentration of organics. Ammonium followed the pattern of sulfate, because of the charge balance and dominance of sulfate in anions. Lastly, the diurnal variation of chloride with lower concentrations in daytime was shaped by the development of boundary layer and temperature-dependent partitioning between gas and particle phases.

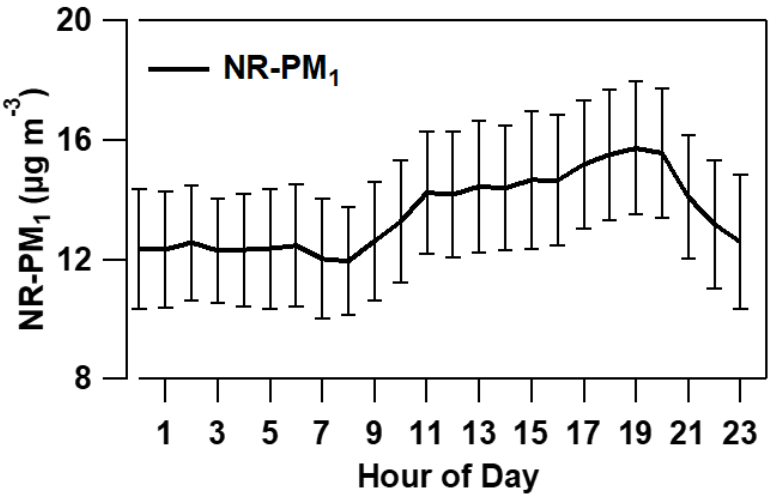

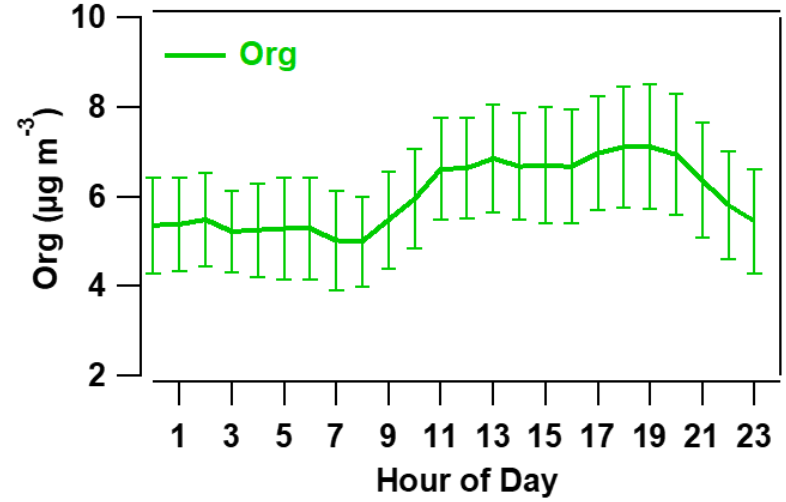
Org
Org (µg m-3)
10
8
6
4
2
1 3 5 7 9 11 13 15 17 19 21 23
Hour of Day

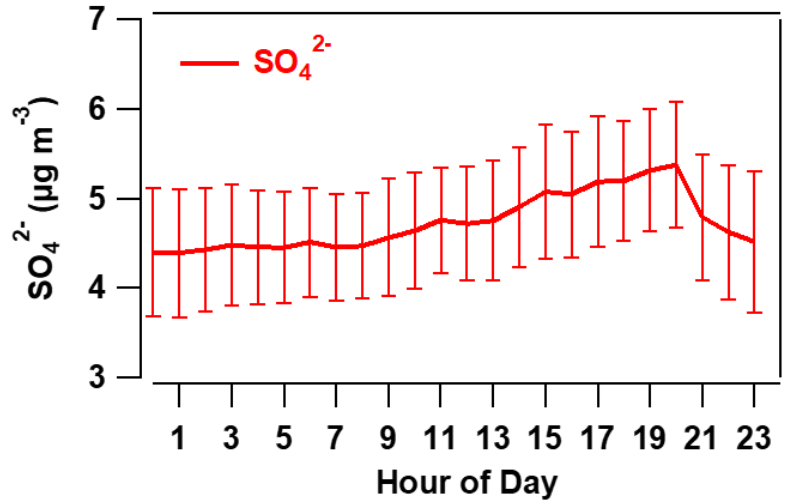
SO4 2-
SO4 2- (µg m-3)
7
6
5
4
3
1 3 5 7 9 11 13 15 17 19 21 23
Hour of Day

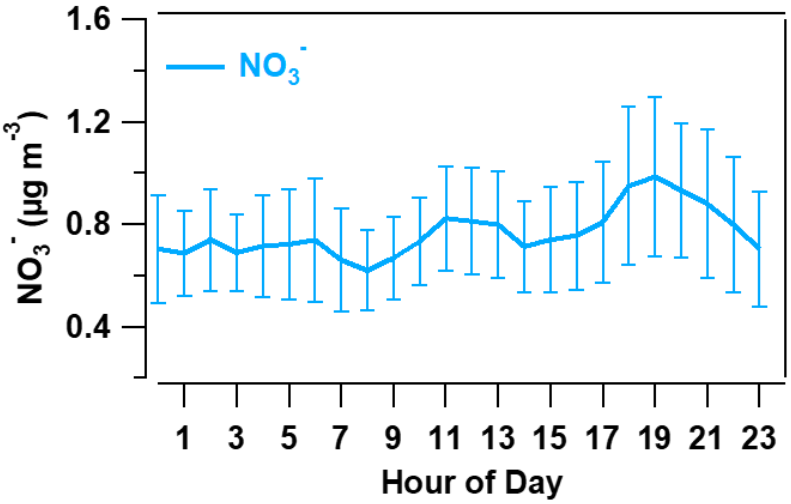
NO3-
NO3- (µg m-3)
1.6
1.2
0.8
0.4
1 3 5 7 9 11 13 15 17 19 21 23
Hour of Day

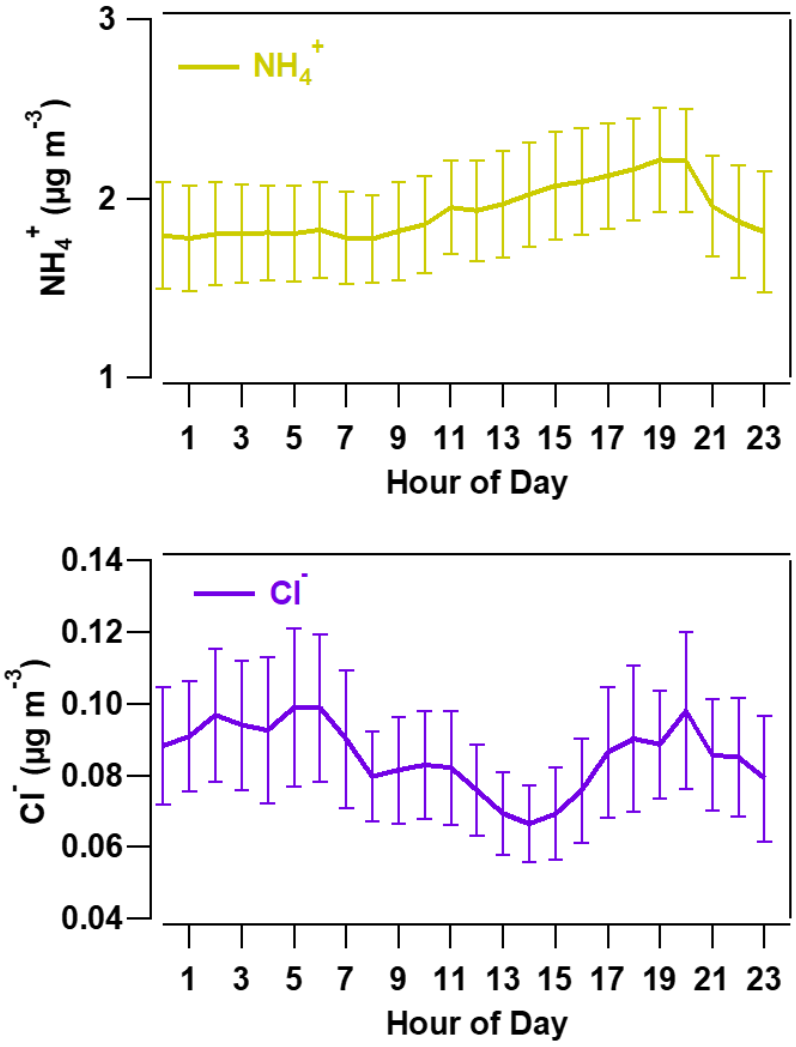

Figure 5-3. Average diurnal variations of NR-PM_1 and the components therein.

5.3 Source apportionment of OA at the background site

To further study the organics in NR-PM_1, it is necessary to break it down to OA components of different characteristics. Hence, source apportionment was applied to the organics. The most appropriate results were determined based on the principles described in previous studies (Ulbrich et al., 2009; Zhang et al., 2011), taking into

account the mathematical criteria and physical meanings of the factors. The number of factors from 2 to 7 was tested, and the corresponding Q/Q_{exp} values were calculated. For the solution with each number of factors, the rotational ambiguity was tested with the FPEAK ranging from -2 to 2 in steps of 0.2. According to the variation of Q/Q_{exp} value with the number of factors and the interpretability of the mass spectra, a 4-factor solution was finally accepted. They included a factor of hydrocarbon-like OA (HOA, a type of POA) and three factors representing OOA (SOA).

The mass spectra of the four identified factors are shown in Figure 5-4(a). HOA is mainly associated with primary emissions of fossil fuel combustion (Zhang et al., 2005; Lanz et al., 2008). Here, the main ions in the HOA factor were the alkyl fragments ($C_nH_{2n+1}^+$ and $C_nH_{2n-1}^+$), such as m/z 41 ($C_3H_5^+$), 43 ($C_3H_7^+$), 55 ($C_4H_7^+$) and 57 ($C_4H_9^+$), in line with the HOA spectra reported before (Ng et al., 2011; Sun et al., 2011). The HOA factor had the highest H:C ratio (1.84) and conversely the lowest O:C ratio (0.24). The O:C ratio was at the upper end of the range for HOA, i.e., 0.05–0.25 (Canagaratna et al., 2015), which was also higher than those at the other sites in Hong Kong (Lee et al., 2015; Yao et al., 2021). This might be due to the fact that air masses at this background site were more aged. Therefore, the contribution of HOA might be somewhat overestimated. The OOA factors had lower loadings of alkyl fragments and higher loadings of oxygenated species than the HOA factor. Consistent with previous studies (Lanz et al., 2007; Ulbrich et al., 2009; Sun et al., 2011), the mass spectra of the OOAs were characterized by dominant fractions of m/z 44 (mainly CO_2^+). Two out of the three OOA factors were less oxidized with the O:C ratio of 0.72 (0.76) and H:C ratio of 1.47 (1.46), referred to as LO-OOA1 (LO-OOA2). The other OOA factor was defined as more oxidized OOA (MO-OOA), because of the much higher O:C ratio (1.12) and lower H:C ratio (1.15).

It is noteworthy that cooking organic aerosol (COA), an important source of OA

identified in urban areas of Hong Kong (Lee et al., 2015; Liu et al., 2019), was not discerned at this site. A possible reason was that the COA was oxidized to OOAs during the transport (Yao et al., 2021; Zhou et al., 2021). Hence, COA and the tracer ions of COA (e.g., $C_3H_3O^+$ at m/z 55 and $C_3H_5O^+$ at m/z 57) are not discussed further in this section. While biomass burning was suspected as a large contributor to OA at the same site (Lyu et al., 2020), the high contributions were determined with a reconstruction method based on the concentrations of molecular tracers and were mainly identified in December 2018 when the AMS data was not available. However, it is difficult to completely eliminate the interferences of other sources.

Overall, OOAs dominated the contribution (86.5 ± 0.07 %) to the total organics, while HOA only accounted for 13.5 ± 0.7% (Figure 5-4(b)). LO-OOA1 was the largest source of OA with the contribution of 43.0 ± 1.1%. Second to it was MO-OOA, which was responsible for 34.5 ± 1.4% of the total organics. The factor LO-OOA2 made the least and relatively stable contribution (8.9 ± 0.5%) throughout the field campaign, likely representing the background levels of OOA at the site.

Figure 5-4(c) shows the diurnal variations of OA assigned to the four sources. The HOA got highest concentrations at ~9:00 and ~ 21:00, later than the corresponding peaks of HOA in urban areas (Lee et al., 2015; Yao et al., 2021). Such delay could be due to the transport of emissions from the upwind cities. While the variation of LO-OOA2 was small throughout the day, the significantly higher levels of LO-OOA1 and MO-OOA in the daytime indicated intensive SOA formation involving photochemical processes. The peak of LO-OOA1 appeared at ~13:00, earlier than the broad peak of MO-OOA during 15:00 – 20:00. When the LO-OOA1 decreased between 13:00 and 16:00, the MO-OOA continued to increase. The different patterns were attributable to different formation mechanisms of the two OOA components and potential transformation between them, which are discussed below.

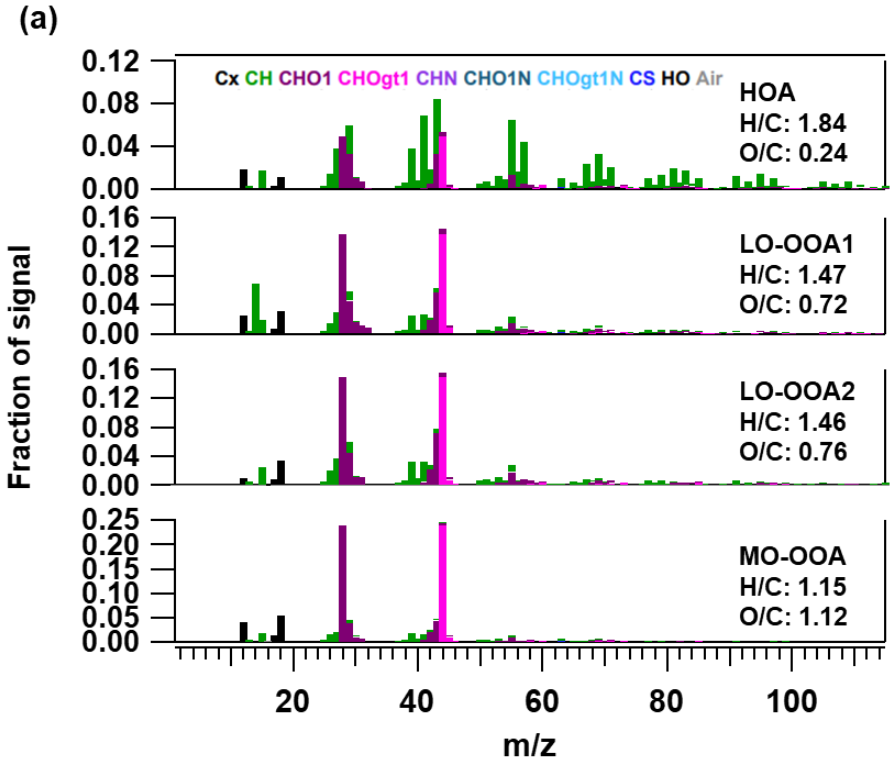
(a)
Cx CH CHO1 CHOgt1 CHN CHO1N CHOgt1N CS HO Air
HOA
H/C: 1.84
O/C: 0.24
LO-OOA1
H/C: 1.47
O/C: 0.72
LO-OOA2
H/C: 1.46
O/C: 0.76
MO-OOA
H/C: 1.15
O/C: 1.12
Fraction of signal
0.12
0.08
0.04
0.00
0.16
0.12
0.08
0.04
0.00
0.16
0.12
0.08
0.04
0.00
0.25
0.20
0.15
0.10
0.05
0.00
20
40
60
80
100
m/z

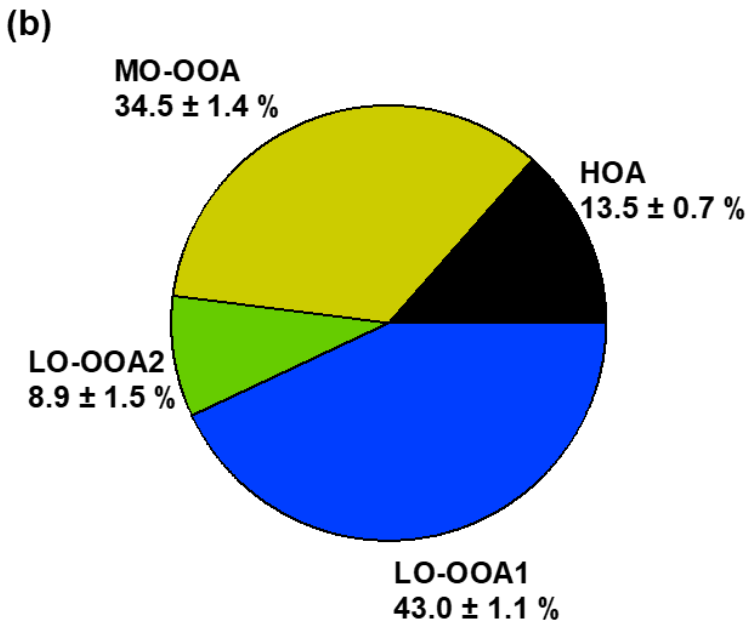
(b)
MO-OOA
34.5 ± 1.4 %
HOA
13.5 ± 0.7 %
LO-OOA2
8.9 ± 1.5 %
LO-OOA1
43.0 ± 1.1 %

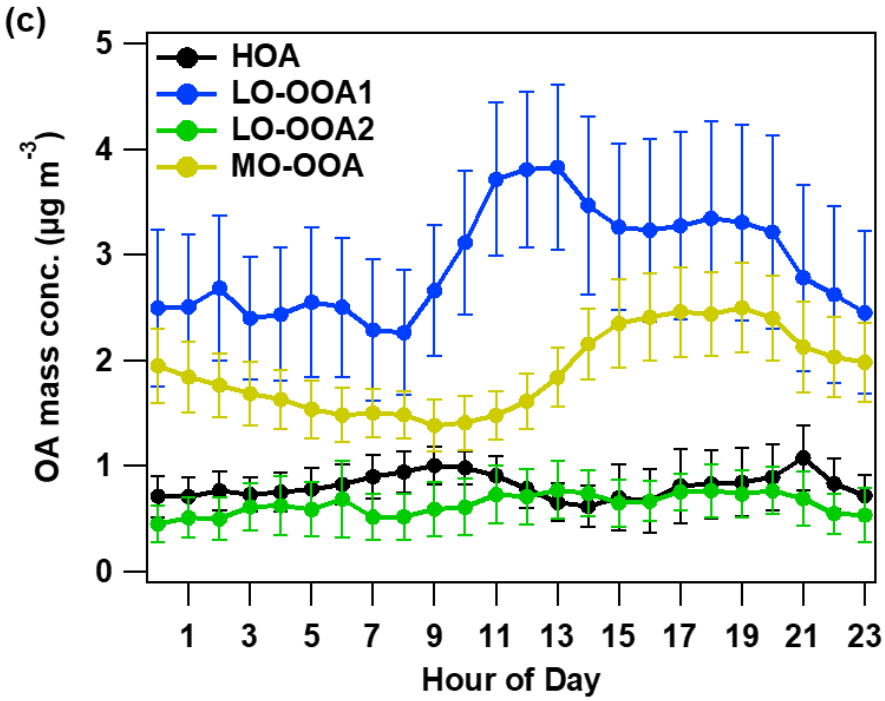

Figure 5-4. Mass spectra of OA factors resolved from source apportionment (a); Percentage contributions to the total organics of the identified sources (b); and Diurnal patterns of the specific sources (c).

5.4 Formation mechanisms of LO-OOA1 and MO-OOA

The above analyses implied the processes of photochemical and aqueous oxidations in SOA formation. To understand the role of photochemical oxidation, we examined the correlations between OOAs and the odd oxygen O_x ($O_x = O_3 + NO_2$) (Clapp and Jenkin, 2001). As a measure to eliminate the interference of diurnal patterns to the correlation, daily averages were used in the analysis. It was found that MO-OOA responded positively to O_x with a moderate correlation ($r^2 = 0.69$), as shown in Figure 5-5 (a). As such, the formation of MO-OOA was associated with photochemical oxidation. Furthermore, the high levels of MO-OOA were accompanied by high LWC values, and the diurnal patterns of MO-OOA and LWC resembled each other. To further reveal the effect of LWC, we plot MO-OOA against LWC in 5 LWC intervals (Figure 5-5 (b)). The method of averaging variables in a few intervals has been widely adopted in correlation analysis (Marshall et al., 2008), which is capable of reducing the influences of other factors. Obviously, the concentration of MO-OOA increased with the rise in LWC level, and the positive correlation was very significant ($r^2 = 0.96$). As such, it was likely that the MO-OOA formation involved aqueous processes. However, we should note that the aqueous processes for SOA formation in this study were mainly those in aerosol liquid water, since LWC is highly correlated with SIAs (sulfate, ammonium and nitrate). In this case, photochemical oxidation and aqueous processes might play roles in different stages of chemical evolution, or they were coupled, e.g., formation of aqueous oxidants through photochemical reactions.

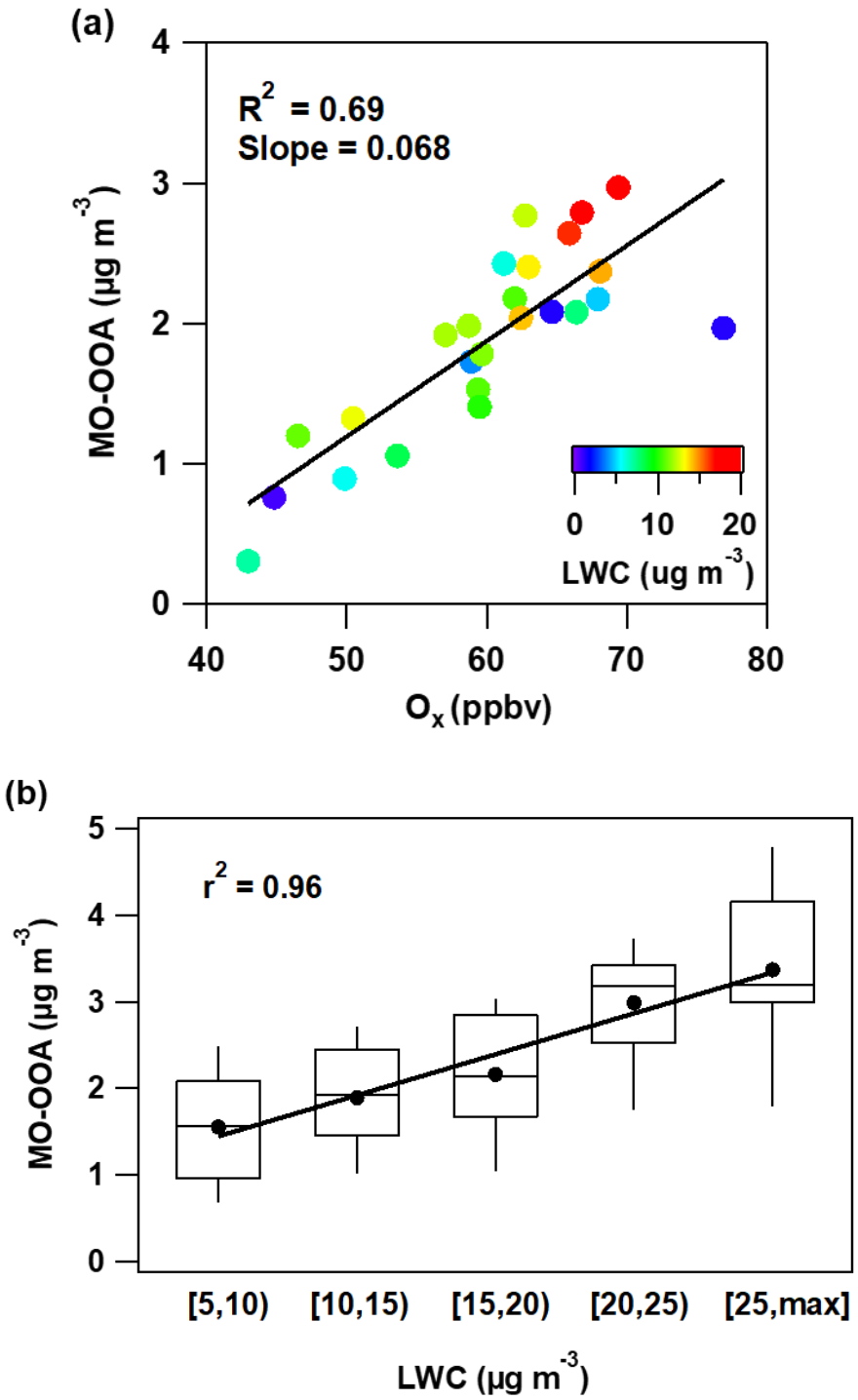

Figure 5-5. Scatter plot of daily average MO-OOA versus O_x as a function of LWC level (a); Variation of MO–OOA with LWC in 5 intervals (b).

It was indicated that some oxygenated compounds of primary emissions might be assigned to LO-OOA due to similarity in elemental compositions, such as saccharides from biomass burning and fatty acids from cooking (Zhou et al., 2021). However, due to the weak correlations with the corresponding molecular tracers (see discussion below), LO-OOA1 was not significantly interfered by either biomass burning or cooking in this study. Even so, there was nearly no correlation between LO-OOA1 and O_x or LWC (Figure 5-6), implying that the formation of LO-OOA1 was regulated by other factors, e.g., precursors and/or oxidants other than O_x, and was independent of aqueous processes.

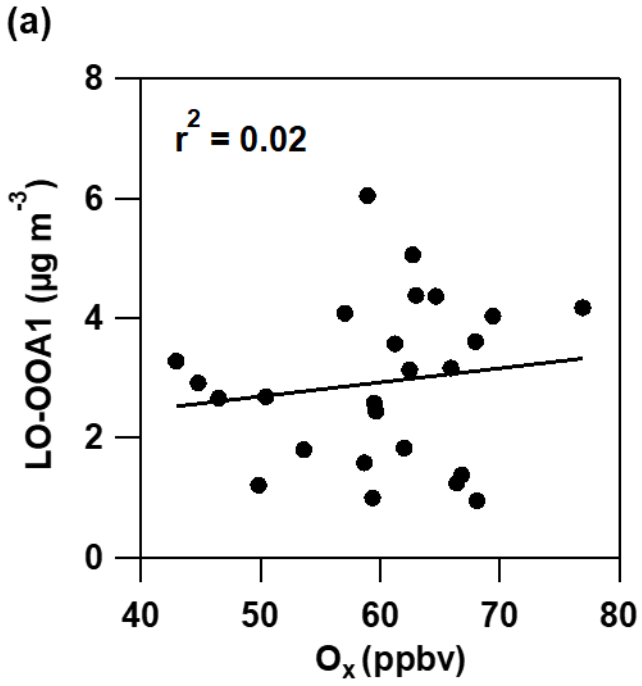

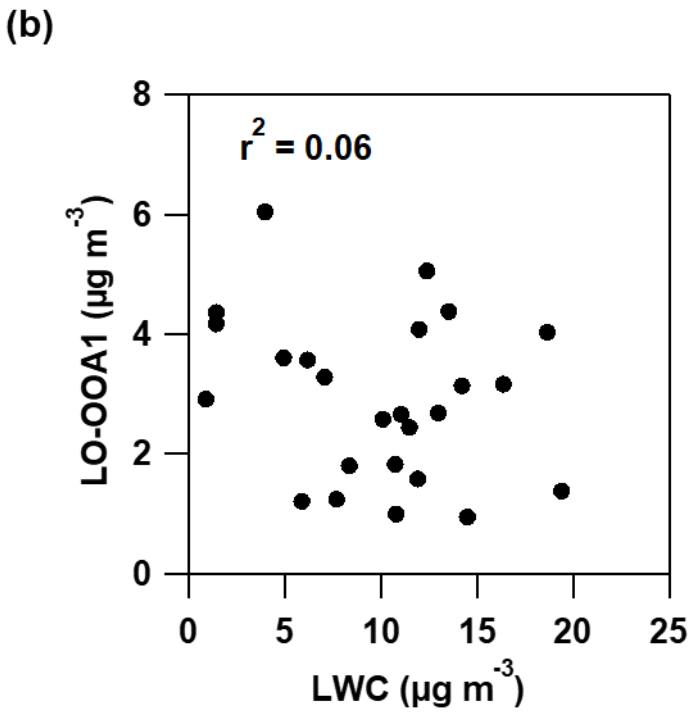

Figure 5-6. Scatter plots of daily average LO-OOA1 versus O_x (a) and LWC (b).

Furthermore, the potential precursors of OOAs were explored. We examined the diurnal patterns of VOCs and noticed that the peaks of LO-OOA1 and MO-OOA were later than those for toluene and biogenic VOCs (isoprene and monoterpenes), respectively (Figure 5-7). While further relationship was not found between OOAs and VOCs, we identified moderate to good correlations between OOAs and OA markers that could be formed through oxidation of VOCs. LO-OOA1 exhibited the best correlation with hydroxybenzoic acids (OHBAs) with r^2 of 0.48 (Figure 5-8 (a)). Besides, the variations of LO-OOA1 were occasionally synchronized with some other OA markers, such as 2,3-dihydroxy-4-oxopentanoic acid (DHOPA). To identify as many factors accounting for the variations of LO-OOA1 as possible, we performed a series of multilinear

regressions between LO-OOA1 and the OA markers. Through tests, the regression with a highest r^2 of 0.66 and OHBAs, DHOPA and malic acid as the independent variables was determined, as summarized in Table 5-1. The r^2 of 0.66 suggests that the sources or processes represented by these OA markers explained 66% of the variations of LO-OOA1. OHBAs have been detected in primary emissions of biomass burning and can also be secondarily formed through oxidation of aromatics, e.g., naphthalene and benzonic acid (Wang et al., 2020). Here, due to the poor correlation between OHBAs and levoglucosan (r^2 = 0.06) and higher concentrations of OHBAs in daytime (Figure 5-9), the OHBAs were most likely secondary products. In addition, DHOPA is a typical tracer of anthropogenic SOA derived from aromatics (Al-Naiema and Stone, 2017). The small and negative coefficient for malic acid implied a potential transformation, which is discussed below. Overall, aromatics were the most likely precursors of LO-OOA1. Due to the relatively low O_3 levels in the morning, hydroxyl-initiated oxidation was a plausible pathway leading to the formation of LO-OOA1, which also explained the poor correlation between LO-OOA1 and O_x.

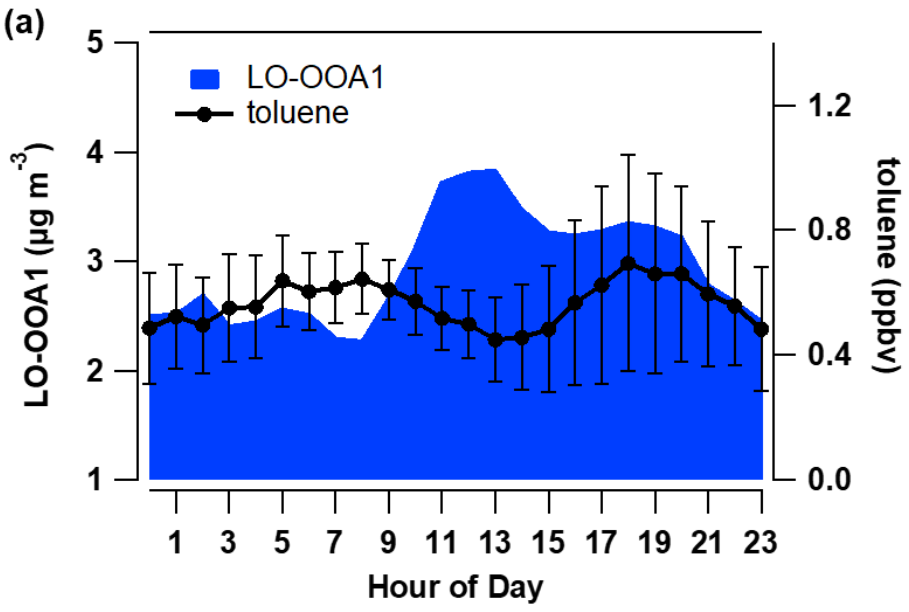

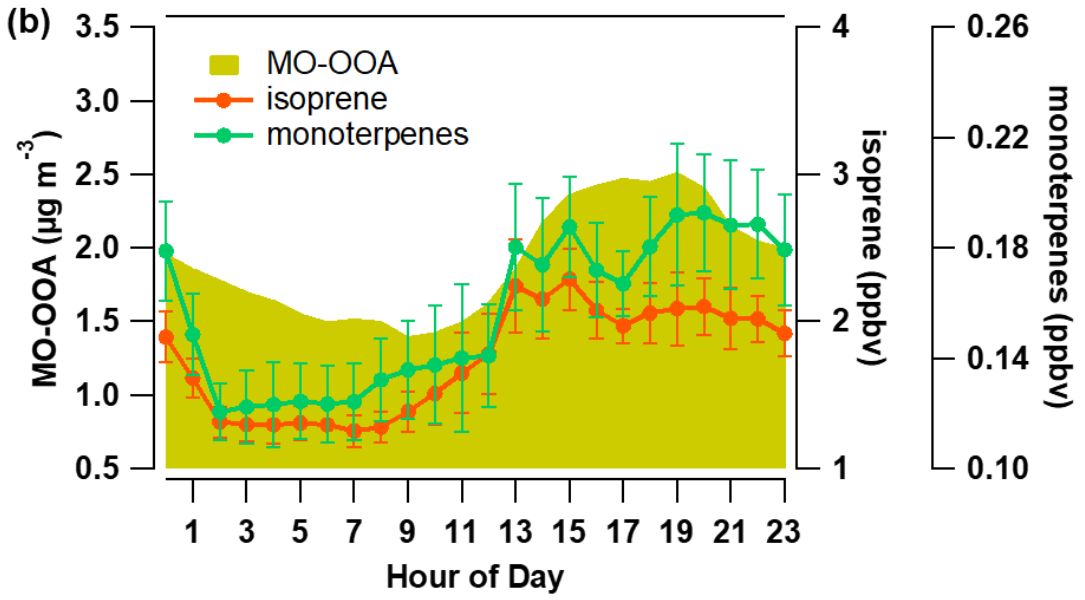

Figure 5-7. Average diurnal variations of LO-OOA1 and toluene (a); and MO-OOA, isoprene and monoterpenes (b).

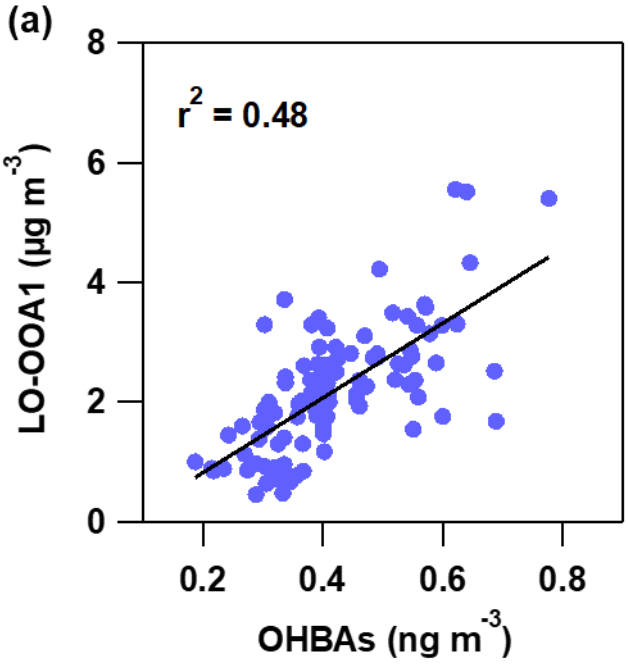

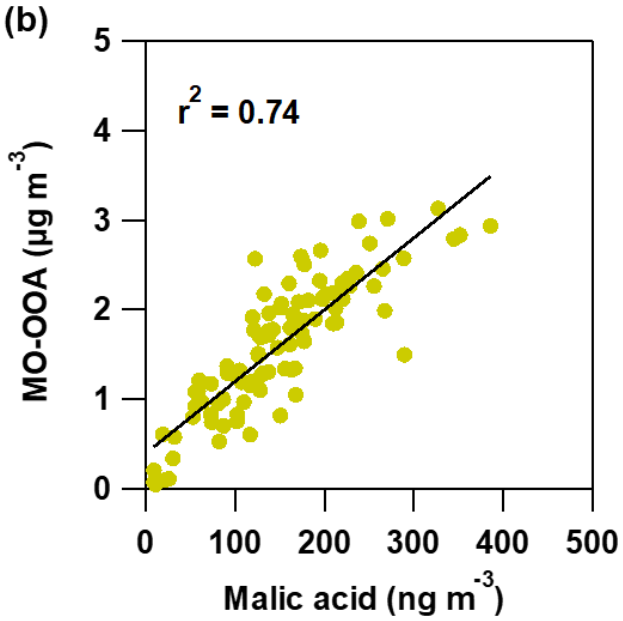

Figure 5-8. Correlations between OOA and molecular markers of OA: LO-OOA1 vs. OHBA (a); and MO-OOA vs. malic acid (b).

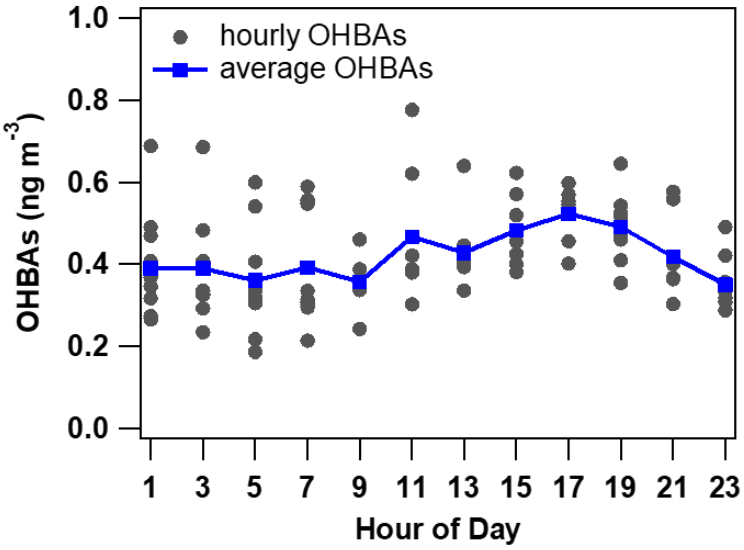

Figure 5-9. Hourly concentrations (grey dots) and average diurnal variations (blue line) of OHBAs.

Table 5-1. Multilinear regression results between LO-OOA1 and OA makers.

	Coefficient	*p* value	Significance F	r^2
Intercept	-0.86	0.005	<0.0001	0.66
INDV-1* (DHOPA)	1.66	0.015		
INDV-2 (OHBAs)	8.95	<0.0001		
INDV-3 (Malic acid)	-0.01	<0.001		

* INDV denotes independent variable.

Malic acid was the OA marker that correlated best with MO-OOA (r^2= 0.74), as shown in Figure 5-8 (b). Multilinear regressions with more OA markers as independent variables did not increase the coefficient of determination too much, which therefore were not adopted. According to Lyu et al. (2020), the evidence of biogenic VOCs fuelling malic acid formation was not found in this campaign. Instead, anthropogenic VOCs were suspected as the main precursors of malic acid, due to the moderate correlation between malic acid and DHOPA (Lyu et al., 2020). As a verification, Figure 5-10 presents the dependences of MO-OOA on the sum of monoterpenes SOA tracers (MT-SOA-T) and the sum of isoprene SOA tracers (Isop-SOA-T) in different air masses. The species included in MT-SOA-T and Isop-SOA-T and classification of air masses were introduced in Lyu et al. (2020). It can be seen that the data points are spread out. While the concentrations of biogenic SOA tracers were higher in continental air, the levels of MO-OOA were lower due likely to the lower O_x. However, the bad correlation ($r^2 < 0.25$) between MO-OOA and MT-SOA-T or Isop-SOA-T in any individual type of air masses suggested that biogenic VOCs might not be the main precursors of MO-

OOA.

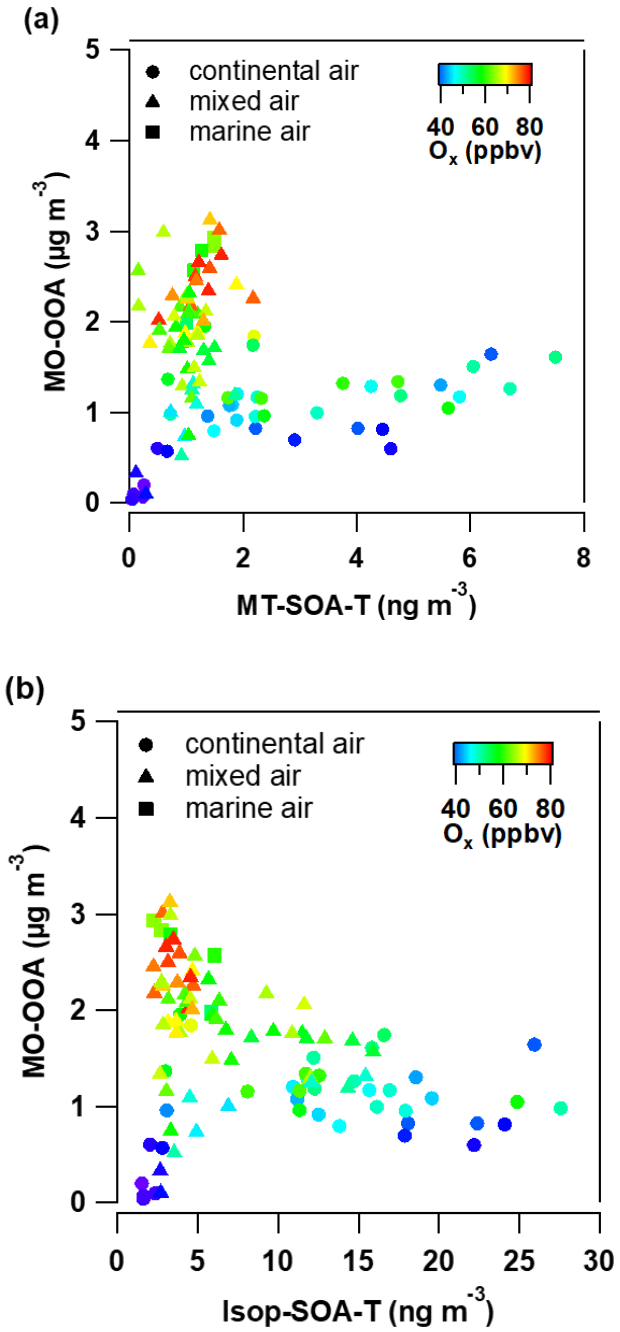

Figure 5-10. Scatter plot of MO-OOA versus MT-SOA-T (a) and Isop-SOA-T (b). MT-SOA-T is the sum of 3-methyl-1,2,3-butanetricarboxylic acid, 3-hydroxy-4,4-

dimethylglutaric acid and pinonic acid. Isop-SOA-T includes 2-methylthritol and 2-methylerythritol. Classification of air masses is identical to that adopted by Lyu et al. (2020).

We further investigated the ratio of MO-OOA/LO-OOA1 to see the potential transformation between OOAs. It is interesting to note that the ratio of MO-OOA/LO-OOA1 showed highly consistent diurnal pattern with that of LWC (Figure 5-11). In particular, the consistency in the early afternoon when LO-OOA1 decreased and MO-OOA increased most likely indicated that aqueous processes were involved in the transformation of LO-OOA1 to MO-OOA. This partly explained the correlation between MO-OOA and DHOPA (r^2=0.59). Therefore, like malic acid, MO-OOA might also be the aging product of anthropogenic organics. However, due to the lack of direct evidence and various precursors of malic acid (Wang et al., 2008; Hu and Yu, 2013), we leave the precursors of MO-OOA an open question to be answered in future research. In fact, we found that malic acid correlated fairly well with some biogenic SOA tracers at the same site in another field campaign in 2020 (unpublished data). The discrepancies could be caused by many factors, such as the fewer biogenic SOA tracers detected in 2018, recent emission control of some anthropogenic sources (e.g., ship emissions), and meteorological differences. In addition, no diurnal cycle of MO-OOA/LO-OOA synchronized with LWC or other factors was observed in the roadside dataset, which may be due to the relatively stable variation of MO-OOA at the roadside site.

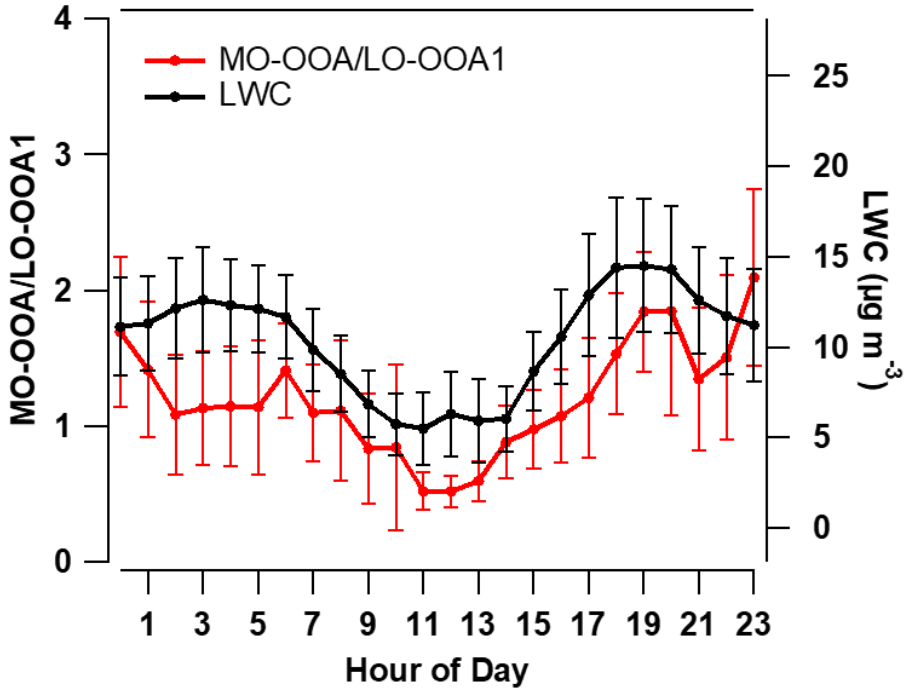

Figure 5-11. Average diurnal variations of the ratio of MO-OOA/LO-OOA1 and LWC at HT.

5.5 Conclusions

SOA in the atmosphere is of serious concern for its impacts on air quality, climate and human health. However, the formation mechanisms of SOA in regions significantly affected by human activities have not been fully understood. In this chapter, at an urban background site on the coastline of South China where the SOA chemistry could be complicated by interactions of air pollutants with different sources and origins and changeable meteorology, we discovered high loadings of organics with absolute dominance of SOA in NR-PM_1 in a cool season. The LO-OOA components dominated over MO-OOA and accounted for more than half of the PM_1-bound organics in mass concentration. We proved that one of the LO-OOA components that was more variable and overwhelmed its counterpart in concentration was mainly formed through photochemical oxidation of aromatics. The formation processes seemed not to be limited by O_x and LWC. Differently, the formation of MO-OOA was associated with both photochemical oxidation and aqueous processes, yet there was no clear conclusion on the precursors of MO-OOA. Even so, we proposed the potential transformation from LO-OOA to MO-OOA involving aqueous processes. Taking advantages of the other measurements in addition to AMS data, such as molecular OA markers measured by TAG, this study advanced our understanding on the formation mechanisms and precursors of SOA. In particular, the importance of anthropogenic VOCs in contributing to SOA formation in coastal air was highlighted, where the high relative humidity and atmospheric oxidative capacity also played significant roles in OA aging. Similar conditions are common in marginal seas and estuaries close to cities, hence more in-depth studies on SOA formation in representative regions are necessary.

Chapter 6 Changes in aerosol chemistry at an urban background site in Hong Kong before and during the COVID-19 pandemic

6.1 Introduction

Particulate pollution has been a major concern in Hong Kong for many years (So et al., 2007; Cheung et al., 2015). Organic aerosols (OAs) make up a large fraction of particulate matters (PMs), which contain POAs directly emitted from various sources and SOAs formed in the atmosphere. Due to diverse precursors, complex meteorological conditions, and complicated evolutionary processes, SOA formation in the atmosphere requires further investigations to formulate appropriate control strategies. In recent years, our research found that due to control measures in Hong Kong, PM and its precursors (e.g. VOCs) emitted from diesel- and LPG-fueled vehicles declined over the years, while VOCs emissions from gasoline-fueled vehicles increased (Lyu et al., 2016, 2017a; Yao et al., 2019). However, these studies did not measure particles of smaller size, such as NR-PM_1 or OAs. In fact, submicron aerosols were found to be the main component of $PM_{2.5}$, and there appeared to be no substantial change between 2005 and 2014 in Beijing, while $PM_{2.5}$ levels decreased significantly (Chen et al., 2017), indicating the dominance of secondary OAs. Hence, understanding the composition and evolution of submicron particles and OAs over the years is of great significance. Furthermore, secondary formation of OAs in remote/rural areas is often chosen to be studied because the background sites are far from primary emissions. It happened that we conducted a sampling campaign at Hok Tsui site in Hong Kong in autumn 2018 to study SOA formation and its relationship with precursors in the absence

of the COVID-19 pandemic (Chapter 5). Two years later (i.e., autumn 2020), when the COVID-19 pandemic hit, we performed another field sampling at the same site. These two sampling campaigns perfectly provided us with the opportunity to study changes in aerosol chemistry due to changes in source emissions and meteorological conditions at this urban background site before and during the pandemic.

A number of studies have explored the effects of changes in emissions and meteorological conditions on aerosol chemistry (Huang et al., 2010; Sun et al., 2016; Zhao et al., 2017; Zhong et al., 2021). Huang et al. (2010) highlighted that strict emission controls and favorable meteorological conditions altered aerosol chemistry and played important roles in improving air quality during the 2008 Beijing Olympics. Zhao et al. (2017) found that primary aerosols decreased more than secondary aerosols during the 2015 Chinese Victory Day military parade due to temporary control measures. Sun et al. (2016) studied a typical haze event in winter 2015, which was much more severe than the same period in 2014, with the difference mainly attributable to meteorological differences between the two years. Zhong et al. (2021) conducted online measurements of organic aerosols at a background site before and during the COVID-19 lockdown in northwestern China and found a large increase in oxidized organic aerosols during the lockdown. However, the relatively short time periods in which the aforementioned emission controls were implemented, ranging from a few days to less than a month, are not representative of the impact of long-term emission changes on aerosol chemistry. In addition, these special events were often accompanied by meteorological changes, bringing more uncertainty. For changes on longer timescales, Zhang et al., (2016) analyzed the long-term variations of submicron OA at a peri-urban background site of France for six years and found that OA factors exhibited distinct seasonal patterns, which were associated with different atmospheric formation

pathways. Young et al., (2015) investigated the annual cycle of submicron particles at an urban background site in the UK and surprisingly showed no change in the extent of SOA oxidation given changes in precursor emissions and photochemical activity. Lee et al. (2015) presented seasonal variations in aerosol composition and characteristics as sampling campaigns were conducted during each season of the year. The proportion of species in NR-PM_1, the contribution of local sources and regional transport to OA, and the degree of oxidation were all strongly season-dependent. Because of complex driving forces, more detailed comparisons of aerosol chemistry over the years are critical to better elucidate the impacts of multiple factors including changes in emissions and meteorological conditions on particulate pollution.

In this chapter, HR-ToF - AMS was deployed along with other online instruments for real-time measurements of gaseous and particulate pollutants at the Hok Tsui site in autumn 2020. The results were compared to those observed during the same period in 2018. Specifically, changes in aerosol composition, pollutant levels and the degree of OA oxidation between 2018 and 2020 sampling campaigns were first investigated. The differences in OA sources and their apportionments were identified and quantified using a receptor model, i.e., PMF model. Lastly, the changes in the formation and evolution of OOA from 2018 to 2020 are elaborated. The findings will help the governments adjust air pollutant control strategies in the region.

6.2 General characteristics of pollutants in 2020

The day-to-day variations and average mass concentrations of NR-PM_1 components are shown in Figure 6-1 ((a)-(b)). The hourly NR-PM_1 concentration ranged from 0.3 to 48.9 μg/m^3 with an average of 12.3 ± 0.3 μg/m^3, much lower than the values at suburban and roadside sites in Hong Kong (Lee et al., 2015; Yao et al., 2021), and slightly lower ($p < 0.01$) than the levels (13.5 ± 0.4 μg/m^3) found in 2018 at the same site. Similar to previous studies in Hong Kong, organics was the most dominant species of all measured components. Concentrations of organics ranged from 0.3 to 31.4 μg/m^3 with an average of 6.4 ± 0.2 μg/m^3 throughout the sampling period. The concentration and average percentage of organics (51.0 ± 0.5 %) were higher than those (6.0 ± 0.2 μg/m^3 and 43.8 ± 0.7 %) in 2018 at this site ($p < 0.01$), but still lower than that of urban roadside sites (54.2 - 57.7 %) (Lee et al., 2015; Yao et al., 2021). This might be due to different source emissions and formation processes this year, which were further analyzed in the following sections. Sulfate, a secondarily formed inorganic ion, was the second most dominant species with an average mass concentration of 4.0 ± 0.1 μg/m^3 and an average fraction of 33.1 ± 0.4 %, slightly below the values (4.7 ± 0.1 μg/m^3 and 35.8 ± 0.7 %) in 2018 ($p < 0.01$), possibly due to the less aqueous-phase formation of particles during sampling period in the Pearl River Delta region while we found that the SO_2 levels were higher in 2020 (2.8 ± 0.04 ppbv vs 1.2 ± 0.05 ppbv). In addition, consistent with the results in 2018, the proportions of total organics and sulfate were followed by ammonium (10.6 ± 0.1 %), nitrate (4.7 ± 0.1 %), and chloride (0.7 ± 0.03 %), with concentrations of 1.3 ± 0.3, 0.6 ± 0.03, and 0.07 ± 0.02 μg/m^3, respectively. The proportion of ammonium was lower ($p < 0.01$) than that in 2018 (14.4 ± 0.2 %), while the average concentrations and proportions of nitrate and chloride were comparable to those in 2018.

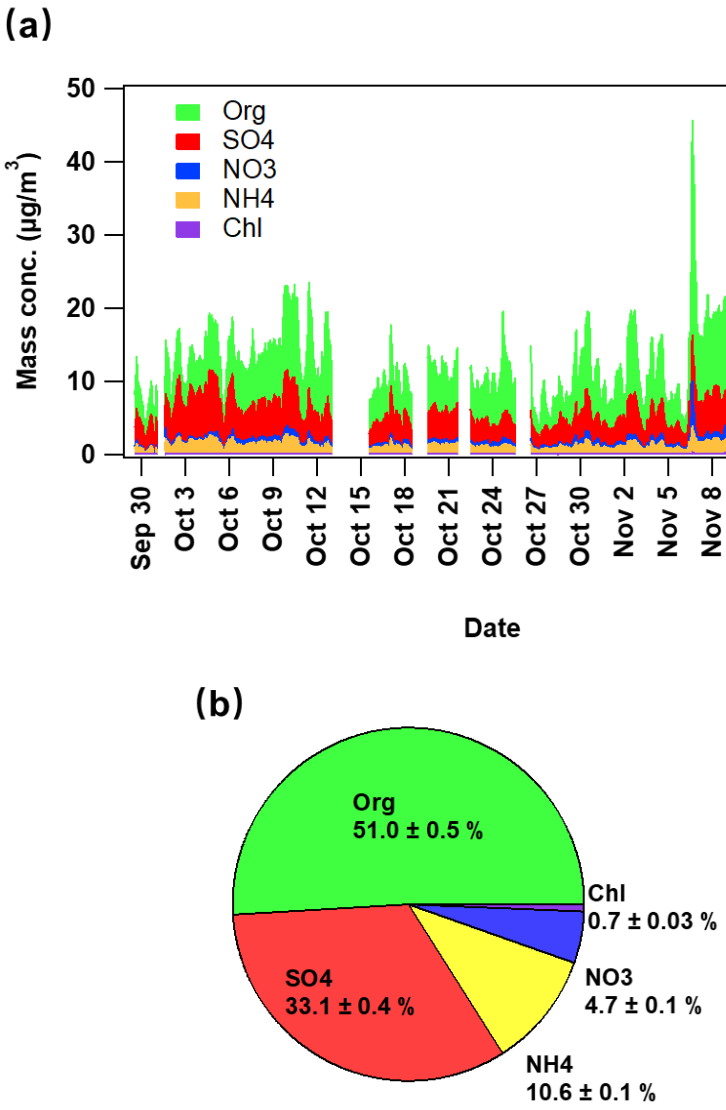

Figure 6-1. Daily-to-daily variations in mass concentration of NR-PM_1 components (a); and average percentages of NR-PM_1 components (b) at HT in 2020

The diurnal variations of bulk composition in NR-PM_1 are shown in Figure 6-2. Higher levels of organics were discovered during the day in the 2020 sampling campaign (p < 0.01), with the highest peak observed at 15:00, indicating strong photochemical

formation of secondary aerosols at this site. This differed from what was observed in the 2018 sampling campaign, where aqueous processes led to the highest levels of organics at night. The diurnal variation of sulfate was similar to the peak of total organics, mainly in the afternoon, with a distinct trough between 10:00-12:00. Nitrate, ammonium and chloride followed the trend of sulfate, with a peak in the afternoon. The simultaneous peaks of these secondary inorganic species (sulfate + nitrate + ammonium, SIAs) in the afternoon indicated intense photochemical processing at the site in the 2020 sampling campaign. While the level of chloride was generally low at noon due to the fact that high temperature limited the gas to aerosol conversion of chloride in the daytime, a slightly enhancement of chloride was observed in the early morning and afternoon which caused by the development of boundary layer. These diel cycles of both organic and secondary inorganic species indicated that this site was greatly affected by photochemical formation of secondary aerosols in the 2020 sampling campaign.

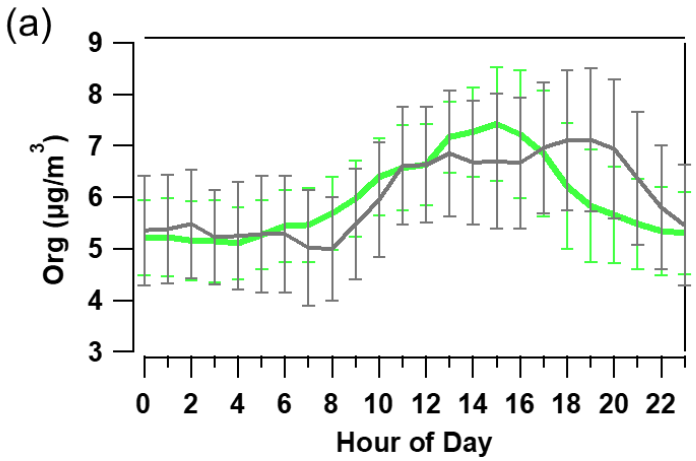

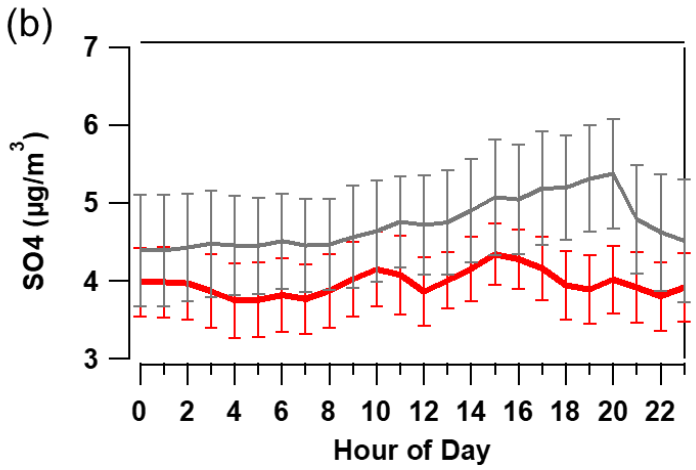
(b)
SO4 (µg/m3)
7
6
5
4
3
0 2 4 6 8 10 12 14 16 18 20 22
Hour of Day

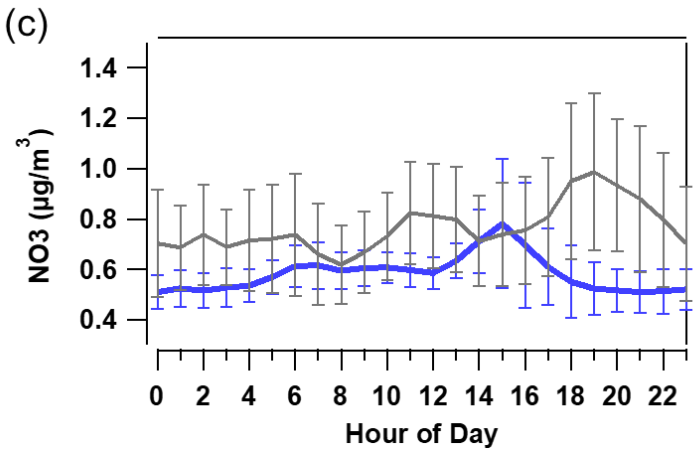
(c)
NO3 (µg/m3)
1.4
1.2
1.0
0.8
0.6
0.4
0 2 4 6 8 10 12 14 16 18 20 22
Hour of Day

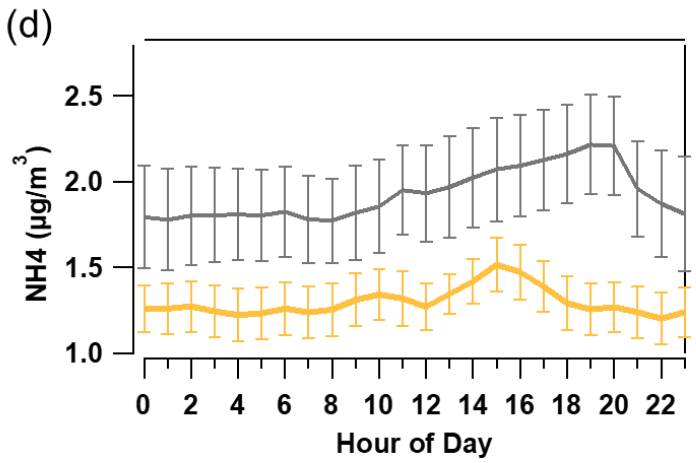
(d)
NH4 (µg/m3)
2.5
2.0
1.5
1.0
0 2 4 6 8 10 12 14 16 18 20 22
Hour of Day

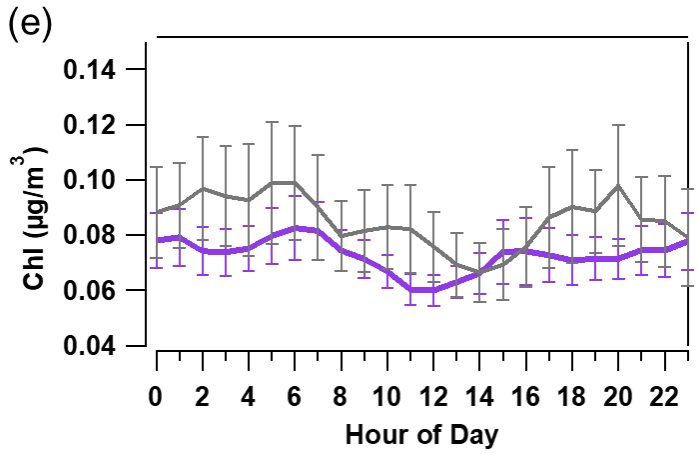

Figure 6-2 Average diurnal variations of the components in NR-PM_1 (a) organics, (b) sulfate, (c) nitrate, (d) ammonia, and (e) chloride. The grey lines are the results in the 2018 sampling campaign.

To further study the pollution characteristics at Hok Tsui site between the 2018 and 2020 sampling campaigns, the diurnal trends of gaseous and particulate-phase pollutants are presented in Figure 6-3. The daytime PM_1 and $PM_{2.5}$ levels in 2020 were higher than in 2018, indicated by the higher afternoon peaks (~16:00) in 2020, suggesting possibly stronger photochemically secondary formation of aerosols in the daytime in 2020. In contrast, the higher levels of PM_1 and $PM_{2.5}$ in the evening in 2018 might be related to the aqueous formation of OAs, as discussed in Sections 5.3 and 5.4. In terms of gaseous pollutants, the NO values in both 2018 and 2020 reached a significant peak around 9:00, consistent with the morning traffic peak in Hong Kong (Lee et al., 2015; Yao et al., 2021), indicating that this site was also influenced by vehicle emissions nearby. Indeed, our observation confirmed that there were several vehicles passing by each morning. Despite similar NO patterns in these two sampling campaigns, the level in 2018 was higher than in 2020 ($p < 0.01$). This might be due the reduction of vehicles on the road in 2020 because of the covid-19 pandemic (HKATC,

2018; HKATC, 2020). This was further confirmed by the fact that the NO_x levels at three roadside sites in Hong Kong were all lower during the 2020 sampling campaign, compared to those during the 2018 sampling campaign (Mong Kok site: 137.64±5.23 μg/m^3 in 2018, 110.60±3.47 μg/m^3 in 2020; Central site: 172.53±8.98 μg/m^3 in 2018, 135.10±4.89 μg/m^3 in 2020; Causeway Bay site: 202.66±9.61 μg/m^3 in 2018, 178.05±5.52 μg/m^3 in 2020). The average diurnal variations of CO and SO_2 at this site were relatively stable in the two years, while the CO levels were comparable and the SO_2 levels were higher in 2020 than in 2018, which might be due to the enhancement of SO_2 emissions in PRD region from 2018 to 2020 by the development of shipping industry in these years (Zhang et al., 2022). Ship emissions contributed to the elevation of SO_2 at this site as the measured SO_2 levels did not increase in 2020 at those roadside sites (Mong Kok site: 3.2±0.2 μg/m^3 in 2018, 2.7±0.1 μg/m^3 in 2020; Central site: 7.1±0.3 μg/m^3 in 2018, 3.8±0.1 μg/m^3 in 2020; Causeway Bay site: 8.3±0.2 μg/m^3 in 2018, 5.6±0.1 μg/m^3 in 2020), which were strongly influenced by vehicle emissions. However, as noted above, sulfate levels in 2020 were lower ($p < 0.01$) compared to 2018, suggesting less formation or less regional transport of sulfate from inland PRD region in 2020 sampling campaign. Furthermore, the diurnal pattern of O_x between these two years was similar, but the daytime O_x values (8:00 – 17:00) were higher in the 2020 sampling campaign, indicating stronger atmospheric oxidative capacity during this sampling period. This might be related to lower anthropogenic emissions, especially the lower levels of O_3 precursors (VOCs and NO_x) in the 2020 sampling campaign, due to less human activities during the COVID-19 pandemic. The temperature and relative humidity during these two sampling campaigns were also compared. It was seen that the diel cycles of both temperature and relative humidity showed similar trends between 2018 and 2020. However, the average temperature was higher in 2020 (25.0 ± 0.1℃) than that in 2018 (22.5 ± 0.1℃) ($p < 0.01$), which was

probably one of the reasons causing higher oxidative capacity in 2020. In contrast, the average relative humidity in 2020 (76.1 ± 0.6%) was lower than in 2018 (79.9 ± 0.8%) ($p < 0.01$), which also led to lower LWC levels in 2020.

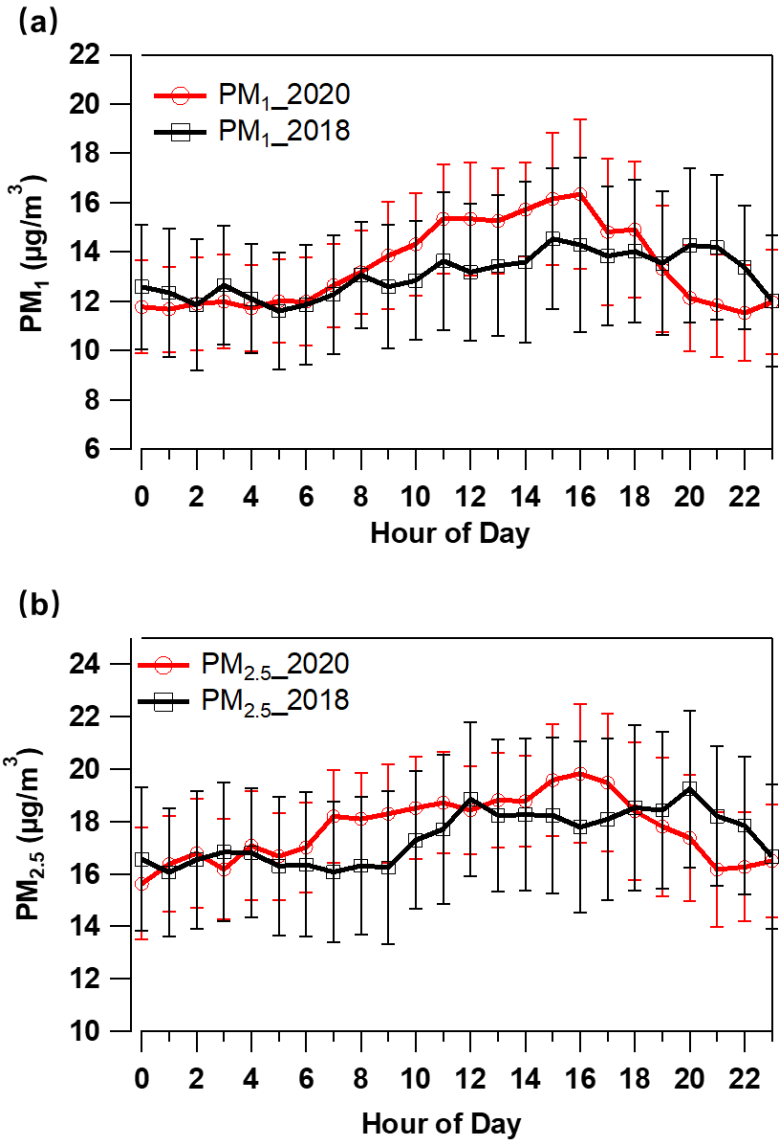

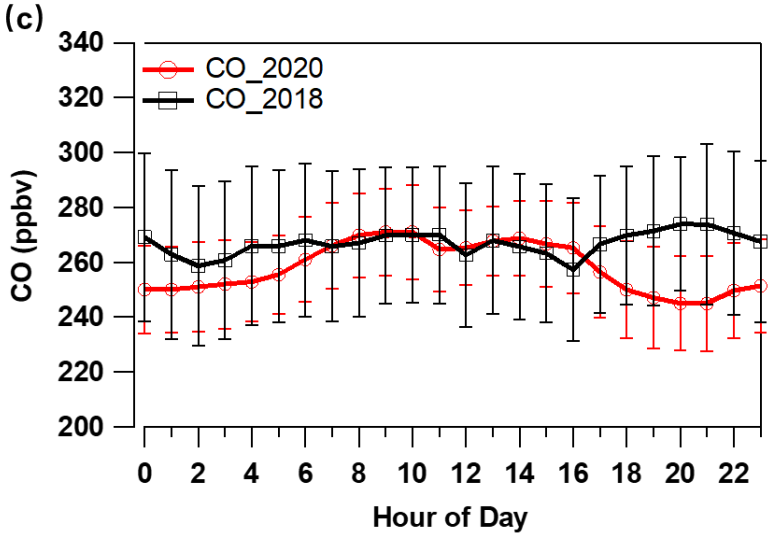
(c)
CO_2020
CO_2018
CO (ppbv)
340
320
300
280
260
240
220
200
0
2
4
6
8
10
12
14
16
18
20
22
Hour of Day

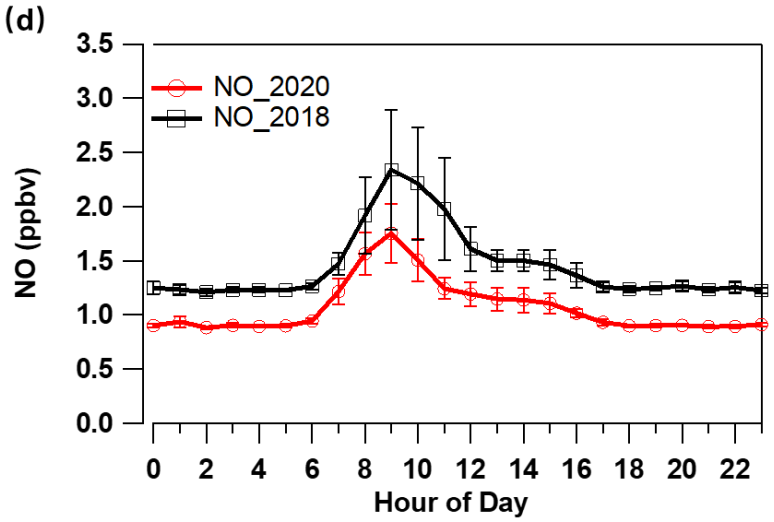
(d)
NO_2020
NO_2018
NO (ppbv)
3.5
3.0
2.5
2.0
1.5
1.0
0.5
0.0
0
2
4
6
8
10
12
14
16
18
20
22
Hour of Day

(e)

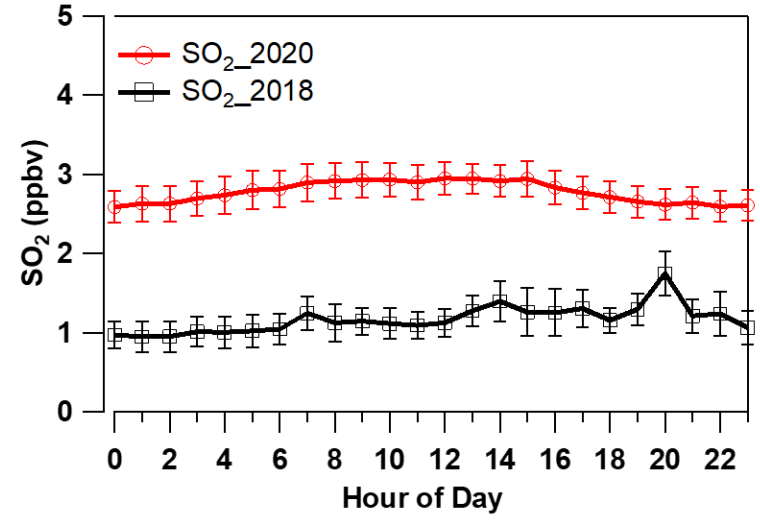
SO2_2020
SO2_2018
SO2 (ppbv)
Hour of Day

(f)

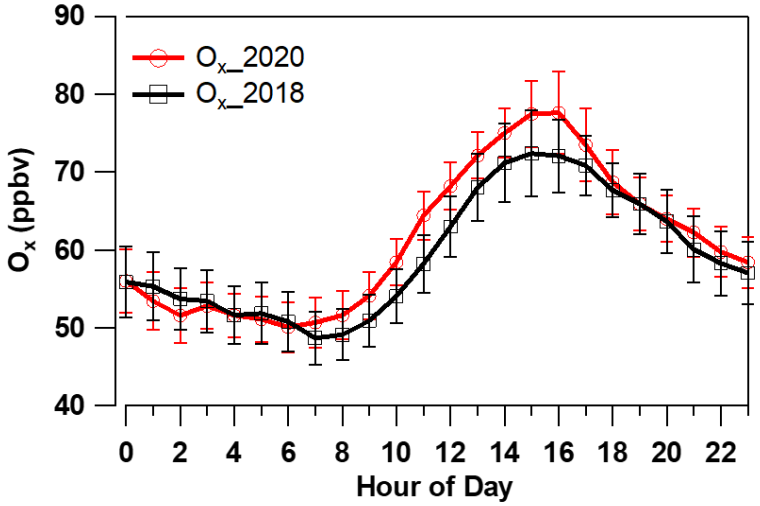
Ox_2020
Ox_2018
Ox (ppbv)
Hour of Day

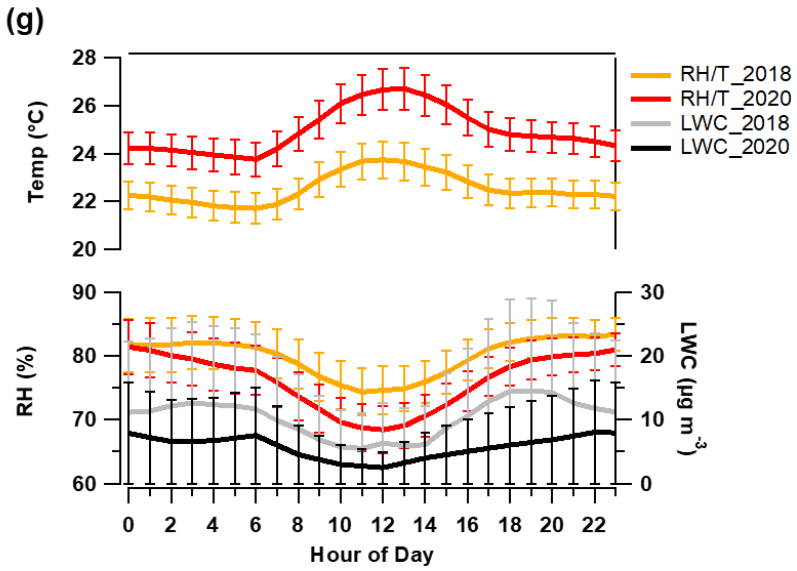

Figure 6-3 Comparison of diel cycles of particle-phase and gas-phase pollutants between 2018 (black) and 2020 (red): (a) PM_1, (b) $PM_{2.5}$, (c) CO, (d) NO, (e) SO_2, (f) O_x, and (g) meteorological conditions and calculated LWC values

The levels of VOCs at this site during the two sampling periods were also compared, as shown in Table 6-1. These data were measured using online GC-FID by HKEPD (Wang et al., 2017). Note: due to the limited data collection rate of online instruments, isoprene data were not compared here. It was clearly seen that all the VOC levels were lower in 2020 than in 2018. Since these VOC species were mainly emitted from anthropogenic sources such as gasoline/diesel exhaust, LPG vehicles and/or solvent use (Ling et al., 2014; Lyu et al., 2017a), the results implied less anthropogenic emissions during the 2020 sampling campaign, compared to the 2018 sampling campaign. As alkanes and alkenes were mainly from different types of vehicles, their emission reductions were due to significantly lower VOCs emitted by vehicles in 2020 compared to 2018 (~ 19.8% - 62.5%). For example, *i*/*n*-butanes were mainly emitted from LPG vehicles. It was found that emissions from LPG vehicles fell by around 46.8% - 48.6% in 2020. In addition, *i*/*n*-pentanes were reduced by 43.4% - 62.5%, meaning less VOC

emissions from gasoline vehicles. These results are consistent with the fact that fewer vehicles were on the road in 2020 due to the COVID-19 pandemic (HKATC, 2018, 2020). Indeed, NO_x levels at the roadside sites were also reduced. Furthermore, among these VOCs, xylenes had the highest reduction, indicating a sharp decline in construction work in Hong Kong, as xylenes were mainly emitted from solvent use. All evidence pointed to significant reductions in anthropogenic emissions during the 2020 sampling campaign due to the impact of COVID-19 on human activities.

Table 6-1. Comparison of VOC levels in 2018 and 2020 sampling periods. The reduction percentage of each VOC is calculated as (VOC mixing ratio$_{2018}$ - VOC mixing ratio$_{2020}$) / VOC mixing ratio$_{2018}$)

VOC species	**2018 (ppbv)**	**2020 (ppbv)**	**Percentage of reduction**
Ethane	1.97±0.06	1.58±0.04	19.8%
Propane	1.53±0.07	1.04±0.04	32.0%
Propene	0.13±0.01	0.09±0.004	30.8%
i-Butane	0.70±0.04	0.36±0.02	48.6%
n-Butane	0.94±0.08	0.50±0.03	46.8%
i-Pentane	0.53±0.03	0.30±0.01	43.4%
n-Pentane	0.48±0.04	0.18±0.007	62.5%
Benzene	0.36±0.01	0.14±0.004	61.1%
Toluene	0.57±0.04	0.27±0.02	52.6%
Ethylbenzene	0.12±0.01	0.04±0.003	66.7%

m,p-Xylene	0.31±0.03	0.03±0.003	90.3%
o-Xylene	0.14±0.02	0.04±0.003	71.4%

Figure 6-4 compares the bulk compositions as a function of NR-PM_1 levels in the two sampling campaigns. Notably, all bulk components (organics, sulfate, nitrate, ammonium, chloride) increased significantly with the increase of NR-PM_1 levels in both years when the NR-PM_1 values were in the range of 0-30 μg/m^3, suggesting the potential roles of photochemical oxidation that promoted the formation of SOAs and SIAs during these two sampling campaigns. Furthermore, sulfate did not show continuous increase when NR-PM_1 was higher than ~30 μg/m^3 in 2020, while it increased continuously with the increase of NR-PM_1 levels in 2018. Since we found in the 2018 sampling campaign that aqueous processes contributed to the formation of submicron particles at this site, differences in sulfate variations implied that aqueous processes may play a less important role in the formation of submicron nonrefractory particles in the 2020 sampling campaign than photochemical processes.

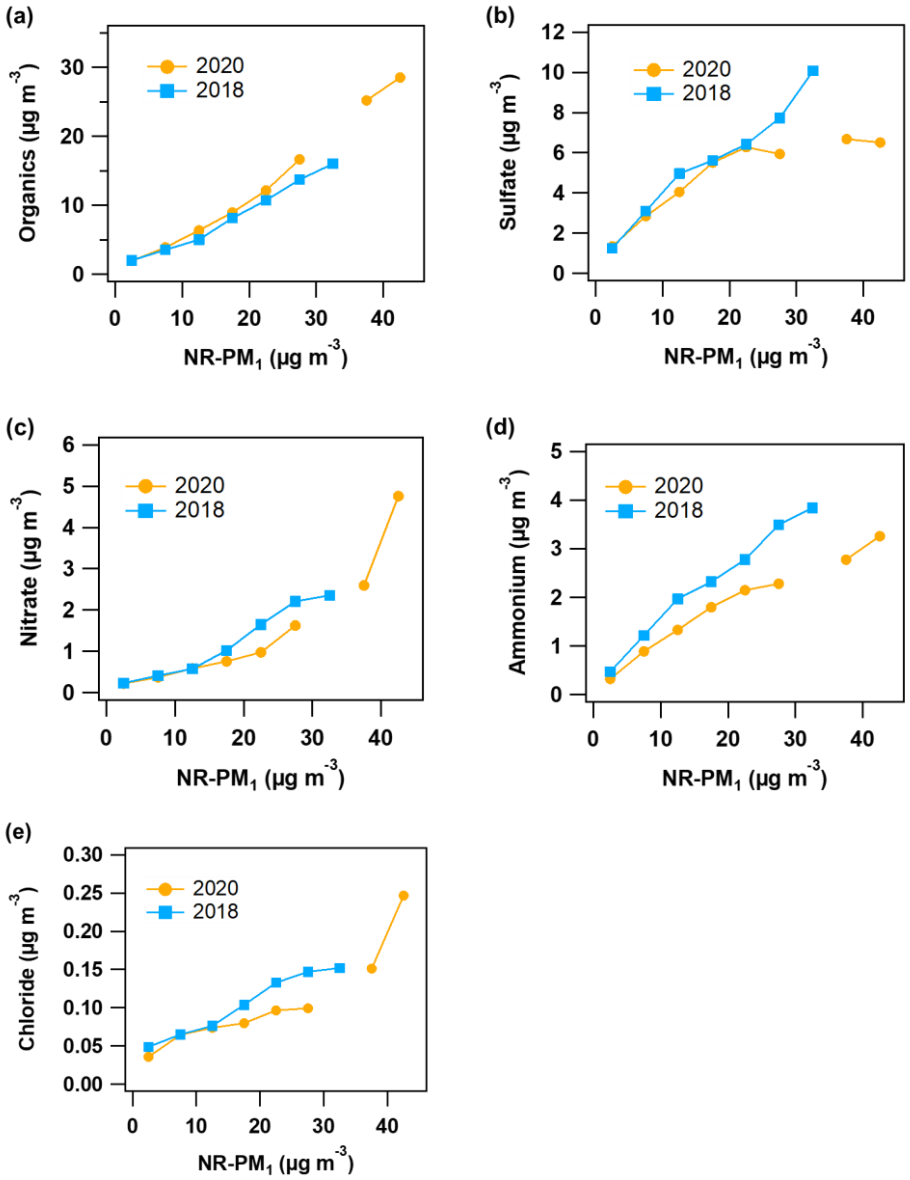

Figure 6-4 Correlations of mass concentrations of bulk compositions with NR-PM_1 levels in the 2020 (yellow) and 2018 (blue) sampling campaigns. The data are grouped in NR-PM_1 bins (5 µg/m^3 increment).

6.3 Source apportionment of OAs at HT in 2020

Receptor model was applied to the measured organics to study the source contributions to OAs. Detailed procedures and criteria for selecting OA factors were discussed in Chapter 5. In brief, 4 factors were identified, including a factor of hydrocarbon-like OA (HOA) and three factors representing OOAs (SOA). The HOA factor contained abundant alkyl fragments ($C_nH_{2n+1}^+$ and $C_nH_{2n-1}^+$), such as m/z 41 ($C_3H_5^+$), 43 ($C_3H_7^+$), 55 ($C_4H_7^+$) and 57 ($C_4H_9^+$), in line with previously reported HOA spectra (Ng et al., 2011; Sun et al., 2011), which are mainly related to primary emissions from fossil fuel combustion (Zhang et al., 2005; Lanz et al., 2008). The OOA factors had lower loadings of alkyl fragments and higher loadings of oxygenated species such as m/z 44 (mainly CO_2^+) than the HOA factor. According to the ratios of H:C and O:C, the three OOA factors were divided into less oxidized OOAs (LO-OOA1 and LO-OOA2), and more oxidized OOA (MO-OOA). The proportions of the four OA sources are shown in Figure 6-5 (a). Overall, POA (HOA) accounted for only 17.9 ± 0.7% of total organics, while OOAs dominated (82.1 %) because the site was less affected by primary emissions. Among the three OOAs, MO-OOA was the largest source of OAs with a contribution of 45.1 ± 1.0%, indicating a high oxidation level of OAs at this site. LO-OOA1 ranked second, accounting for an average of 31.7 ± 0.8% of total organics throughout the sampling campaign. The factor LO-OOA2 made the smallest and relatively stable contribution (5.3 ± 0.3%) throughout the field campaign, possibly representing the background level of OOA at the site.

Figure 6-5 (b) shows the diurnal variations of the four PMF-resolved OA sources. HOA source had the highest concentration in the morning (~8:00, local time), corresponding to the peak of HOA in urban areas (Lee et al., 2015; Yao et al., 2021). Both LO-OOA1 and MO-OOA peaked around 3:00 pm, indicating strong photochemical secondary

formation of OOAs at this site in 2020. While there was a potential transformation from LO-OOA1 to MO-OOA at this site, the peaks appeared at the same time of the day implied different formation processes of these two OOA components in 2020 from those in 2018. Similar to the patterns in 2018, the diurnal variation of LO-OOA2 was small and flat.

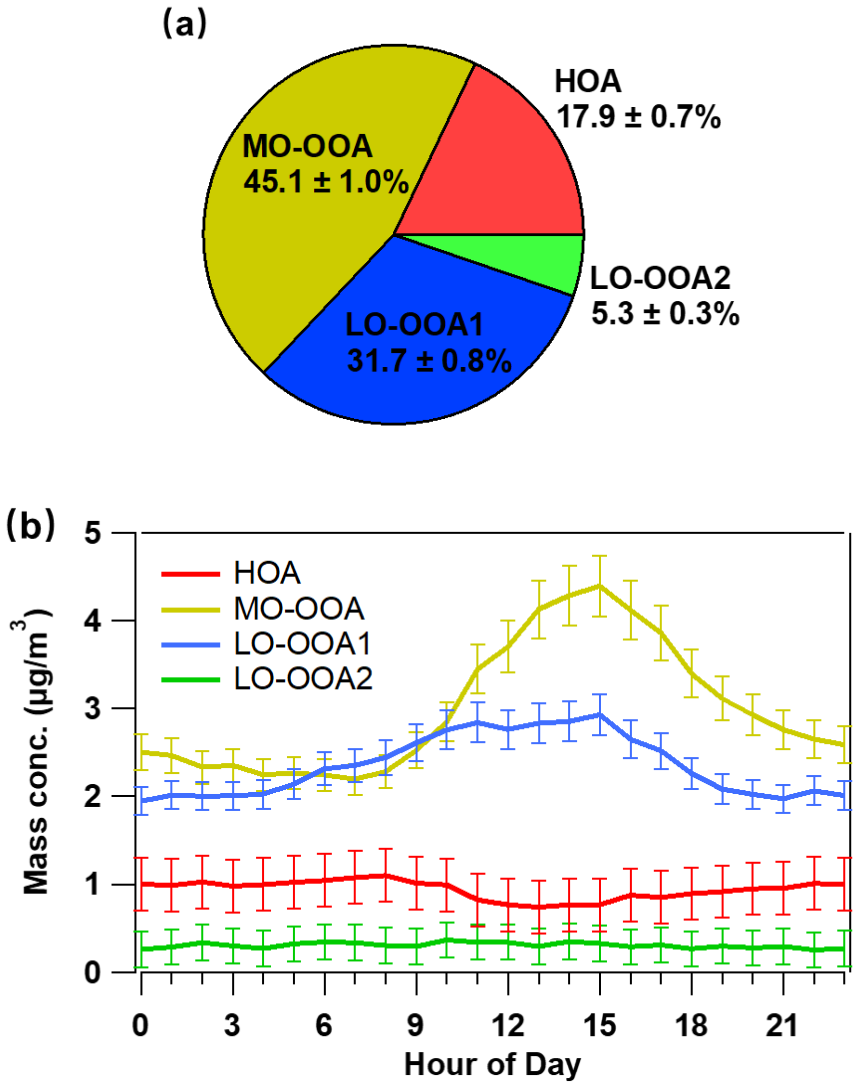

Figure 6-5. (a) Source contributions to total OAs. (b) Diurnal patterns of the OA sources.

The variations of individual sources in the sum of PMF-resolved OAs for the two

sampling campaigns are shown in Figure 6-6 ((a) – (d)). Likewise, the mass concentrations of MO-OOA and LO-OOA1 increased with total OA levels during the 2018 and 2020 sampling campaigns, suggesting that the high OA levels were mainly attributable to these two OOAs. In contrast, the mass concentration of HOA did not increase with total OAs, implying that POA was not a major contributor when OA levels were high at this background site. In addition, the levels of LO-OOA2 elevated with increasing total OAs, indicating that the background OA concentrations might also enhance during periods of high OA. Due to the relatively stable feature of background OOA, the mass concentration of LO-OOA2 was significantly lower than that of MO-OOA and LO-OOA1 ($p < 0.01$).

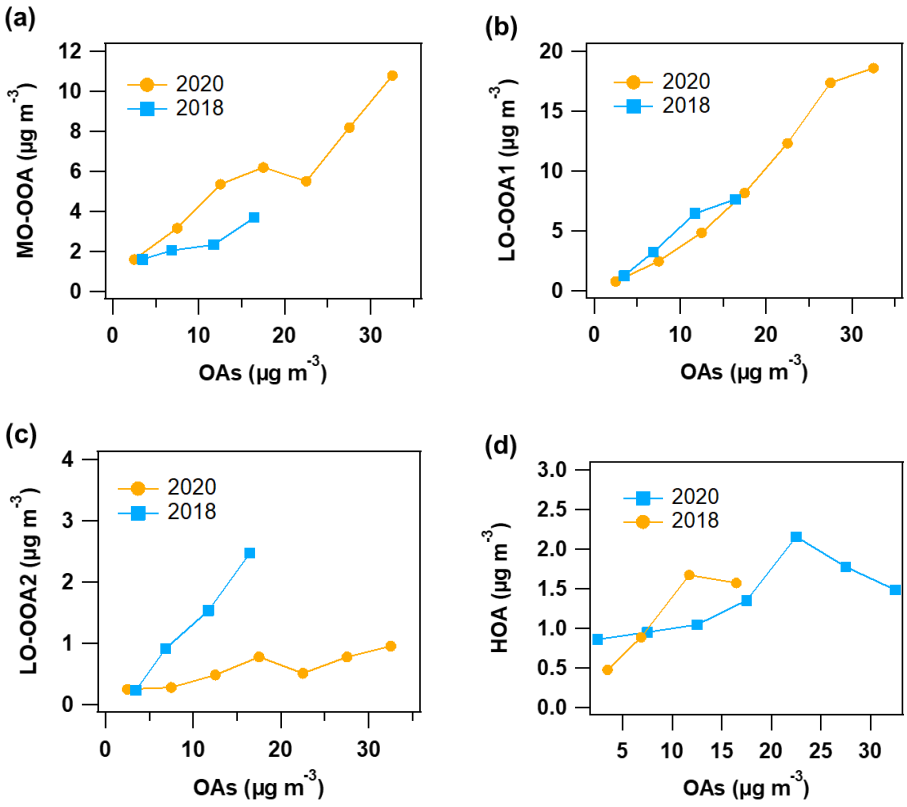

Figure 6-6. Mass concentrations of MO-OOA (a); LO-OOA1 (b); LO-OOA2 (c) and

HOA (d) as a function of OAs in 2020 (yellow) and 2018 (blue). The data are grouped in OA bins (5 μg/m^3 increment).

To understand the similarities and differences in the evolution and formation processes of OOAs between 2018 and 2020, the diurnal variations of LO-OOA1 and MO-OOA in each year are shown in Figure 6-7. Clearly, LO-OOA1 levels were generally higher in 2018, while MO-OOA values were higher in 2020, indicating a higher degree of OA oxidation in 2020. Although LO-OOA1 started to rise in the morning in these two years, the peak time in 2018 (~13:00) was earlier than that in 2020 (~15:00), reflecting the difference in OA evolution processes between 2018 and 2020. In contrast, the peak of MO-OOA in 2018 (~19:00) was later than in 2020 (~15:00) due to the influence of aqueous processes. The rates of increase in daytime MO-OOA and LO-OOA1 were calculated (ΔOA/ Δhour) for the two sampling campaigns. The levels of MO-OOA were found to increase much faster in 2020 (2018: 0.11 μg m^{-3} h^{-1} vs. 2020: 0.30 μg m^{-3} h^{-1}) while the growth rate of LO-OOA1 was higher in 2018 (2018: 0.31 μg m^{-3} h^{-1} vs. 2020: 0.07 μg m^{-3} h^{-1}), further suggesting the different evolution and oxidation processes of OAs between the two years. The evening peak of MO-OOA observed in 2018 implied that aqueous processes might promote the formation of MO-OOA through LO-OOA1, while the same peak hour of MO-OOA and LO-OOA1 (also with O_x) in 2020 suggested that photochemical processes might play a more important role in the formation of OOAs, especially in the formation of MO-OOA.

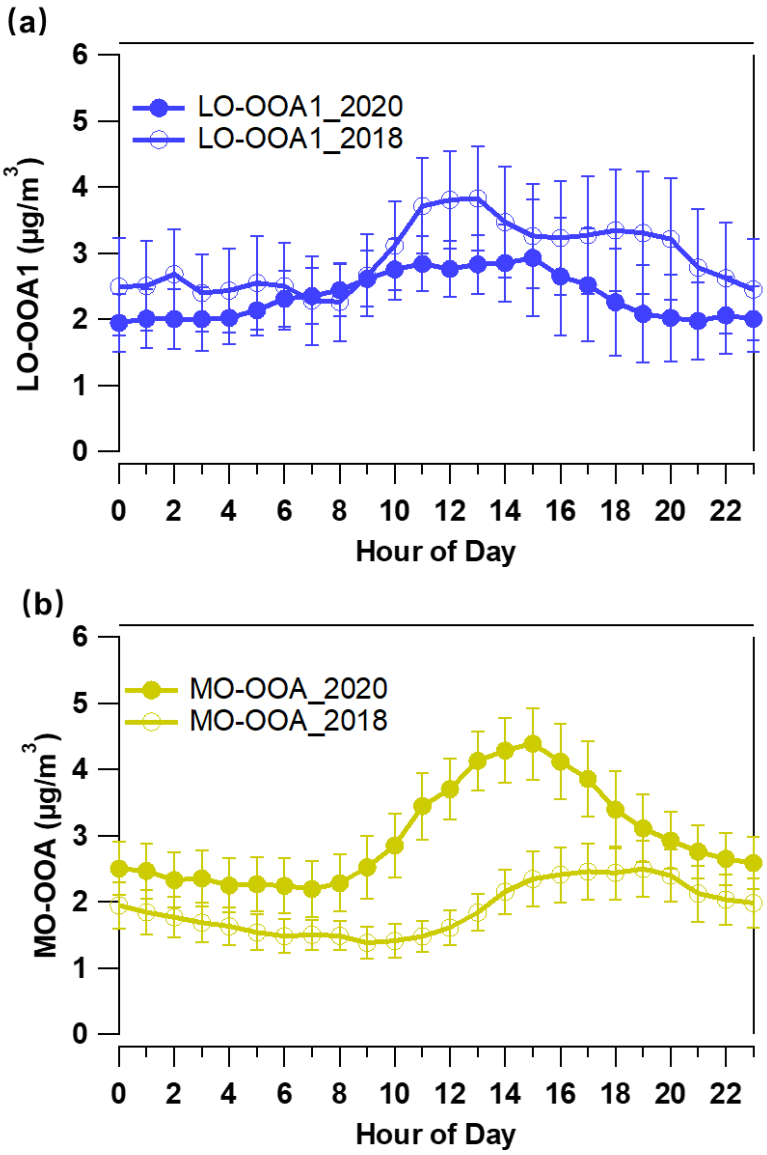

Figure 6-7 Average diurnal cycles of LO-OOA1 (a) and MO-OOA (b) in the two sampling campaigns.

Figure 6-8 compares the average diurnal cycles of H:C and O:C ratios for further insight into aerosol chemistry in these two sampling campaigns. The diurnal trends of H:C and O:C ratios in the two sampling campaigns were basically similar, that is, the H:C ratio showed the highest peak in the morning, and the O:C ratio presented a broad peak from

the afternoon to early evening. Although the variations and peaks in H:C ratios were analogous in these two campaigns, there was a time lag between them, implying differences in photochemical processes between the two years. The daytime O:C ratio from 8:00 to 17:00 in 2020 was generally higher than in 2018, consistent with the high O_x levels during the day in 2020, indicating that secondary organics were more abundant in 2020, possibly due to higher temperatures and O_x levels in the afternoon in 2020, which resulted in stronger photochemical oxidation.

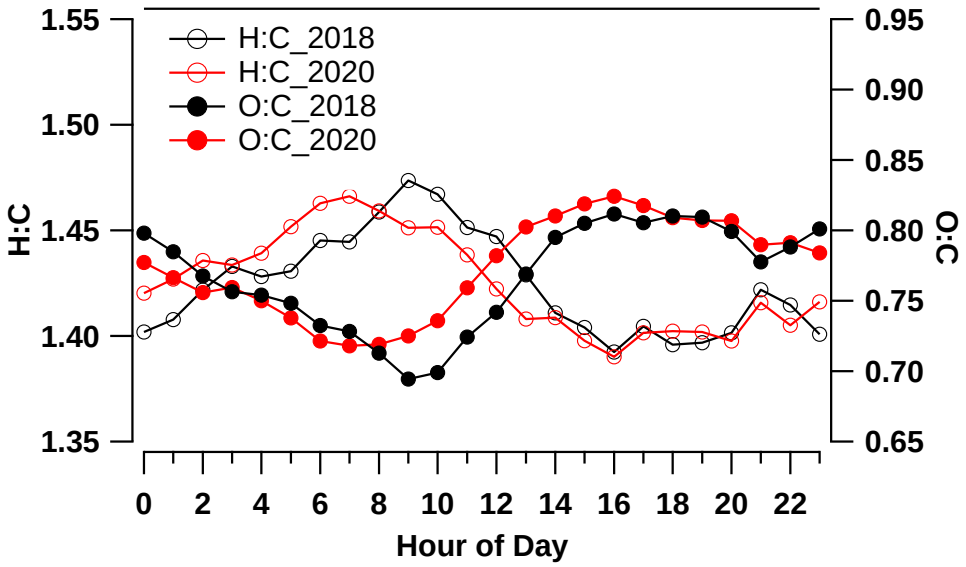

Figure 6-8 Average diurnal cycles of H:C and O/C ratios in the two sampling campaigns

6.4 Similarity and differences of evolution and formation processes of OAs between 2018 and 2020

Since LO-OOA1 and MO-OOA remained the major contributors to OAs in the 2020 sampling campaign, the processes of photochemical oxidation and aqueous formation of these two OOAs were further investigated. Measured O_x levels and RH values were used as indicators of photochemical and aqueous processes, respectively. As shown in Figure 6.9 ((a) – (c)), total organics, MO-OOA and LO-OOA1 all increased significantly with O_x levels. Notably, all OOAs were significantly enhanced in 2020 when O_x was above ~100ppbv, whereas no such high levels of O_x were observed in the 2018 sampling campaign. While we found that photochemical oxidation contributed to the formation of OOAs in 2018 (Section 5.4), the results in 2020 suggested that the levels of OAs could be further enhanced when the photochemical processes were stronger. In contrast, OAs did not show a sustained increase as a function of RH (Figure 6.9 ((d) – (f))). MO-OOA and LO-OOA1 increased with changes in RH at low levels (< 60%) and then decreased at RH> ~60%. This was due to the phase transition of the particles from solid/semisolid to liquid at RH = 40–60% (Liu et al., 2017). Exceptionally, MO-OOA in 2018 increased even at 60% < RH < ~90%, consistent with the finding that aqueous processes contributed to the formation of MO-OOA in 2018 (Section 5.4). The results implied that photochemical processes may play a more important role in the formation of OOAs than aqueous processes in 2020.

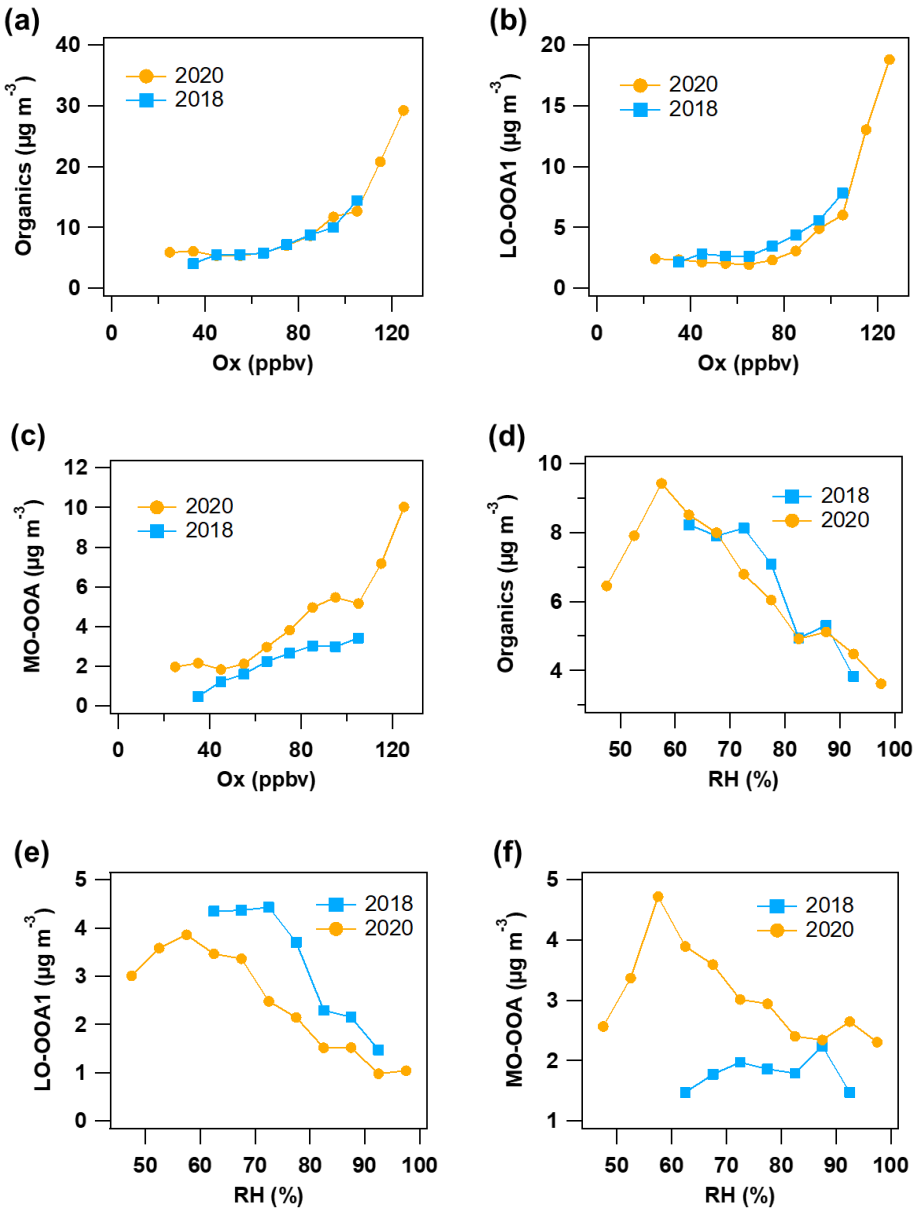

Figure 6-9. Correlations of organics, MO-OOA and LO-OOA1 with O_x ((a)-(c)) and RH ((d)-(f)) in 2020 (yellow) and 2018 (blue). The data are grouped in O_x bins (10 ppbv increment) and RH bins (5% increment), respectively.

To identify specific precursors and formation pathways of SOA, AMS data were uniquely combined with hourly TAG measurements of specific SOA tracers, which

could help us enhance our understanding of OOAs. Figure 6-10 (a) – (h) shows the diurnal patterns of typical OA tracers measured by TAG during the two sampling campaigns. All SOA tracers showed similar diurnal patterns in 2018 and 2020 sampling campaigns, perhaps suggesting relatively stable chemical and physical characteristics between the two sampling campaigns at this site. As typical SOA tracers, malic acid and citramalic acid followed the diurnal pattern of O_x with a peak in the afternoon, so did hydroxybenzoic acids (OHBAs) and 2,3-dihydroxy-4-oxopentanoic acid (DHOPA), suggesting photochemical formation of these OA markers. OHBAs and DHOPA have been reported as SOA tracers derived from oxidation of anthropogenic aromatics (Al-Naiema and Stone, 2017). Since malic acid and citramalic acid also presented similar diurnal trends to OHBAs and DHOPA, anthropogenic VOCs were suspected to be their major precursors (Lyu et al., 2020). In addition, biogenic SOA tracer MT-SOA-T also peaked in the afternoon, implying that its photochemical formation of biogenic VOCs also contributed to the high OOAs in the afternoon. Conversely, Isop-SOA-T concentrations showed a similar pattern to levoglucosan and oleic acid, being higher at night and lowest at noon, suggesting a planetary boundary layer (PBL) effect (Lyu et al., 2020). The same phenomenon was observed in the 2018 campaign by Lyu et al. (2020), who claimed that the detected Isop-SOA-T was a regional background signal that was more influenced by PBL height than by daytime photo-oxidation. However, there was another possibility which was not considered in Lyu et al. (2020). That is, as the precursor of Isop-SOA-T, isoprene peaked at 13:00-15:00 when sea-breezes prevailed at this coastal site, bringing isoprene-containing air masses to the upper atmosphere, where intensive photo-oxidation of isoprene occurred. Due to the unique meteorological characteristics of the study region, sea breezes could persist into late night and then switched to land breezes which recirculated the aged Isop-SOA-T containing air masses to the sampling site after midnight and before dawn. In addition,

the levels of combustion tracer, i.e., levoglucosan were higher in the evening and lowest in early afternoon, perhaps related to the development of PBL, causing downward transport of levoglucosan originated from other regions in the evening (Lyu et al., 2020). Moreover, the diurnal pattern of oleic acid showed a peak at 19:00-20:00, coincident with the regular dinner time of Hong Kong residents (Section 4.3). In conclusion, the above results indicated that photochemical oxidation of anthropogenic and biogenic VOCs was one important pathway for the formation of SOAs and primary OAs could still be detected at this background coastal site. In addition, the diurnal patterns of SOA markers further supported that SOAs in 2020 were more generated from photochemical processes rather than aqueous processes.

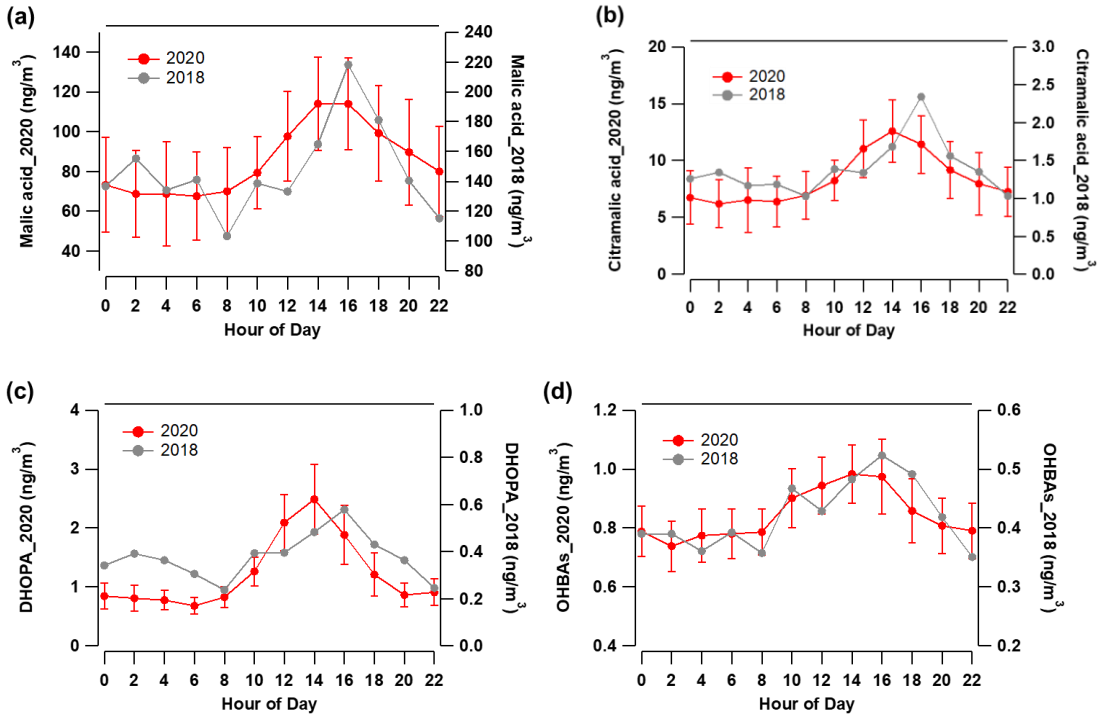

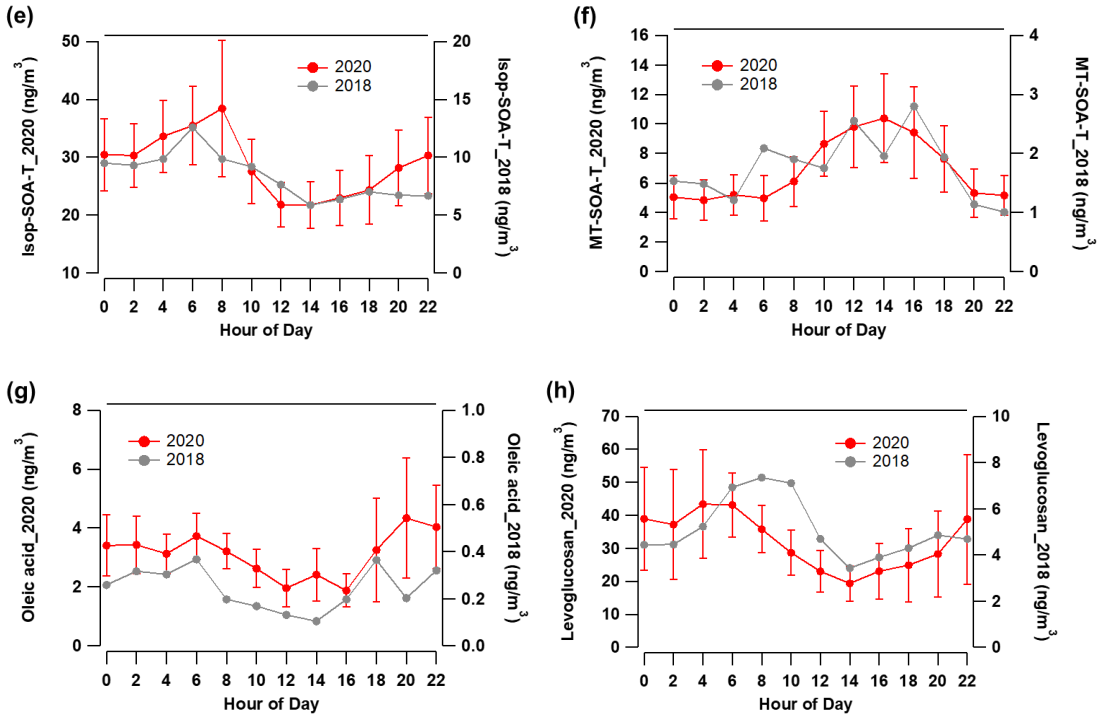

Figure 6-10 Average diurnal variations of SOA tracers measured by TAG: (a) malic acid; (b) citramalic acid; (c) DHOPA; (d) OHBAs; (e) Isop-SOA-T; (f) MT-SOA-T; (g) oleic acid; and (h) levoglucosan and in 2020. Note: Isop-SOA-T stands for isoprene-derived SOA tracers, including 2-methylthreitol, 2-methylerythritol and 2-methylglyceric acid. MT-SOA-T stands for monoterpenes-derived SOA tracers, including 3-methyl-1,2,3-butanetricarboxylic acid, 3-hydroxy-4,4-dimethylglutaric acid and Pinic acid. The grey lines and dots in these figures are data from the 2018 sampling campaign.

To identify possible components of OOAs, we calculated the coefficient of determination (r^2) of LO-OOA1 and MO-OOA with selected OA markers measured by TAG. Similar to what was found in the 2018 sampling campaign, OHBAs and DHOPA showed a diel cycle synchronized with LO-OOA1, suggesting that the potential precursors of LO-OOA1 were aromatics, as OHBAs and DHOPA are likely anthropogenic SOAs formed from aromatics. Furthermore, Figure 6-11 (a) presents the

dependence of LO-OOA1 with OHBAs in different air masses. The moderate correlation between LO-OOA1 and OHBAs in long-range (r^2 = 0.47) and coastal air masses (r^2 = 0.57) also suggested that anthropogenic VOCs might be the main precursors of LO-OOA1 in these cases.

In the 2018 sampling campaign, of all the OA markers, MO-OOA had the best correlation with malic acid (r^2= 0.74), and anthropogenic VOCs were suspected to be the main precursors of malic acid in this sampling campaign (Section 5.4). However, only weak correlation was found between MO-OOA and malic acid in 2020 (r^2= 0.24). Instead, malic acid was found to be related to biogenic emissions in the 2020 sampling campaign (r^2= 0.69 with 2-methylglyceric acid in coastal air masses, and r^2= 0.66 in continental air masses), indicating potential contribution of biogenic SOA to MO-OOA in 2020. Figure 6-11 (b)-(c) presents the scatter plots of MO-OOA with 2-methylglyceric acid and pinic acid in different air masses. Moderate correlations of MO-OOA with 2-methylglyceric acid in continental air mass (r^2= 0.66), with pinic acid in coastal (r^2= 0.64) and long-range (r^2= 0.59) air masses, were found. One possible reason for the difference in the formation of MO-OOA between 2018 and 2020 was that 2-methylglyceric acid was not detected in the 2018 sampling campaign, while the improvement in measuring more OA markers in 2020 allowed us to better interpret the formation of OOAs. Another possible reason was that the higher daytime temperature and oxidative capacity of the 2020 sampling campaign also facilitated the formation of OOA through biogenic emissions. Note that the highest correlation between MO-OOA and 2-methylglyceric acid was found in continental air masses. This may be because 2-methylglyceric acid is usually formed at high NO_x concentrations (Surratt et al., 2010), and the continental air mass in the PRD region is rich in NO_x. The role of these OA markers suggested that, unlike LO-OOA1, which was primarily derived from anthropogenic SOAs, biogenic SOA might also contribute to MO-OOA. In addition,

the red data points with high O_x levels mostly fell on the upper left and upper middle panels of the MO-OOA charts with OA markers, further suggesting that photochemical oxidation played a more important role in the formation of MO-OOA in 2020. In addition, in the graph of the relationship between LO-OOA1 and OHBAs, the red dots appeared in both the middle and the lower right panels, which might be due to the fact that LO-OOA1 was relatively fresh and less affected by photochemical processes than MO-OOA. To sum up, the formation of MO-OOA in 2018 was mainly related to anthropogenic emissions, but primarily to biogenic emissions in 2020. Moreover, the photochemical oxidative capacity in 2020 was higher than that in 2018. The combined effects of stronger photochemical oxidation and biogenic emissions led to more MO-OOA formation in 2020.

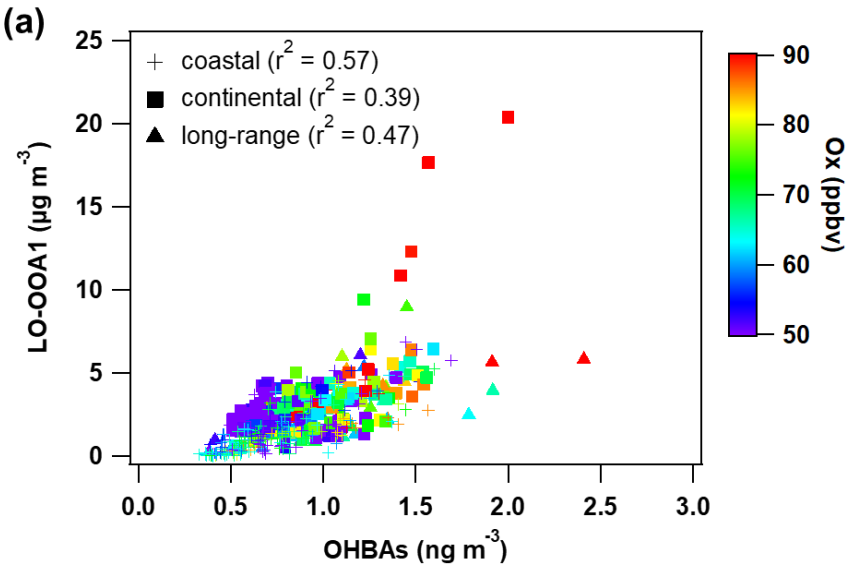

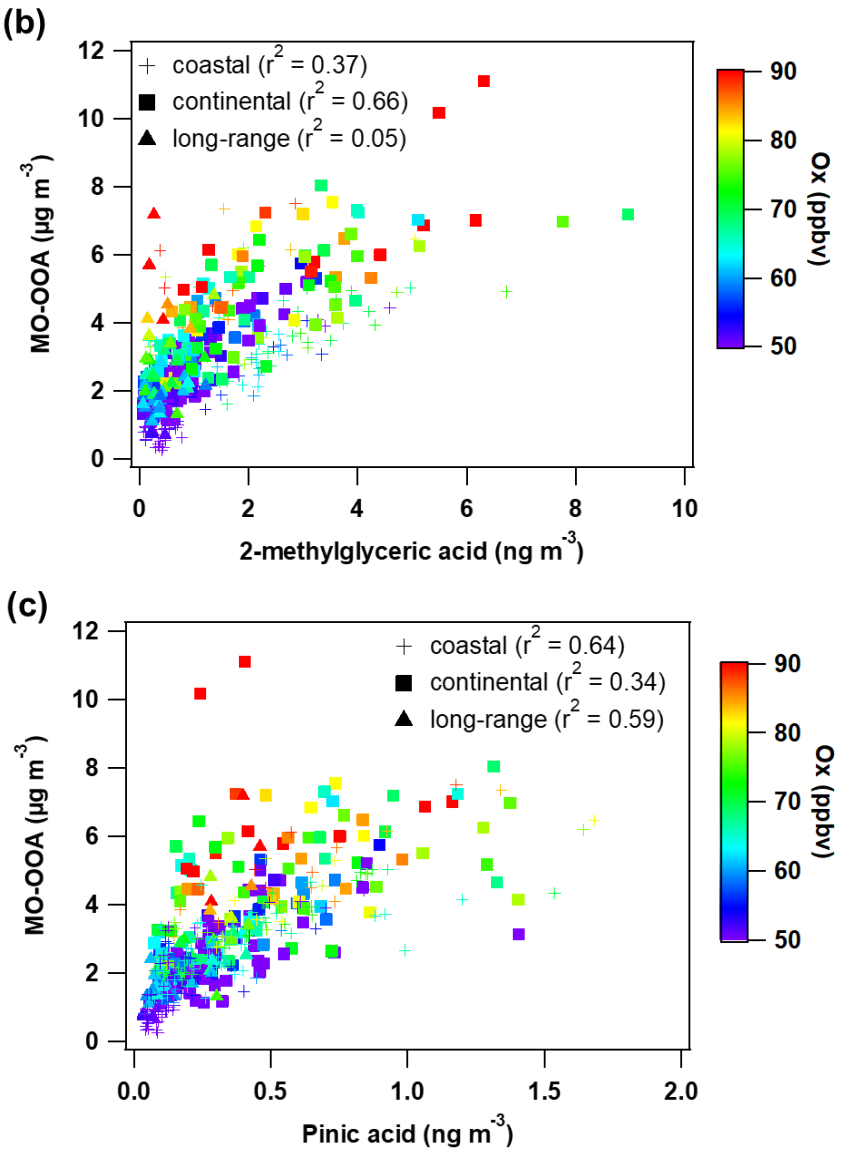

Figure 6-11. Scatter plot of LO-OOA1 versus OHBAs (a), MO-OOA versus 2-methylglyceric acid (b), MO-OOA versus pinic acid (c). OHBAs are the sum of hydroxybenzoic acids. The 72-hour backward trajectories were simulated every 2 hours for the air masses arriving at the site (300 m) using the Hybrid Single-Particle Lagrangian Integrated Trajectory model. The air parcels originated from the coastline of southeast China (coastal), continent with short-range (continental) and long-range trajectory, respectively.

6.5 Conclusion

Comparing aerosol chemistry across years to understand the impacts of changes in emissions and meteorological conditions before and after COVID-19 is critical. In this chapter, a comprehensive sampling campaign was conducted at an urban background site in Hong Kong in autumn 2020 during a similar time period to the 2018 sampling campaign to investigate changes in aerosol sources and formation mechanisms. Organics remained the predominant of all measured components with an average of 6.4 ± 0.2 μg/m^3 and an average fraction of 51.0 ± 0.5 %, higher than the values (6.0 ± 0.2 μg/m^3 and 43.8 ± 0.7 %) at this site in 2018. The diurnal variations of organics and all SIAs in NR-PM_1 showed the highest peak at 15:00, indicating intense photochemical formation of secondary aerosols at this site. Higher daytime (8:00 – 17:00) O_x levels and temperatures during the sampling campaign than in 2018 indicated stronger photochemical processes in 2020. The diurnal peaks of MO-OOA and LO-OOA1 were the same at 15:00, and the levels generally increased with the increase of O_x, implying that the formation of both OOAs was related to photochemical oxidation. The higher O:C ratios during the daytime (8:00-17:00) in 2020 than in 2018 also implied more abundant secondary organics in the afternoon in 2020 than in 2018. By examining molecular OA markers measured by TAG, we sought to explore the formation mechanisms and precursors of SOA. The diel cycles of malic acid, citramalic acid, DHOPA, OHBAs and MT-SOA-T all showed the highest peaks in the afternoon, consistent with OOAs and O_x. These results further suggested that photochemical oxidation played an important role in the formation of SOAs regardless of anthropogenic/ biogenic sources at this site. By calculating the multilinear regression between LO-OOA1/MO-OOA and OA markers measured by TAG, we found that LO-OOA1 was mainly derived from anthropogenic SOAs, while biogenic SOA also

contributed to MO-OOA in 2020, especially in high O_x conditions. These findings, showing different formation processes of OAs at the same site, could enhance our understanding of OAs in urban background areas.

Chapter 7 Conclusions and suggestions for future study

7.1 Conclusions

This thesis investigated the characteristics, sources, and formation processes of OAs in urban roadside site and urban background site in Hong Kong. The proportion and evolution process of COA and two OOAs was well studied. In addition, this thesis attempted to conduct an in-depth study of the relationship between OAs and precursors. Furthermore, this study explored the interannual and inter-site variabilities of OA pollution in Hong Kong. The main findings of this study are as follows:

1) The characteristics, sources and evolution of OAs in the roadside environment were studied. A significant contribution of cooking emissions to OAs was found at the high-traffic site, even greater than that of vehicular emissions. Especially on Sundays, the peak COA levels were even higher, implying that COA was the main cause of high OA concentrations in urban roadside environments in Hong Kong.
2) The oxidation degree of cooking emissions in the atmosphere was investigated and found to be related to atmospheric O_x. The variation of $C_3H_3O^+$ / $C_3H_5O^+$ in this study was opposite to the daytime pattern of O_x, indicating that COA emitted elsewhere was progressively oxidized, resulting in enhanced OOA in the roadside environment, especially in the afternoon when photochemical reactions are usually strong.
3) High loadings of SOA-dominated organics in NR-PM_1 in cool season were found at an urban background site along the southern coastline of China, where organic aerosol chemistry might be complicated due to interactions of air pollutants from different source origins and variable meteorological conditions.

It has been demonstrated that a more variable and more concentrated LO-OOA component than its counterpart was primarily formed by photochemical oxidation of aromatics. The formation processes seemed not to be limited by O_x and LWC due to poor correlations.

4) The formation of MO-OOA was related to photochemical oxidation and aqueous processes in the 2018 sampling campaign. However, there was no clear conclusion about the precursors of MO-OOA. Nevertheless, a potential shift from LO-OOA to MO-OOA has been proposed involving aqueous processes.
5) A detailed comparison of aerosol chemistry before and during the COVID-19 pandemic was performed at an urban background site in Hong Kong. Temporal variations in chemical species of NR-PM_1 and air pollutants suggested that this site was more photochemically reactive in the 2020 sampling campaign than in 2018. Higher values of daytime OOAs and O:C ratios in 2020 implied stronger photochemical oxidation, leading to more abundant secondary organics in 2020. The diurnal patterns of SOA markers supported the inference that MO-OOA and LO-OOA1 were more related to photochemical processes in 2020, which caused by the stronger photochemical capacity in the atmosphere.
6) Photochemical oxidation of anthropogenic and biogenic VOCs was one important pathway for the formation of SOAs, and primary OAs could still be detected at the background coastal site. Analysis on the relationships of LO-OOA1 and MO-OOA with OA molecular markers suggested that LO-OOA1 mainly consisted of anthropogenic SOAs, while biogenic SOAs might contribute to MO-OOA.

7.2 Limitations and suggestions for future study

Although this study enriched the literature archives in the field of OA pollution in Hong Kong, there are still limitations. To further understand the OA pollution, the following suggestions are made for future research.

1) In this study, source apportionment of OAs was conducted at roadside and urban background sites in Hong Kong. While AMS provides high time resolution data for source apportionment, it can only give information on fragments of submicron particles, making it difficult to identify some specific emission sources. For example, HOA resolved in ambient air could from different types of vehicles and some burning sources (Mohr et al., 2009; Collier et al., 2015). It was also found that ambient LO-OOA could be overestimated due to the high similarities with other factors such as COA (Zhou et al., 2021). To improve the interpretability of the resolved factors through AMS data, it was useful to explore the AMS chemical profiles of specific sources and the aging products. Through the chassis dynamometer tests, we could get the specific source profiles from gasoline or diesel vehicles. It was also worth studying the elemental compositions of OOA generated from oxidation of known VOC precursors by combining AMS and potential aerosol mass (PAM) oxidation flow reactors. Besides, further modification of AMS by connecting an online GC in front of AMS or combine AMS data with in-situ data of OA markers measured by TAG-ToF-MS could enhance the ability of source apportionment of atmospheric OAs.
2) Due to the influence of transboundary transport and the spatially variable characteristics of OA sources, regional contribution and spatial characteristics of local sources in Hong Kong needed further investigation. It was important to

integrate observations at multiple locations and identify differences in OA sources by air mass origins. Field observation in the upwind region could also be done to separate the OAs from local sources and transboundary transport. Besides, vehicle cruise measurement of OAs would provide a detailed map of organic aerosols and the sources in different areas in Hong Kong.

3) In this study, we provided the insights of the potential precursors of MO-OOA and LO-OOA1. However, the exact precursors of OOAs are highly uncertain, making it hard to provide clear policy recommendations. To determine the specific precursors of OOAs, the correlation between OOA components and VOCs or OA markers derived from defined VOCs (e.g., isoprene SOA, monoterpenes SOA, and aromatics SOA measured by TAG-ToF-MS) could be studied. Combination of AMS and PAM could get the OOA yields of different VOC precursors and some specific source emission mixtures, thus understanding the precursors of OOAs in the atmosphere.
4) We found oxidation of COA (a significant OA in Hong Kong) in the atmosphere and potential conversion from LO-OOA to MO-OOA, but it is unknown how COA and LO-OOA were oxidized and what the influencing factors were (e.g. liquid water content, particle acidity, and particle surface area). The more detailed OA evolution and oxidation processes in the atmosphere could be further investigated. One possible way was to examine the evolutions of characteristic ion fragments of OA components to explore the processes. The processes could be speculated through looking into the conversion of OA tracers. The relationship between the potential influencing factors and OAs could also be checked. In addition, chamber experiments could also be used to investigate the evolution processes of OAs. COAs or LO-OOA from PAM could be used as

seed aerosols. Different gradients of oxidants (ozone or OH) and influencing factors could be set in the experiments.

References

Aiken, A. C., DeCarlo, P. F., Kroll, J. H., Worsnop, D. R., Huffman, J. A., Docherty, K. S., Ulbrich, I. M., Mohr, C., Kimmel, J. R., Sueper, D., Sun, Y., Zhang, Q., Trimborn, A., Northway, M., Ziemann, P. J., Canagaratna, M. R., Onasch, T. B., Alfarra, M. R., Prevot, A. S. H., Dommen, J., Duplissy, J., Metzger, A., Baltensperger, U., and Jimenez, J. L.: O/C and OM/OC ratios of primary, secondary, and ambient organic aerosols with High-Resolution Time-of-Flight Aerosol Mass Spectrometry, Environ. Sci. Technol., 42, 4478–4485, doi: 10.1021/es703009q, 2008.

Al-Naiema, I. M. and Stone, E. A.: Evaluation of anthropogenic secondary organic aerosol tracers from aromatic hydrocarbons, Atmos. Chem. Phys., 17, 3, 2053-2065, doi: org/10.5194/acp-17-2053-2017, 2017.

Brege, M., Paglione, M., Gilardoni, S., Decesari, S., Facchini, M. C. and Mazzoleni, L. R.: Molecular insights on aging and aqueous-phase processing from ambient biomass burning emissions-influenced Po Valley fog and aerosol, Atmos. Chem. Phys., 18(17), 13197-13214, doi: org/10.5194/acp-18-13197-2018, 2018.

Canagaratna, M. R., Jayne, J. T., Jimenez, J. L., Allan, J. D., Alfarra, M. R., Zhang, Q., Onasch, T. B., Drewnick, F., Coe, H., Middlebrook, A., Delia, A., Williams, L. R., Trimborn, A. M., Northway, M. J., DeCarlo, P. F., Kolb, C. E., Davidovits, P., and Worsnop, D. R.: Chemical and microphysical characterization of ambient aerosols with the aerodyne aerosol mass spectrometer, Mass Spectrom. Rev., 26, 185-222, doi: 10.1002/mas.20115, 2007.

Canagaratna, M. R., Onasch, T. B., Wood, E. C., Herndon, S. C., Jayne, J. T., Cross, E. S., Miake-Lye, R. C., Kolb, C. E., and Worsnop, D. R.: Evolution of vehicle exhaust

particles in the atmosphere, J. Air Waste Manage. Assoc., 60, 1192–1203, doi: 10.3155/1047-3289.60.10.1192, 2010.

Canagaratna, M. R., Jimenez, J. L., Kroll, J. H., Chen, Q., Kessler, S. H., Massoli, P., Hildebrandt Ruiz, L., Fortner, E., Williams, L. R., Wilson, K. R., Surratt, J. D., Donahue, N. M., Jayne, J. T., and Worsnop, D. R.: Elemental ratio measurements of organic compounds using aerosol mass spectrometry: characterization, improved calibration, and implications, Atmos. Chem. Phys., 15, 253- 272, doi:10.5194/acp-15-253-2015, 2015.

Chan, H.: Removal and recycling of pollutants from Hong Kong restaurant wastewaters, Bioresour. Technol., 17, 6859-6867, doi: 10.1016/j.biortech.2010.03.104, 2010.

Cheung, H. C., Wang, T., Baumann, K., and Guo, H.: Influence of regional pollution outflow on the concentrations of fine particulate matter and visibility in the coastal area of southern China, Atmos. Environ., 39, 6463-6474, doi: 10.1016/j.atmosenv.2005.07.033, 2005.

Cheung K, Ling Z. H., Wang D. W., Wang Y, Guo H., Lee B., Li Y. J., and Chan C. K.: Characterization and source identification of sub-micron particles at the HKUST Supersite in Hong Kong, Sci. Total Environ., 527-528, 287-296, doi: 10.1016/j.scitotenv.2015.04.087, 2015.

Chirico, R., DeCarlo, P. F., Heringa, M. F., Tritscher, T., Richter, R., Prévôt, A. S. H., Dommen, J., Weingartner, E., Wehrle, G., Gysel, M., Laborde, M. and Baltensperger, U.: Impact of aftertreatment devices on primary emissions and secondary organic aerosol formation potential from in-use diesel vehicles: results from smog chamber experiments, Atmos. Chem. Phys., 10, 11545-11563, doi: 10.5194/acp-10-11545-2010, 2010.

Clapp, L. J., and Jenkin, M. E.: Analysis of the relationship between ambient levels of O_3, NO_2 and NO as a function of NO_x in the UK, Atmos. Environ., 35, 6391-6405, doi: org/10.1016/S1352-2310(01)00378-8, 2001.

Collier, S., Zhou, S., Kuwayama, T., Forestieri, S., Brady, J., Zhang, M., Kleeman, M., Cappa, C., Bertram, T., and Zhang, Q.: Organic PM Emissions from Vehicles: Composition, O /C Ratio, and Dependence on PM Concentration, Aerosol Sci. Tech., 49, 86–97, 2015.

DeCarlo, P. F., Kimmel, J. R., Trimborn, A., Northway, M. J., Jayne, J. T., Aiken, A. C., Gonin, M., Fuhrer, K., Horvath, T., Docherty, K. S., Worsnop, D. R., and Jimenez, J. L.: Field-deployable, high-resolution, time-of-flight aerosol mass spectrometer, Anal. Chem., 78, 8281-8289, doi: 10.1021/ac061249n, 2006.

DeCarlo, P. F., Dunlea, E. J., Kimmel, J. R., Aiken, A. C., Sueper, D., Crounse, J., Wennberg, P. O., Emmons, L., Shinozuka, Y., Clarke, A., Zhou, J., Tomlinson, J., Collins, D. R., Knapp, D., Weinheimer, A. J., Montzka, D. D., Campos, T., and Jimenez, J. L.: Fast airborne aerosol size and chemistry measurements above Mexico City and Central Mexico during the MILAGRO campaign, Atmos. Chem. Phys., 8, 4027–4048, doi: org/10.5194/acp-8-4027-2008, 2008.

DeCarlo, P. F., Ulbrich, I. M., Crounse, J., de Foy, B., Dunlea, E. J., Aiken, A. C., Knapp, D., Weinheimer, A. J., Campos, T., Wennberg, P. O., and Jimenez, J. L.: Investigation of the sources and processing of organic aerosol over the Central Mexican Plateau from aircraft measurements during MILAGRO, Atmos. Chem. Phys., 10, 5257–5280, doi: 10.5194/acp-10-5257-2010, 2010.

de Gouw, J. and Jimenez, J. L.: Organic aerosols in the Earth's atmosphere, Environ. Sci. Technol., 43, 7614–7618, doi: 10.1021/es9006004, 2009.

Dockery, D. W., Pope, C. A., Xu, X., Spengler, J. D., Ware, J. H., Fay, M. E., Ferris, B. G. and Speizer, F. E.: An association between air pollution and mortality in six US cities, N. Engl. J. Med., 329, 1753-1759, doi: 10.1056/NEJM199312093292401, 1993.

Elser, M., Huang, R. J., Wolf, R., Slowik, J. G., Wang, Q., Canonaco, F., and Prévôt, A. S.: New insights into $PM_{2.5}$ chemical composition and sources in two major cities in China during extreme haze events using aerosol mass spectrometry, Atmos. Chem. Phys., 16(5), 3207-3225, 2016.

Friese, E. and Ebel, A.: Temperature dependent thermodynamic model of the system $H^+ - NH_4^+ - Na^+ - SO_4^{2-} - NO_3^- - Cl^- - H_2O$, J. Phys. Chem. A, 114(43), 11595-11631, 2010.

Gordon, T. D., Presto, A. A., Nguyen, N. T., Robertson, W. H., Na, K., Sahay, K. N., Zhang, M., Maddox, C., Rieger, P., Chattopadhyay, S., Maldonado, H., Maricq, M. M. and Robinson, A. L.: Secondary organic aerosol production from diesel vehicle exhaust: impact of aftertreatment, fuel chemistry and driving cycle, Atmos. Chem. Phys., 14, 4643-4659, doi: 10.5194/acp-14-4643-2014, 2014a.

Gordon, T. D., Presto, A. A., May, A. A., Nguyen, N. T., Lipsky, E. M., Donahue, N. M., Gutierrez, A., Zhang, M., Maddox, C., Rieger, P., Chattopadhyay, S., Maldonado, H., Maricq, M. M. and Robinson, A. L.: Secondary organic aerosol formation exceeds primary particulate matter emissions for light-duty gasoline vehicles, Atmos. Chem. Phys., 14, 4661-4678, doi: 10.5194/acp-14-4661-2014, 2014b.

Guo, H., Ding, A. J., So, K. L., Ayoko, G., Li, Y. S., and Hung, W. T.: Receptor modeling of source apportionment of Hong Kong aerosols and the implication of urban and regional contribution, Atmos. Environ., 43, 1159-1169, doi: 10.1016/j.atmosenv.2008.04.046, 2009.

Han, L., Zhou, W., and Li, W.: Fine particulate ($PM_{2.5}$) dynamics during rapid urbanization in Beijing, 1973–2013, Sci. Rep., 6, 23604, doi: 10.1038/srep23604, 2016.

He, L. Y., Hu, M., Huang, X. F., Yu, B. D., Zhang, Y. H., and Liu, D. Q.: Measurement of emissions of fine particulate organic matter from Chinese cooking, Atmos. Environ., 38, 6557-6564, doi: 10.1016/j.atmosenv.2004.08.034, 2004.

Heald, C. L., Kroll, J. H., Jimenez, J. L., Docherty, K. S., DeCarlo, P. F., Aiken, A. C., Chen, Q., Martin, S. T., Farmer, D. K., and Artaxo, P.: A simplified description of the evolution of organic aerosol composition in the atmosphere, Geophys. Res. Lett., 37, L08803, doi:10.1029/ 2010gl042737, 2010.

Hildebrandt Ruiz, L., Paciga, A. L., Cerully, K., Nenes, A., Donahue, N. M., and Pandis, S. N.: Aging of secondary organic aerosol from small aromatic VOCs: changes in chemical composition, mass yield, volatility and hygroscopicity, Atmos. Chem. Phys. Discuss., 14, 31441–31481, doi:10.5194/acpd-14-31441-2014, 2014.

Hong Kong Annual Traffic Census 2017 Edition (HKATC). Accessible at: https://www.td.gov.hk/filemanager/en/content_4915/annual%20traffic%20census%202017.pdf, 2017.

Hong Kong Annual Traffic Census 2018 Edition (HKATC). Accessible at: https://www.td.gov.hk/filemanager/en/content_4953/annual%20traffic%20census%202018.pdf, 2018.

Hong Kong Annual Traffic Census 2020 Edition (HKATC). Accessible at: https://www.td.gov.hk/filemanager/en/content_5114/annual%20traffic%20census%202020.pdf, 2020.

Hong Kong Environmental Protection Department (HKEPD), Air Quality in Hong Kong 2017, Accessible at http://www.aqhi.gov.hk/api_history/english/report/files/AQR2017e_final.pdf, 2017.

Hu, D., Bian, Q., Lau, A. K., and Yu, J. Z.: Source apportioning of primary and secondary organic carbon in summer PM2.5 in Hong Kong using positive matrix factorization of secondary and primary organic tracer data, J. Geophys. Res., 115, D16204, doi: 10.1029/2009JD012498, 2010.

Hu, D., and Yu, J. Z.: Secondary organic aerosol tracers and malic acid in Hong Kong: seasonal trends and origins, Environ. Chem., 10, 5, 381-394, doi:org/10.1071/EN13104, 2013.

Hu, W., Hu, M., Hu, W., Jimenez, J. L., Yuan, B., Chen, W., Wang, M., Wu, Y., Chen, C., Wang, Z., Peng, J., Zeng, L., and Shao, M.: Chemical composition, sources and aging process of sub-micron aerosols in Beijing: contrast between summer and winter, J. Geophys. Res., 121, 1955–1977, doi: 10.1002/2015JD024020, 2016.

Hu, W., Hu, M., Hu, W. W., Zheng, J., Chen, C., Wu, Y., and Guo, S.: Seasonal variations in high time-resolved chemical compositions, sources, and evolution of atmospheric submicron aerosols in the megacity Beijing, Atmos. Chem. Phys., 17, 9979-10000, doi: 10.5194/acp-17-9979-2017, 2017.

Huang, X. H., Bian, Q. J., Louie, P. K., and Yu, J. Z.: Contributions of vehicular carbonaceous aerosols to PM2.5 in a roadside environment in Hong Kong, Atmos. Chem. Phys., 14, 9279-9293, doi: 10.5194/acp-14-9279-2014, 2014.

Huang, D. D., Kong, L., Gao, J., Lou, S., Qiao, L., Zhou, M., and Huang, C.: Insights into the formation and properties of secondary organic aerosol at a background site in Yangtze River Delta region of China: Aqueous-phase processing vs. photochemical

oxidation, Atmos. Environ., 239, 117716, doi: org/10.1016/j.atmosenv.2020.117716, 2020.

Huang, R., Zhang, Y., Bozzetti, C. et al: High secondary aerosol contribution to particulate pollution during haze events in China, Nature, 514, 218–222, doi: org/10.1038/nature13774, 2014.

Jacob, D. J. and Winner, D. A.: Effect of climate change on air quality, Atmos. Environ., 43(1), 51-63, doi: org/10.1016/j.atmosenv.2008.09.051, 2009.

Jayne, J. T., Leard, D. C., Zhang, X. F., Davidovits, P., Smith, K. A., Kolb, C. E., and Worsnop, D. R.: Development of an aerosol mass spectrometer for size and composition analysis of submicron particles, Aerosol Sci. Tech., 33, 49-70, doi: 10.1080/027868200410840, 2000.

Jimenez, J. L., Jayne, J. T., Shi, Q., Kolb, C. E., Worsnop, D. R., Yourshaw, I., Seinfeld, J. H., Flagan, R. C., Zhang, X., Smith, K. A., Morris, J. W., and Davidovits, P.: Ambient aerosol sampling with an Aerosol Mass Spectrometer, J. Geophys. Res.-Atmos., 108, 8425, doi:8410:1029/2001JD001213, 2003.

Jimenez, J. L., Canagaratna, M. R., Donahue, N. M., Prevot, A. S. H., Zhang, Q., Kroll, J. H., DeCarlo, P. F., Allan, J. D., Coe, H., Ng, N. L., Aiken, A. C., Docherty, K. S., Ulbrich, I. M., Grieshop, A. P., Robinson, A. L., Duplissy, J., Smith, J. D., Wilson, K. R., Lanz, V. A., Hueglin, C., Sun, Y. L., Tian, J., Laaksonen, A., Raatikainen, T., Rautiainen, J., Vaattovaara, P., Ehn, M., Kulmala, M., Tomlinson, J. M., Collins, D. R., Cubison, M. J., Dunlea, J., Huffman, J. A., Onasch, T. B., Alfarra, M. R., Williams, P. I., Bower, K., Kondo, Y., Schneider, J., Drewnick, F., Borrmann, S., Weimer, S., Demerjian, K., Salcedo, D., Cottrell, L., Griffin, R., Takami, A., Miyoshi, T., Hatakeyama, S., Shimono, A., Sun, J. Y., Zhang, Y. M., Dzepina, K., Kimmel, J. R.,

Sueper, D., Jayne, J. T., Herndon, S. C., Trimborn, A. M., Williams, L. R., Wood, E. C., Middlebrook, A. M., Kolb, C. E., Baltensperger, U., and Worsnop, D. R.: Evolution of organic aerosols in the atmosphere, Science, 326, 1525-1529, doi: 10.1126/science.1180353, 2009.

Kanawade, V. P., Tripathi, S. N., Chakraborty, A., and Yu, H.: Chemical characterization of sub-micron aerosols during new particle formation in an urban atmosphere, Aerosol and Air Quality Research, 20(6), 1294-1305, 2020.

Kaltsonoudis, C., Kostenidou, E., Louvaris, E., Psichoudaki, M., Tsiligiannis, E., Florou, K., Liangou, A., and Pandis, S. N.: Characterization of fresh and aged organic aerosol emissions from meat charbroiling, Atmos. Chem. Phys., 17, 7143-7155, doi: org/10.5194/acp-17-7143-2017, 2017.

Kim, H., Zhang, Q., Bae, G. N., Kim, J. Y., and Lee, S. B.: Sources and atmospheric processing of winter aerosols in Seoul, Korea: insights from real-time measurements using a high-resolution aerosol mass spectrometer, Atmos. Chem. Phys., 17, 2009-2033, doi:10.5194/acp-17-2009-2017, 2017.

Kim, H., Zhang, Q., and Heo, J.: Influence of intense secondary aerosol formation and long-range transport on aerosol chemistry and properties in the Seoul Metropolitan Area during springtime: results from KORUS-AQ, Atmos. Chem. Phys., 18, 10, 7149-7168, 2018.

Klein, F., Farren, N. J., Bozzetti, C., Daellenbach, K. R., Kilic, D., Kumar, N. K., Pieber, S. M., Slowik, J. G., Tuthill, R. N., Hamilton, J. F., Baltensperger, U., Prévôt, A. S. H., and El Haddad, I.: Indoor terpene emissions from cooking with herbs and pepper and their secondary organic aerosol production potential, Sci. Rep., 6, 36623, doi: 10.1038/srep36623, 2016.

Kleindienst, T. E., Jaoui, M., Lewandowski, M., Offenberg, J. H., Lewis, C. W., Bhave, P. V. and Edney, E. O.: Estimates of the contributions of biogenic and anthropogenic hydrocarbons to secondary organic aerosol at a southeastern US location, Atmos. Environ., 41, 8288-8300, doi: 10.1016/j.atmosenv.2007.06.045, 2007.

Knote, C., Brunner, D., Vogel, H., Allan, J., Asmi, A., Äijälä, M., Carbone, S., van der Gon, H. D., Jimenez, J. L., Kiendler-Scharr, A., Mohr, C., Poulain, L., Prévôt, A. S. H., Swietlicki, E., and Vogel, B.: Towards an online-coupled chemistry-climate model: evaluation of trace gases and aerosols in COSMO-ART, Geosci. Model Dev., 4, 1077–1102, doi: org/10.5194/gmd-4-1077- 2011, 2011.

Kroll, J. H., Donahue, N. M., Jimenez, J. L., Kessler, S. H., Canagaratna, M. R., Wilson, K. R., Altieri, K. E., Mazzoleni, L. R., Wozniak, A. S., Bluhm, H., Mysak, E. R., Smith, J. D., Kolb, C. E., and Worsnop, D. R.: Carbon oxidation state as a metric for describing the chemistry of atmospheric organic aerosol, Nat. Chem., 3, 133-139, doi: 10.1038/nchem.948, 2011.

Lanz, V. A., Alfarra, M. R., Baltensperger, U., Buchmann, B., Hueglin, C., and Prévôt, A. S. H.: Source apportionment of submicron organic aerosols at an urban site by factor analytical modelling of aerosol mass spectra, Atmos. Chem. Phys., 7, 1503-1522, doi:10.5194/acp-7-1503-2007, 2007.

Lanz, V. A., Alfarra, M. R., Baltensperger, U., Buchmann, B., Hueglin, C., Szidat, S., Wehrli, M. N., Wacker, L., Weimer, S., Caseiro, A., Puxbaum, H., and Prevot, A. S. H.: Source attribution of submicron organic aerosols during wintertime inversions by advanced factor analysis of aerosol mass spectra, Environ. Sci. Technol., 42, 214–220, doi:10.1021/es0707207, 2008.

Lee, B. P., Li, Y. J., Yu, J. Z., Louie, P. K., and Chan, C. K.: Characteristics of submicron particulate matter at the urban roadside in downtown Hong Kong- Overview of 4 months of continuous high-resolution aerosol mass spectrometer measurements, J. Geophys. Res., 120, 7040-7058, doi: 10.1002/2015JD023311, 2015.

Lee, B. P., Louie, P. K. K., Luk, C., and Chan, C. K.: Evaluation of traffic exhaust contributions to ambient carbonaceous submicron particulate matter in an urban roadside environment in Hong Kong, Atmos. Chem. Phys., 17, 15121-15135, doi: doi.org/10.5194/acp-17-15121-2017, 2017.

Li, Y. J., Lee, B. Y. L., Yu, J. Z., Ng, N. L., and Chan, C. K.: Evaluating the degree of oxygenation of organic aerosol during foggy and hazy days in Hong Kong using high-resolution time-of-flight aerosol mass spectrometry (HR-ToF-AMS), Atmos. Chem. Phys., 13, 8739-8753, doi: 10.5194/acp-13-8739-2013, 2013.

Li, Y. J., Lee, B. P., Su, L., Fung, J. C. H., and Chan, C. K.: Seasonal characteristics of fine particulate matter (PM) based on high-resolution time-of-flight aerosol mass spectrometric (HR-ToF-AMS) measurements at the HKUST Supersite in Hong Kong, Atmos. Chem. Phys., 15, 37-53, doi: 10.5194/acp-15-37-2015, 2015.

Lin, C., Li, Y., Lau, A. K. H., Li, C. C. and Fung, J. C. H.:15-year $PM_{2.5}$ trends in the Pearl River Delta region and Hong Kong from satellite observation, Aerosol Air. Qual. Res., 8, 2355-2362, doi: org/10.4209/aaqr.2017.11.0437, 2018.

Ling, Z. H. and Guo, H.: Contribution of VOC sources to photochemical ozone formation and its control policy implication in Hong Kong, Environmental science & policy, 38, 180-191, doi: org/10.1016/j.envsci.2013.12.004, 2014.

Liu, T., Liu, Q., Li, Z., Huo, L., Chan, M., Li, X., Zhou, Z. and Chan, C. K.: Emission of volatile organic compounds and production of secondary organic aerosol from stir-frying spices, Sci. Total Environ., 599-600, 1614-1621, doi: 10.1016/j.scitotenv.2017.05.147, 2017a.

Liu, T., Li, Z., Chan, M., and Chan, C. K.: Formation of secondary organic aerosols from gas-phase emissions of heated cooking oils, Atmos. Chem. Phys., 17, 7333-7344, doi: 10.5194/acp-17-7333-2017, 2017b.

Liu, T., Wang, Z., Huang, D. D., Wang, X. and Chan, C. K.: Significant production of secondary organic aerosol from emissions of heated cooking oils, Environ. Sci. Technol. Lett., 5, 32-37, doi: doi.org/10.1021/acs.estlett.7b00530, 2018.

Liu, T., Zhou, L., Liu, Q., Lee, B. P., Yao, D., Lu, H., Lyu, X., Guo, H., and Chan, C. K.: Secondary organic aerosol formation from urban roadside air in Hong Kong, Environ. Sci. Technol., 53, 3001-3009, doi: 10.1021/acs.est.8b06587, 2019.

Liu, Y., Wu, Z., Wang, Y., Xiao, Y., Gu, F., Zheng, J.: Submicrometer particles are in the liquid state during heavy haze episodes in the urban atmosphere of Beijing, China. Environ. Sci. Technol. Letters, 4(10), 427–432. doi: org/10.1021/acs. estlett.7b00352, 2017.

Louie, P. K., Watson, J. G., Chow, J. C., Chen, A., Sin, D. W., and Lau, A. K.: Seasonal characteristics and regional transport of $PM_{2.5}$ in Hong Kong, Atmos. Environ., 39, 1695-1710, doi: 10.1016/j.atmosenv.2004.11.017, 2005.

Liu, X., Wang, N., Lyu, X., Zeren, Y., Jiang, F., Wang, X., Zou, S., Ling, Z. and Guo, H.: Photochemistry of ozone pollution in autumn in Pearl River Estuary, South China, Sci. Total Environ., 754, 141812, doi: org/10.1016/j.scitotenv.2020.141812, 2021.

Lyu, X.P., Guo, H., Simpson, I. J., Meinardi, S., Louie, P. K., Ling, Z.H., Wang, Y., Liu, M., Luk, C.W.Y., Wang, N., and Blake, D. R.: Effectiveness of replacing catalytic converters in LPG-fueled vehicles in Hong Kong, Atmos. Chem. Phys., 16, 6609-6626, doi: org/10.5194/acp-16-6609-2016, 2016.

Lyu, X. P., Zeng, L. W., Guo, H., Simpson, I. J., Ling, Z. H., Wang, Y., Murray, F., Louie, P. K. K., Saunders, S. M., Lam, S. H. M. and Blake, D. R.: Evaluation of the effectiveness of air pollution control measures in Hong Kong, Environ. Pollut., 220, 87-94, doi: 10.1016/j.envpol.2016.09.025, 2017a.

Lyu, X. P., Guo, H., Cheng, H. R., Wang, X. M., Ding, X., Lu, H. X., YAO, D. W. and Xu, C.: Observation of SOA tracers at a mountainous site in Hong Kong: Chemical characteristics, origins and implication on particle growth, Sci. Total Environ., 605, 180-189, doi: 10.1016/j.scitotenv.2017.06.161, 2017b.

Lyu, X., Guo, H., Yao, D., Lu, H., Huo, Y., Xu, W., Kreisberg, N., Goldstein, A. H., Jayne, J., Worsnop, D., Tan, Y., Lee, S. C. and Wang, T.: In situ measurements of molecular markers facilitate understanding of dynamic sources of atmospheric organic aerosols, Environ. Sci. Technol., 54(18), 11058-11069, doi: org/10.1021/acs.est.0c02277, 2020.

Marshall, J. D., Nethery, E. and Brauer, M.: Within-urban variability in ambient air pollution: comparison of estimation methods, Atmos. Environ., 42, 1359-1369, doi: org/10.1016/j.atmosenv.2007.08.012, 2008.

Middlebrook, A. M., Bahreini, R., Jimenez, J. L., and Canagaratna, M. R.: Evaluation of composition-dependent collection efficiencies for the Aerodyne Aerosol Mass Spectrometer using field data, Aerosol Sci. Tech., 46, 258–271, doi:10.1080/02786826.2011.620041, 2012.

Mohr, C., Huffman, J. A., Cubison, M. J., Aiken, A. C., Docherty, K. S., Kimmel, J. R., Ulbrich, I. M., Hannigan, M., and Jimenez, J. L.: Characterization of primary organic aerosol emissions from meat cooking, trash burning, and motor vehicles with high-resolution aerosol mass spectrometry and comparison with ambient and chamber observations, Environ. Sci. Technol., 43, 2443–2449, doi:10.1021/es8011518, 2009.

Mohr, C., DeCarlo, P. F., Heringa, M. F., Chirico, R., Slowik, J. G., Richter, R., Reche, C., Alastuey, A., Querol, X., Seco, R., Peñuelas, J., Jiménez, J. L., Crippa, M., Zimmermann, R., Baltensperger, U., and Prévôt, A. S. H.: Identification and quantification of organic aerosol from cooking and other sources in Barcelona using aerosol mass spectrometer data, Atmos. Chem. Phys., 12, 1649–1665, doi:10.5194/acp-12-1649-2012, 2012.

Ng, N. L., Canagaratna, M. R., Zhang, Q., Jimenez, J. L., Tian, J., Ulbrich, I. M., Kroll, J. H., Docherty, K. S., Chhabra, P. S., Bahreini, R., Murphy, S. M., Seinfeld, J. H., Hildebrandt, L., Donahue, N. M., DeCarlo, P. F., Lanz, V. A., Prévôt, A. S. H., Dinar, E., Rudich, Y., and Worsnop, D. R.: Organic aerosol components observed in Northern Hemispheric datasets from Aerosol Mass Spectrometry, Atmos. Chem. Phys., 10, 4625-4641, doi: 10.5194/acp-10-4625-2010, 2010.

Ng, N. L., Canagaratna, M. R., Jimenez, J. L., Chhabra, P. S., Seinfeld, J. H., and Worsnop, D. R.: Changes in organic aerosol composition with aging inferred from aerosol mass spectra, Atmos. Chem. Phys., 11, 6465-6474, doi: 10.5194/acp-11-6465-2011, 2011.

Nordin, E. Z., Eriksson, A. C., Roldin, P., Nilsson, P. T., Carlsson, J. E., Kajos, M. K., Hellén, H., Wittbom, C., Rissler, J., Löndahl, J., Swietlicki, E., Svenningsson, B., Bohgard, M., Kulmala, M., Hallquist, M. and Pagels, J. H.: Secondary organic aerosol

formation from idling gasoline passenger vehicle emissions investigated in a smog chamber. Atmos. Chem. Phys., 13, 6101-6116, doi: 10.5194/acp-13-6101-2013, 2013.

Offenberg, J. H., Lewis, C. W., Lewandowski, M., Jaoui, M., Kleindienst, T. E. and Edney, E. O.: Contributions of toluene and α-pinene to SOA formed in an irradiated toluene/α-pinene/NOx/air mixture: comparison of results using 14C content and SOA organic tracer methods, Environ. Sci. Technol., 41, 3972-3976, doi: 10.1021/es070089+, 2007.

Paatero, P. and Tapper, U.: Positive matrix factorization- A nonnegative factor model with optimal utilization of error-Estimates of data values, Environmetrics, 5, 111- 126, doi:10.1002/env.3170050203, 1994.

Paglione, M., Gilardoni, S., Rinaldi, M., Decesari, S., Zanca, N., Sandrini, S., and Fuzzi, S: The impact of biomass burning and aqueous-phase processing on air quality: a multi-year source apportionment study in the Po Valley, Italy, Atmos. Chem. Phys., 20, 1233-1254, doi: org/10.5194/acp-20-1233-2020, 2020.

Pagonis, D.; Krechmer, J. E.; de Gouw, J.; Jimenez, J. L. and Ziemann, P. J.: Effects of gas−wall partitioning in Teflon tubing and instrumentation on time-resolved measurements of gas-phase organic compounds, Atmos. Meas. Tech. 10, 4687−4696, doi: 10.5194/amt-10-4687-2017, 2017.

Pope, C.A. and Dockery, D.W.: Health effects of fine particulate air pollution: lines that connect, J. Air Waste Manage. Assoc., 56, 709-742, doi: 10.1080/10473289.2006.10464485, 2006.

Qin, Y. M., Li, Y. J., Wang, H., Lee, B. P., Huang, D. D. and Chan, C. K.: Particulate matter (PM) episodes at a suburban site in Hong Kong: evolution of PM characteristics

and role of photochemistry in secondary aerosol formation, Atmos. Chem. Phys., 16, 14131-14145, doi: 10.5194/acp-16-14131-2016, 2016.

Racherla, P. N., and Adams, P. J.: Sensitivity of global tropospheric ozone and fine particulate matter concentrations to climate change, J. Geophys. Res., 111, D24, doi:10.1029/2005JD006939, 2006.

Seinfeld, J. and Pandis, S.: Atmospheric Chemistry and Physics, 1997, New York, doi: org/10.12987/9780300150315, 2008.

Setyan, A., Zhang, Q., Merkel, M., Knighton, W. B., Sun, Y., Song, C., Shilling, J. E., Onasch, T. B., Herndon, S. C.,Worsnop, D. R., Fast, J. D., Zaveri, R. A., Berg, L. K., Wiedensohler, A., Flowers, B. A., Dubey, M. K., and Subramanian, R.: Characterization of submicron particles influenced by mixed biogenic and anthropogenic emissions using high-resolution aerosol mass spectrometry: results from CARES, Atmos. Chem. Phys., 12, 8131–8156, doi: 10.5194/acp-12-8131-2012, 2012.

So, K. L., Guo, H., and Li, Y. S.: Long-term variation of $PM_{2.5}$ levels and composition at rural, urban and roadside sites in Hong Kong: Increasing impact of regional air pollution, Atmos. Environ., 41, 9427-9434, doi: 10.1016/j.atmosenv.2007.08.053, 2007.

Sun, C., Lee, B. P., Huang, D., Li, Y. J., Schurman, M. I., Louie, P. K., Luk, C., and Chan, C. K.: Continuous measurements at the urban roadside in an Asian megacity by Aerosol Chemical Speciation Monitor (ACSM): particulate matter characteristics during fall and winter seasons in Hong Kong. Atmos. Chem. Phys., 16, 1713-1728, doi: org/10.5194/acp-16-1713-2016, 2016.

Sun, J., Zhang, Q., Canagaratna, M. R., Zhang, Y., Ng, N. L., Sun, Y., Jayne, J. T., Zhang, X., Zhang, X., and Worsnop, D. R.: Highly time- and size-resolved

characterization of submicron aerosol particles in Beijing using an Aerodyne Aerosol Mass Spectrometer, Atmos. Environ., 44, 131-140, doi: 10.1002/mas.20115, 2010.

Sun, Y. L., Zhang, Q., Schwab, J. J., Demerjian, K. L., Chen, W. N., Bae, M. S., Hung, H. M., Hogrefe, O., Frank, B., Rattigan, O. V., and Lin, Y. C.: Characterization of the sources and processes of organic and inorganic aerosols in New York city with a high-resolution time-of-flight aerosol mass spectrometer, Atmos. Chem. Phys., 11, 1581–1602, doi:10.5194/acp-11-1581- 2011, 2011.

Schauer, J. J., Kleeman, M. J., Cass, G. R., Simoneit, B. R: Measurement of emissions from air pollution sources. 4. C1- C27 organic compounds from cooking with seed oils, Environ. Sci. Technol, 36, 567−575, doi: org/10.1021/es002053m, 2002.

Surratt, J.D., Chan, A.W.H., Eddingsaas, N.C. Chan, M., Loza, C.L., Kwan, A.J., Hersey, S.P., Flagan, R.C., Wennberg, P.O., Seinfeld, J.H.: Reactive intermediates revealed in secondary organic aerosol formation from isoprene, Proc. Natl. Acad. Sci., 107, pp. 6640-6645, 2010.

Tai, A. P., Mickley, L. J., and Jacob, D. J.: Correlations between fine particulate matter ($PM_{2.5}$) and meteorological variables in the United States: Implications for the sensitivity of $PM_{2.5}$ to climate change, Atmos. Environ., 44, 3976-3984, doi: 10.1016/j.atmosenv.2010.06.060, 2010.

Tan, Y., Han, S., Chen, Y., Zhang, Z., Li, H., Li, W., Yuan, Q., Li, X., Wang, T., and Lee, S. C.: Characteristics and source apportionment of volatile organic compounds (VOCs) at a coastal site in Hong Kong, Sci. Total Environ., 777, 146241, doi: org/10.1016/j.scitotenv.2021.146241, 2021.

Ulbrich, I. M., Canagaratna, M. R., Zhang, Q., Worsnop, D. R., and Jimenez, J. L.: Interpretation of organic components from Positive Matrix Factorization of aerosol

mass spectrometric data, Atmos. Chem. Phys., 9, 2891-2918, doi:10.5194/acp-9-2891-2009, 2009.

Vu, H. Q., Li, G., Law, R., and Zhang, Y.: Tourist activity analysis by leveraging mobile social media data, J. Travel Res., 57, 883-898, doi: org/10.1177/0047287517722232, 2018.

Wang, Y., Wang, H., Guo, H., Lyu, X, Cheng, H., Ling, Z., Louie, P.K., Simpson, I.J., Meinardi I.J. and Blake, D.R.: Long-term O_3-precursor relationships in Hong Kong: field observation and model simulation, Atmos. Chem. Phys., 17, 10919-10935, doi: org/10.5194/acp-17-10919-2017, 2017.

Wang, T.; Dai, J.; Lam, K. S.; Poon, C. N. and Brasseur, G. P.: Twenty-Five Years of Lower Tropospheric Ozone Observations in Tropical East Asia: The Influence of Emissions and Weather Patterns, Geophys. Res. Lett. 2019, 46 (20), 11463−11470.

Wang, W., Wu, M. H., Li, L., Zhang, T., Li, H. J., Wang, Y. J., Liu, X. D., Sheng, G. Y., Claeys, M. and Fu, J. M.: Polar organic tracers in $PM_{2.5}$ aerosols from forests in eastern China, Atmos. Chem. Phys., 8, 7507. doi:10.5194/ACP-8-7507-2008, 2008.

Wexler, A. S. and Clegg, S. L.: Atmospheric aerosol models for systems including the ions H^+, NH_4^+, Na^+, SO_4^{2-}, NO_3^-, Cl^-, Br^-, and H_2O, J. Geophys. Res., 107(D14), ACH-14, 2002.

Xiao, Y., Hu, M., Zong, T., Wu, Z., Tan, T., Zhang, Z., Fang, X., Chen, S., and Guo, S.: Insights into aqueous-phase and photochemical formation of secondary organic aerosol in the winter of Beijing, Atmos. Environ., 118535. doi: org/10.1016/j.atmosenv.2021.118535, 2021.

Xu, L., Guo, H., Boyd, C. M., Klein, M., Bougiatioti, A., Cerully, K. M., Hite, J. R., Isaacman-VanWertz, G., Kreisberg, N. M., Knote, C., Olson, K., Koss, A., Goldstein A. H., Hering, S. V., Gouw, J., Baumann, K., Lee, S. H., Nenes, A., Weber, R. J. and Ng, N. L.: Effects of anthropogenic emissions on aerosol formation from isoprene and monoterpenes in the southeastern United States, Proc. Natl. Acad. Sci., 112, 1, 37-42, doi: 10.1073/pnas.1512277112, 2015.

Xu, L., Pye, H. O. T., He, J., Chen, Y., Murphy, B. N., Ng, N. L.: Experimental and model estimates of the contributions from biogenic monoterpenes and sesquiterpenes to secondary organic aerosol in the southeastern United States, Atmos. Chem. Phys. 18, 12613-12637, doi: org/10.5194/acp-18-12613-2018, 2018.

Xu, W., Sun, Y., Wang, Q., Zhao, J., Wang, J., Ge, X., ... & Coe, H. (2019). Changes in aerosol chemistry from 2014 to 2016 in winter in Beijing: Insights from high-resolution aerosol mass spectrometry. Journal of Geophysical Research: Atmospheres, 124(2), 1132-1147.

Yao, D, Lyu, X, Murray, F., Morawska, L., Yu, W., Wang, J., and Guo, H.: Continuous effectiveness of replacing catalytic converters on liquified petroleum gas-fueled vehicles in Hong Kong, Sci. Total Environ., 648, 830-838, doi: org/10.1016/j.scitotenv.2018.08.191, 2019.

Young, D. E., Allan, J. D., Williams, P. I., Green, D. C., Flynn, M. J., Harrison, R. M., and Coe, H.: Investigating the annual behaviour of submicron secondary inorganic and organic aerosols in London, Atmos. Chem. Phys., 15, 11, 6351-6366, doi:10.5194/acp-15-6351-2015, 2015.

Zhao, Y., Hu, M., Slanina, S., and Zhang, Y.: The molecular distribution of fine particulate organic matter emitted from western-style fast food cooking, Atmos. Environ., 41, 8163-8171, doi: org/10.1016/j.atmosenv.2007.06.029, 2007.

Zhang, Q., Alfarra, M. R., Worsnop, D. R., Allan, J. D., Coe, H., Canagaratna, M. R., and Jimenez, J. L.: Deconvolution and quantification of hydrocarbon-like and oxygenated organic aerosols based on aerosol mass spectrometry, Environ. Sci. Technol., 39, 4938–4952, doi:10.1021/es048568l, 2005.

Zhang, Q., Jimenez, J. L., Canagaratna, M. R., Ulbrich, I. M., Ng, N. L., Worsnop, D. R., and Sun, Y.: Understanding atmospheric organic aerosols via factor analysis of aerosol mass spectrometry: a review, Anal. Bioanal. Chem., 401, 3045–3067, doi: 10.1007/s00216-011-5355-y, 2011.

Zhang, X., Xu, J., Kang, S., Zhang, Q., and Sun, J.: Chemical characterization and sources of submicron aerosols in the northeastern Qinghai–Tibet Plateau: insights from high-resolution mass spectrometry, Atmos. Chem. Phys., 19, 7897-7911, doi: 10.5194/acp-19-7897-2019, 2019.

Zhang, Y. N.; Zhang, Z. S.; Chan, C. Y.; Engling, G.; Sang, X. F.; Shi, S., and Wang, X. M.: Levoglucosan and carbonaceous species in the background aerosol of coastal southeast China: case study on transport of biomass burning smoke from the Philippines, Environ. Sci. Pollut. Res. 2012, 19 (1), 244−255.

Zhang, Y., Favez, O., Petit, J. E., Canonaco, F., Truong, F., Bonnaire, N., and Albinet, A.: Six-year source apportionment of submicron organic aerosols from near-continuous highly time-resolved measurements at SIRTA (Paris area, France), Atmos. Chem. Phys., 19, 23, doi: org/10.5194/acp-19-14755-2019, 14755-14776, 2019.

Zhang, Y., Zhou, R., Chen, J. and Rangel-Buitrago, N: The effectiveness of emission control policies in regulating air pollution over coastal ports of China: Spatiotemporal variations of NO_2 and SO_2, Ocean & Coastal Management, 219, 106064, 2022.

Zhou, L., Liu, T., Yao, D., Guo, H., Cheng, C. and Chan, C. K.: Primary emissions and secondary production of organic aerosols from heated animal fats, Sci. Total Environ., 148638, doi: org/10.1016/j.scitotenv.2021.148638, 2021.